New protocols for exploring the auxin metabolic network

A Dissertation
SUBMITTED TO THE FACULTY OF
UNIVERSITY OF MINNESOTA
BY

Qian Tang

IN PARTIAL FULFILLMENT OF THE REQUIREMENTS
FOR THE DEGREE OF
DOCTOR OF PHILOSOPHY

Advisor: Jerry D. Cohen

August 2022

Acknowledgements

First of all, I would like to express my deepest thanks to my advisor, Dr. Jerry Cohen for his exceptional mentorship through my Ph.D. study. I will forever thank him for his support and guidance not only in my academic career but also in my personal life. His knowledge and enthusiasm in science, and empathy and optimism in life countlessly encouraged me to overcome challenges and finding the strength to carry on. I am also grateful that Jerry created such a trustful and open-minded research environment that my time working in his lab has always been enjoyable and a great opportunity to learn and explore. I appreciated his help and advice in my research throughout these years, and efforts he put in revising manuscripts and this dissertation. Jerry is a great mentor in life, a role model that motivates me to become a genuine, self-driven and inspiring scientist.

Next, I would like to thank my advisory committee for giving me all the thoughtful feedback, insightful suggestions and encouragement along the way. I wish to express my great gratitude to Dr. Adrian Hegeman for sharing his expertise in biochemistry and metabolomics and helping with data analysis and visualization, to Dr. Neil Olszewski for providing valuable feedback and constructive criticism to shape my research, and to Dr. Changbin Chen for sharing his academic and career experience and giving helpful comments on my thesis.

I thank all the present and past members of the Cohen/Gardner/Hegeman lab group who have shared ideas and given valuable discussions in group meetings. In particular, I wish to thank Dr. Gary Gardner for his mentorship in the field of photobiology and constructive suggestions on my thesis, Dr. Yuan Xu for being my mentor when I first joined the Ph.D. program and helping me settle down in Jerry's lab, Dr. Molly Tillmann for her collaboration and help with designing experiments and polishing my research projects, Dr. Dana Freund, Dr. Renata Pincelli-Souza and Kate Sammons for their expertise and assistance, and Doug Brinkman for growth chambers set-up and support.

I would also like to express my sincere thanks to the Plant and Microbial Biology (PMB) graduate program and the Department of Horticultural Science for hosting my graduate studies and providing professional administrative support, and I am deeply thankful for the advice and assistance I received from my fellow graduate students.

I wish to extend my special thanks to Dr. Janet Slovin for the collaboration of the strawberry project. She is not only a great scientist but also a good friend who has enlightened me a lot about maintaining work/life balance. I enjoyed very much having yoga lessons with her.

My research was supported by the National Science Foundation (NSF) Plant Genome Research Program grant IOS-1238812, the US Department of Agriculture National Institute of Food and Agriculture (USDA-NIFA) No. 2018-67013-27503 and 2019-51181-30025, Minnesota Department of Agriculture grant CON000000092336_2021 SCBG and by funds from the Minnesota Agricultural Experiment Station and the Gordon and Margaret Bailey Endowment for Environmental Horticulture. I am also thankful for the summer fellowships and travel grants provided by the PMB graduate program and the Department of Horticultural Science, as well as the travel grants provided by the Microbial and Plant Genomics Institute (MPGI) and American Society of Plant Biologists (ASPB), which allowed me to attend academic conferences and workshops and exchange with scientists from all over the world.

Last but not least, I would like to thank my friends and family who have offered me tremendous support and encouragement. Special thank you to Xin for her courage, persistence, and all of her amazing artistic creations that have inspired me and helped me get through tough times. An enormous thank you to my parents for their unconditional love and support no matter how far we are apart, and their help with finding peace of life and balance in being a mother and a graduate student. Finally, deepest thank you to my son, Ethan, for being the sunshine of my life and helping me learn to love, give and forgive.

Dedication

This dissertation is dedicated to my mother Mrs. Zhenbao Wang and my father Dr. Liangjie Tang.

Abstract

The phytohormone auxin plays a critical role in plant growth and development. Maintenance of auxin homeostasis involves a complex interaction between biosynthesis, formation and hydrolysis of conjugates, catabolism and transport. Despite significant progress in elucidating metabolic pathways of the primary bioactive auxin, indole-3-acetic acid (IAA), over the past few decades, key components such as intermediates and enzymes have not been fully characterized, and the dynamic regulation of IAA metabolism in response to environmental signals has not been completely revealed. Using a highly sensitive liquid chromatography-mass spectrometry (LC-MS) method, I identified auxin-amino acid conjugates in achenes of *F. vesca* as consisting of indole-3-acetylaspartate (IAasp) and indole-3-acetylglutamate (IAglu). In contrast to what has been proposed to occur in Arabidopsis, I determined that IAasp and IAglu are hydrolyzed by seedlings to provide a source of free IAA for growth. I also describe the methods for pathway analysis in *Arabidopsis thaliana* seedlings by monitoring incorporation of multiple stable isotopes from labeled precursors to IAA biosynthetic pathway intermediates coupled with chemical inhibitors application and high-performance LC-MS techniques. These methods were then adapted to survey Arabidopsis seedlings for their changing indolic profile. I describe in detail the Stable Isotope Labeled Kinetics (SILK) methods employing a rapid stable isotope labeling that allows for tracing the turnover rates of IAA pathway precursors and product concurrently with a time scale of seconds to minutes. By measuring the entire pathways over time and using different isotopic tracer techniques, I demonstrate that these methods offer more detailed information about this complex interacting network of IAA biosynthesis, and should prove to be useful for studying auxin metabolic network in vivo in a variety of plant tissues and under different environmental conditions.

Tables of Contents

List of Tables

List of Figures

Chapter 1. Introduction

Plant life and its orderly development has to be strictly controlled to achieve optimum growth and reproduction. For example, to be successful, germination has to occur at the right time and under the correct environmental conditions. Early seedling growth should be rapid to defend against various biotic or abiotic stresses. During its adult life, the plant will compete for resources such as light and water, then allocate its resources for shoot growth, leaf numbers and energy storage in order to survive until flowering. The coordination of all these difficult tasks is due to the action of an extremely complex hormonal signaling network and the plant growth hormone auxin plays a central role in this regulatory process. Indeed, auxin regulates almost all aspects of plant growth and development including embryogenesis, tissue architecture and tropic responses. Maintenance of auxin homeostasis involves multi-pathways for biosynthesis of indole-3-acetic acid (IAA), the principal auxin in plants, conjugation and conjugate hydrolysis and its subsequent catabolic processes including deactivation by ring oxidation of IAA and its conjugated forms (Guo et al., 2022; Hayashi et al., 2021; Ross & Gélinas-Marion, 2021; Tuominen et al., 1994; Woodward & Bartel, 2005). IAA signaling affects the expression pattern of many genes (Paponov et al., 2008; Simon & Petrášek, 2011). A number of proteins involved in auxin responses, including receptors and transporters, have been proposed (Calderon-Villalobos et al., 2010; Zazímalová et al., 2010). With the advancement of analytical and computational capacities, significant progress in elucidating IAA metabolic pathways has been made. However, key components such as intermediates and enzymes involved in IAA metabolic pathways have not been fully characterized, and the dynamic regulation of IAA metabolism in response of endogenous and environmental signals has not been completely understood (Ljung, 2013). In this dissertation critical advances in methodology that enables new ways for studying regulation of IAA metabolism will be described in its subsequent chapters.

Several IAA biosynthetic pathways have been proposed based on genetic analysis and biochemical measurements (Korasick et al., 2013). These pathways can be classified

into three categories: the IPyA pathway, other tryptophan (Trp)-dependent pathways and tryptophan-independent pathway (Wang et al., 2015). Pathway Figure 3-1 shows major components and pathways implicated in IAA biosynthesis. Until recently the enzymes of all the Trp-dependent IAA biosynthesis pathways were thought to be uniquely present in the cytosol (Chandler, 2009; Tzin & Galili, 2010), however, more recent studies (Kriechbaumer et al., 2017) clearly showed that both YUCCA and TAA-like genes encode proteins targeted to different cellular compartments. In addition, various publication have proposed that IAA is synthesized through potentially four interconnected Trp-dependent pathways, as defined by their key intermediates: the indole-3-acetaldoxime (IAOx), indole-3-acetamide (IAM), tryptamine (TAM), and indole-3-pyruvic acid (IPyA) pathways Tivendale et al., 2014; Woodward & Bartel, 2005). The IPyA pathway, however, has been considered as the potential major contributor, among those pathways proposed, to cellular IAA production (Stepanova et al., 2008; Won et al., 2011; Zhao, 2012). The simplicity of this pathway was first shown by genetic and analytic methods in maize (Phillips et al., 2011) and later in Arabidopsis (Won et al., 2011) to involve the two-step conversion of Trp to IPyA by the TAA1 family of Trp aminotransferases (Tao et al., 2008; Zhou et al., 2011), followed by decarboxylation to produce IAA by the YUCCA (YUC) family of flavin monooxygenase enzymes (Won et al., 2011). *TAA1* and *YUC* gene families are highly conserved across different plant species and these genes are coexpressed in a spatial and temporal manner (Stepanova et al., 2011). Other Trp-dependent pathways, based on the isolation of precursors, have also been suggested to function in a number of species including maize (*Zea mays*), pumpkin (*Cucurbita maxima*), tobacco (*Nicotiana tabacum*), rice (*Oryza sativa*) and various *Brassica* species including Arabidopsis (Korasick et al., 2013).

There were three lines of evidence supporting the Trp-independent auxin pathway. First, it was shown by examining the rate of turnover of IAA and its metabolic precursors, that biosynthesis of IAA from Trp occurs at rates too low to provide the full needs of the plant (Baldi et al., 1991). This finding was followed by studies using stable isotope labeling analysis of Trp auxotrophic mutants. It was further shown that while the auxotrophic mutants were unable to synthesize Trp they still were able to synthesize IAA from Trp

precursors (Normanly et al., 1993; Wright et al., 1991). In the maize *orange pericarp* (*orp*) mutant containing mutations in both *TSB* genes (Wright et al., 1991), and in Arabidopsis *trp3-1* and *trp2-1* mutants, deficient in the α- and β-subunits of Trp synthase (TSA and TSB, respectively (Normanly et al., 1993) de novo biosynthesis of IAA could be demonstrated by growing seedling on $^{2}H_2O$, resulting in deuterium labeling of IAA, but label was incorporated into Trp pools only in the non-mutant control seedlings. The third line of evidence for a Trp-independent route to IAA comes from using an *in vitro* maize enzyme system, where a partially purified enzyme system could synthesize IAA only from indole and not from Trp. Two Trp precursors, indole-3-glycerol phosphate (IGP) and indole, have been suggested as the possible branch point to Trp-independent IAA biosynthesis (Ouyang et al., 2000; R. Zhang et al., 2008) and consistent with this idea, it was shown that the cytosolic TSA-like indole synthase (INS) participates in catalyzing the first step separating the Trp-dependent and independent pathways in Arabidopsis (Wang et al., 2015). However, Nonhebel (2015) argued that the evidence provided by those early labeling studies with seedling from the Trp auxotrophic mutants did not, by itself, provide strong support for the proposed Trp-independent IAA biosynthesis. However, notably, her arguments did not reference the work by Baldi et al. (1991) on the rate of turnover of IAA and its metabolic precursors nor the studies on in vitro enzyme activities, both of which were historically important. For example, she argued that the isotope labeling data assumed a single pool of Trp from which IAA is produced, because, at the time of her review, one hypothesis was that IAA synthesis might be highly localized due to tissue-specific expression of *YUC* genes (Zhao, 2008). If that were true, then one could propose that IAA might be made at different rates from different pools of Trp. Indeed, since L-Trp is a precursor for the synthesis of IAA as well as many defense compounds and proteins, the Trp pool, although a minor amino acid, is still large compared with that of IAA (Tzin & Galili, 2010). Thus, IAA production might be better regulated if the Trp pool were to be compartmentalized within the cell or, alternatively, if the downstream steps in IAA biosynthesis are tightly regulated (Sairanen et al., 2012). Over the last ten years, however, many of these ideas have not been substantiated or have remained speculative. For example, in silico, physical and GFP localization of fused protein analysis of enzymes

suggested to be involved in the IPyA pathway showed a plethora of different subcellular localizations, from cytosol, non-cytosolic, nucleous, and ER (Kriechbaumer et al., 2017) making Nonhebel's (2015) concept of highly localized IAA biosynthesis highly unlikely at the cellular level. Also, labeling of the bulk Trp and IPyA pools seem to be closely interrelated (Tillmann et al., 2022) suggesting no significant pool segregation, contrary to what would be predicted for a compartmentalized Trp pool for IAA biosynthesis. In spite of these limitations, both omissions and newer contradicting data, the Nonhebel (2015) review provides important insights that can be used to guide further investigations.

The deactivation of auxin is another important process maintaining auxin homeostasis (Hayashi et al., 2021; Ljung, 2013). The pathway of IAA degradation through ring oxidation had been characterized and the genes/enzymes involved in this process identified (Normanly et al., 2010; Zhao et al., 2013). The formation of 2-oxindole-3-acetic acid (oxIAA) from IAA oxidation likely plays essential roles in plant reproductive development, since blocking this process leads to altered seed formation in rice (Zhao et al., 2013). oxIAA, being the major primary IAA catabolite found in *Arabidopsis thaliana* root tissues, participates in the regulation of auxin gradients (Aleš Pěnčík et al., 2013).

The conjugation of auxin is also an important mechanism to maintain the level of bioactive hormone. Various forms of conjugated IAA have been identified and characterized including 1-O-indole-3-acetyl-β-glucose (IAGlc), indole-3-acetyl-*myo*-inositol (IAA-*myo*-inositol) and its sugar derivatives, and a number of IAA amino acid conjugates. These IAA conjugates are involved in many hormonally related processes such as IAA transport and protection within the plant (Chisnell & Bandurski, 1988; Cohen & Bandurski, 1978), stress responses and disease resistance (González-Lamothe et al., 2012; Oetiker & Aeschbacher, 1997), and plant tissue growth and production (Ishimaru et al., 2013; Iyer et al., 2005; Rampey et al., 2004).

Until very recently, this division between two processes, oxidation and amino acid conjugation, were considered distinct and IAA was either directly conjugated to amino acids (by GH3 enzymes) or directly 2-oxidized to form 2-oxindole-3-acetic acid (oxIAA) by DAO1 dioxygenase type activities. The studies reported by Hayashi et al. (2021) have

effectively linked these two processes by showing that conjugation to amino acids and 2-oxidation are actually part of the same pathway (Ross & Gélinas-Marion, 2021) where DAO1 dioxygenase irreversibly oxidizes IAA-aspartate (IAasp) and IAA-glutamate (IAglu) into 2-oxindole-3-acetic acid-aspartate and 2-oxindole-3-acetic acid-glutamate, which are subsequently hydrolyzed by ILR1-like hydrolases to release inactive oxIAA. In addition, the operation of this pathway has been shown to be developmentally linked to normal development of flowers and roots (Guo et al., 2022).

Mass spectrometry (MS) has been an invaluable tool in elucidating auxin metabolic network, enabling identification and quantification of IAA metabolites. In chapter 2, a high resolution and accurate mass mass spectrometry (HR/AM-MS) approach was utilized to investigate auxin-amino acid conjugates in achenes of the diploid strawberry *F. vesca.* These auxin conjugates would serve as sources of free IAA for seed germination and seedling growth (Cohen & Bandurski, 1982). By using this powerful analytical approach, we were able to identify and quantify the 3-substituted low molecular weight indole compounds from a crude plant sample extract and demonstrate how these IAA conjugates are hydrolyzed by *F. vesca* for IAA regulated subsequent growth. This finding was important as it overturns an important aspect of 'conventional wisdom', that IAasp and IAglu, unlike other IAA-amino acid conjugates, are not hydrolysed back to IAA in the plant (Ross & Gélinas-Marion, 2021). This aspect of auxin metabolism, the *in vivo* hydrolysis of these conjugates, has recently been confirmed by the studies of Hayashi et al. (2021) where they used a different approach but came to the same conclusion.

A complete understanding of auxin metabolism should take into account metabolic flux information. The flow of metabolites through metabolic pathways can be measured based on the pool size (i.e., concentration) and the turnover (i.e., biosynthesis and degradation) of a given metabolite (Pratt et al., 2002; Roscher et al., 2000; Yuan et al., 2008). In chapter 3, HR/AM-MS methods combining with stable isotope labeling are described to monitor the path of carbon from IAA precursor to intermediate pools and to concurrently identify and quantify all indolic compounds involved in IAA biosynthesis. The application of chemical inhibitors targeting IAA biosynthesis allows blockage of

certain pathway steps to better address the contribution of the inhibited pathway and to re-direct the synthesis to alternative pathways.

Previous studies of auxin metabolism present certain limitations due to lack of measurements of dynamic changes and the longer labeling times required for the studies. In chapter 4 we describe HR/AM-MS-based rapid stable isotope labeling approaches to obtain kinetic information of the IAA metabolic network. These methods were used first to determine when Arabidopsis seedlings make the transition from heterotrophic to autotrophic auxin biosynthesis, then to analyze the incorporation of stable isotopic labels into newly synthesized precursors and IAA with a time scale of seconds to minutes. This kinetic labeling method, coupled with sensitive analytical instrumentation, allowing the evaluation of the entire auxin metabolic network over time, is a method that promises insight into novel intermediates and the potential for discovery of new pathways involved in IAA biosynthesis and insight into other aspects of auxin metabolism.

Chapter 2. Indole-3-acetyl-aspartate and indole-3-acetyl-glutamate, the IAA-amide conjugates in the diploid strawberry achene, are hydrolyzed in growing seedlings

Introduction[1]

Strawberry is a horticultural product of considerable economic importance worldwide. The edible part is botanically a pseudocarp originating mainly from the expansion of the receptacle, which has the true fruits (the achenes) attached to the outside. From early studies by Nitsch (1950) it is known that achene-derived auxin is the phytohormone regulating the expansion of the receptacle that occurs after fertilization. In subsequent investigations, auxin was also shown to slow the ripening of the receptacle at later stages of development (Given et al., 1988). Early bioassay studies (Nitsch, 1955), chromatographic isotope dilution analysis (Archbold & Dennis, 1984) and mass spectral studies (Archbold & Dennis, 1984; Symons et al., 2012) have all confirmed that indole-3-acetic acid (IAA) in achenes and receptacles is the endogenous auxin.

The pattern of free auxin accumulation in combined achenes and receptacles, rising during the first 7-12 days and returning to low levels quickly after that point (Nitsch 1955; Lis et al., 1978; Archbold & Dennis 1984; Symons et al., 2012) suggests active metabolic or transport activity following the period of embryo growth, that sustains longer periods of receptacle development until ripening (Archbold & Dennis, 1985). Embryo growth is typically completed by ten days after fertilization (Perkins-Veazie, 1995) and based on transcriptome data from developing achenes, it has been suggested that during embryo development auxin possibly moves from the young achene to the receptacle in conjugated form (Kang et al., 2013).

Lis (1974) showed that strawberry tissues are capable of conjugating exogenous auxin. When enlarging receptacles were supplied with [^{14}C]IAA, they synthesized [^{14}C]indoleacetyl-aspartate (IAasp) as well as [^{14}C]indoleacetyl-glucose. Archbold and

[1]Tang et al., 2019

Dennis (1984) used base hydrolysis to show that amide-linked auxin conjugates accumulated during achene development after a spike in free IAA levels, but they did not identify the conjugates present in the extracts. Park et al. (2006) found a protein with IAA in amide linkage in strawberry achenes as well as in receptacle tissue. IAA-conjugates can serve as storage forms of active, free IAA, as well as being entry points into the hormone degradation pathways (Zhang & Peer, 2017). Free IAA for plant growth and development is cleaved from amino acid conjugates by a group of amidohydrolases of the M20 peptidase family first characterized in Arabidopsis (Bartel & Fink, 1995; LeClere et al., 2002) These hydrolases are conserved in higher plants (Campanella et al., 2003, 2014; Smolko et al., 2018).

The common commercial strawberry *F. ×ananassa* is an octoploid, which can be an impediment to genetic characterizations with this species. As for other polyploid crop species, such as alfalfa and potato, where diploid relatives have been utilized as reference species (Jansky et al., 2014; S. Yang et al., 2008), we are using an inbred line of a diploid strawberry, *F. vesca*, for studies of how auxin metabolism in the achene regulates berry growth. *F. vesca* is a progenitor species of *F. ×ananassa*, and a high-quality genome sequence is available for this species (Edger et al., 2018), allowing easy reference to the better-studied reference species for auxin metabolism, *Arabidopsis thaliana*.

We initially focused on identification of all the low molecular weight indole-auxin amino acid conjugates in the mature diploid strawberry achene. These would be expected to act as rapid sources of free IAA for germination and seedling growth (J. D. Cohen & Bandurski, 1982). Our relatively new mass spectrometric approach was utilized, employing high sensitivity/high resolution LC-MS/MS to isolate and identify the 3-substituted low molecular weight indole compounds from a crude plant extract. This protocol has the advantage of not requiring major prior assumptions about the chemical structures being determined. The results of this analysis raised the question of whether strawberry, unlike what is accepted for Arabidopsis (Sauer et al., 2013), hydrolyzes IAasp and IAglu to release free IAA for subsequent growth, and we report here our work to address this uncertainty.

Materials and methods

Plant materials

Achenes were obtained from several lines of strawberry, as detailed in Table 2-1. Plants were grown in a greenhouse with a diurnal cycle of 16 h light and 8 h darkness following normal cultivation practices. Mature fruits were collected and fertilized achenes devoid of receptacle tissue were harvested using the blender method (Morrow, 1954). Clean achenes were collected on filter paper by vacuum filtration, air dried and stored at 4-10°C.

Chemicals and standards

Acetonitrile, 2-isopropanol and methanol (ChromaSolv) were from Sigma-Aldrich (Saint Louis, MO USA). Formic acid was from Fisher Scientific (Hampton, NH USA). Water was distilled in house in a glass still from reverse osmosis treated deionized feed water.

The unlabeled auxin conjugate standards were obtained from commercial sources: IAasp was from Sigma-Aldrich and indole-3-acetyl-L-glutamic acid (IAglu) was custom synthesized by Labseeker (Wujiang City, China). All chemical reagents used in syntheses described below were from Sigma-Aldrich, unless otherwise noted.

Labeled conjugates, [$^{13}C_6$]IAglu and [$^{13}C_6$]IAsp, were synthesized essentially as described (J. D. Cohen, 1981): L-glutamic acid di-tert-butyl ester (Sigma-Aldrich) or L-aspartic acid di-tert-butyl ester (Serva Fine Chemicals, Heidelberg, Germany) was linked to [$^{13}C_6$]IAA (Cambridge Isotope Laboratories, Tewksbury, MA USA) via dicyclohexylcarbodiimide mediated acylation in acetonitrile at 4°C overnight. The solvent was evaporated and the product was then hydrolyzed in 2N KOH in 50% methanol/water (v/v) at 60°C for 2 h to yield the labeled conjugate. The [$^{13}C_6$]IAasp was then purified on lipophilic Sephadex LH-20 (Sigma-Aldrich), as described (Cohen 1981). The [$^{13}C_6$]IAglu product was purified by preparative HPLC on an Agilent (Santa Clara, CA USA) ZORBAX Eclipse XDB-C_{18} 21.2 x 250 mm column. Distilled water and methanol were

used as a solvent system with a gradient starting with methanol at 10% and ending at 90% over 20 min. [$^{13}C_6$]IAglu eluted at 13 min. Identity was confirmed for both compounds using IAglu and IAasp standards through thin-layer chromatography (E. Merck, Darmstadt, Germany); Silica gel 60; ethyl acetate: methyl ethyl ketone:ethanol:water, 5:3:1:1) with indication by Ehmann's reagent (Ehmann, 1977) and by GC-MS analysis as the methyl esters (Cohen, 1982; Epstein et al., 1986).

Mass spectrometric detection

IAA amino acid conjugate discovery and quantitation in strawberry achenes

Typically, a 50 mg sample of H4F7-3 achenes was ground into a fine powder then extracted in 50% 2-isopropanol (kept at -20°C) in a 1.5 ml microcentrifuge tube followed by constant vortexing for 30 min at room temperature. The sample was then centrifuged at 25,000 *g*, at 25°C for 20 min, then 100 µl of the supernatant was diluted 10 times with water. The resulting sample was sufficient for 50-100 analytical determinations at the levels employed in this study.

The extract was analyzed on a Dionex Ultimate 3000 RSLC HPLC coupled to a hybrid quadrupole Orbitrap mass spectrometer (Q Exactive, Thermo Scientific, San Jose, CA USA). 20 µL extract was injected onto a 2.1x100 mm Kinetex XB-C_{18}, 1.7 µm, column (Phenomenex, Torrance, CA USA) and eluted with a solvent gradient. Solvents were A: 0.1% formic acid in water, B: 0.1% formic acid in acetonitrile. Flow rate was 0.2 ml min^{-1}. Gradient was: 0-3.99 min: 3% B, 3.99-4.00 min: 3-16% B, 4-15 min: 16-46.3% B, 15-15.5 min: 46.3-80% B, 15.5-18 min: 80% B. A Heated Electrospray Ionization II probe was used to interface the HPLC and MS. Ion source conditions were: spray voltage: 3.6 kV, capillary temperature: 350°C, probe heater temperature: 300°C, sheath gas: 35 arbitrary units, aux gas: 8 arbitrary units, S-lens RF level: 47. MS was set to acquire one full MS scan followed by 8 targeted-MS2 in positive ionization mode. Full MS conditions were: 1 microscan at 70,000 resolution with an automatic gain control target of $1x10^6$. Maximum accumulation time was 50 ms. Scan range was from 216 to 370 *m/z*. MS^2 conditions were: 1 microscan at 17,500 resolution with automatic gain control target of

$2x10^5$. Isolation width was 10 *m/z* with multiplexing count of 2. 40% normalized collision energy was used with fixed first mass at 60 *m/z*. All data were saved in profile mode.

Using a Q Exactive mass spectrometer the quinolinium signature ion (*m/z* = 130.0651) produced from indolic compounds was monitored with high mass accuracy (Yu et al., 2014). The mass spectrometer was set to acquire a limited full scan (216-370 *m/z*) followed by a series of data independent MS/MS scans. We focused on only IAA amino acid conjugates and thus we only covered a mass range of *m/z* 216-370. Eight data independent scans with a 20 *m/z* isolation window (segment) each were done for each sample. Mass spectra were then extracted for 130.0651 *m/z* signatures. Segments containing the signatures were then divided into smaller segments and analyzed for the signature ion in subsequent reinjections. This process was continued until unambiguous precursor ions were identified. The exact mass and fragmentation patterns of these precursors were obtained for compound identification. To further improve the sensitivity and speed of the analysis of suspected compounds, a targeted MS/MS approach was used. We examined *m/z* values corresponding to those predicted for each of the IAA amino acid conjugates to determine whether they were present *in situ*. The compound identifications were based on HPLC retention time and MS spectra as compared with their respective standards. Once the identity of the compounds had been established, similar procedures were employed except that [$^{13}C_6$]-labeled quantitative standards were added to allow isotope dilution quantitative calculations (Barkawi et al., 2010).

Free IAA quantitation in strawberry achenes

Free IAA in the H4F7-3 achenes was measured by isotope dilution as previously described, except the methylation step was omitted and the samples were analyzed by LC-MS/MS at high resolution on the Q Exactive system used for conjugate analysis. The internal standard, 0.25 ng of [$^{13}C_6$]IAA, was added in 30 µL homogenization buffer (Liu et al., 2012) to each of twelve biological replicates, each weighing 8-12 mg, prior to homogenization with a 3 mm tungsten carbide bead using a Mixer Mill MM 400 (Qiagen, Germantown, MD USA). After incubating the homogenate approximately 1 h on ice, 275 µL water was added to each sample. Samples were then centrifuged and IAA was extracted

from the supernatant using amino and polymethylmethacrylate epoxide (PMME) solid phase extraction resins in Top Tips spin tips (Glygen, Columbia, MD USA) as described by Liu et al. (2012). After elution from PMME tips with 2 × 50 µL volumes of methanol into 1.5 ml microcentrifuge tubes, sample volumes were reduced to approximately 20 uL with a SpeedVac vacuum concentrator (Savant/Thermo, Milford, MA USA). Concentrated samples were transferred to 50 µL inserts in amber autosampler vials for LC-MS/MS analysis with a Dionex Ultimate 3000 RSLC HPLC coupled to a hybrid quadrupole Orbitrap Q Exactive mass spectrometer (Thermo Scientific). 5 µL of strawberry achene extract were injected onto a 50 × 2.1 mm Force C_{18} column with 1.8 µm particle size (Restek, Bellefonte, PA USA) and run with a solvent gradient of 0.1% formic acid in water (solvent A) and 0.1% formic acid in acetonitrile (solvent B) at a flow rate of 0.4 ml min^{-1}. Gradient parameters were as follows: -1-0 min, 5% B; 0-3 min, 5-20% B; 3-6 min, 20-80% B; and 6-6.5 min, 80% B. Mass spectrometry data was collected in the Parallel Reaction Monitoring scan mode with the [M+1] for IAA and [$^{13}C_6$]IAA at *m/z* 176.1 and 182.1, respectively, in the inclusion list and with the following settings: isolation width of 2.0 *m/z*, resolution of 17,500, automatic gain control target of 2 x 10^5, maximum accumulation time of 50 ms, and normalized collision energy of 20%.

Hydrolysis of IAasp and IAglu in growing strawberry seedlings

To determine if IAasp and IAglu were hydrolyzed and provide a source of free IAA during seedling growth, ~175 mg of YW5AF7 achenes were surface sterilized by shaking in 95% ethanol for five minutes followed by 5 rinses in sterile H_2O. The achenes were left in the final rinse and imbibed by rocking on a shaker overnight at 6°C. The achenes were further disinfected by shaking for 15 min in 30% commercial bleach (to a final concentration of ~2% sodium hypochlorite) followed by 5 rinses with sterile water. The achenes were left in the final rinse and poured into a deep Petri dish that was then taped with Micropore tape (3M, St. Paul, MN USA) and kept at 27°C for 4 days until the radicle just emerged. Square Petri dishes (100 x 100 mm with grid), were prepared to contain 15 ml 0.5X Murashige and Skoog medium (Caisson Laboratories, Smithfield, UT USA), pH 6.0, 0.8% Phytoblend agar (Caisson) and 40 µM of either [$^{13}C_6$]IAasp or

[$^{13}C_6$]IAglu. Germinated achenes were placed along the mid-line in a single band spaced at ~3 mm intervals and the plates sealed with Micropore tape (3M). These were then incubated in vertical racks in a growth chamber at 24°C under constant cool white fluorescent lights at ~100 µmol $m^{-2}s^{-1}$ for 6 days. Seedlings were collected from the plates, rinsed with sterile water, blotted dry, weighed, and frozen in liquid N_2, stored at -80°C and shipped between labs on dry ice. Samples from each independent Petri dish were homogenized in a bead mill in 65% isopropanol buffer with 0.2 M imidazole, pH 7.0 containing 1, 1.5 or 3 ng of [$^2H_4$]IAA internal standard (depending of fresh weight of the sample from each plate, which ranged from 19-57 mg). IAA was extracted from plant tissue by micro solid phase extraction using NH_2 and PMME resins, essentially as described in Liu et al. (2012). Samples were derivatized with diazomethane prior to GC-MS/MS analysis to form the IAA methyl ester, using ethereal diazomethane synthesized as described (Barkawi & Cohen, 2010; Cohen, 1984). Samples were analyzed on a Thermo Trace GC Ultra gas chromatograph with a 5 m Zebron Z-Guard GC guard column connected to a 15 m Zebron ZB5MS analytical column with a 0.25 mm diameter and 0.25 µm film thickness (Phenomenex), coupled with a Thermo TSQ Quantum XLS mass spectrometer. The GC temperature profile was set to 70°C for 1 minute, then increased by 50°C per minute to 240° and was held at 240° for 1.5 minutes. Compounds eluted from the GC column were ionized by electron ionization with an emission current of 100 µA. Selected reaction monitoring acquisition mode was used to select the molecular ions of *m/z* 189, 193, and 195 and detect quinolinium product ions of *m/z* 130, 134 and 136 of native IAA, [$^2H_4$]IAA and [$^{13}C_6$]IAA methyl esters, respectively. Quinolinium product ions were produced by collision with argon gas using a collision energy of 10 V and 1.5 mTorr collision gas pressure and detected using scan times of 0.025 s. Peak areas were calculated using Qual Browser in Xcalibur software, and were then used to determine concentration of both native IAA and [$^{13}C_6$]IAA in treated tissue by isotope dilution (Barkawi et al., 2010; Cohen et al., 1986).

IAA amino acid hydrolases in *F. vesca*

IAA amino acid hydrolase genes in the *F. vesca* 4.0 reference genome (Edger et al., 2018) were identified by homology to the protein sequences of the seven Arabidopsis hydrolase sequences (Table 2-2; LeClere et al. 2002) using BLASTp (Altschul et al., 1997) at the GDR website (Jung et al., 2014). Signal peptide predictions were made using SignalP 4.1 (Petersen et al., 2011), and protein localization predictions were made using WoLF PSORT (Horton et al., 2007). Protein sequences were aligned and phylogenetic analyses conducted using MEGA version X with Clustal alignment (Kumar et al., 2018). Gene expression values were estimated from *F. vesca* transcriptome data (Kang et al., 2013) at Strawberry Genome Resources (Darwish et al., 2013) and from *F. ×ananassa* transcriptome data (Sánchez-Sevilla et al., 2017).

Results

Identification of endogenous IAA conjugates

Because of the low levels of indolic compounds that were the target of this study, a highly sensitive and selective mass spectrometric method was required to analyze from what was essentially a crude extract. Using high resolution detection of the quinolinium ion for the detection of 3-substituted indoles, only two IAA conjugates, IAasp and IAglu, were identified in achenes from the diploid strawberry, *F. vesca* inbred line H4F7-3 (Figure 2-1). IAasp [CID 446620] was identified by the presence of a significant $[M^{+}H]$ at *m/z* 291.0878 (predicted for $C_{14}H_{15}N_2O_5$ - 291.0981) and a clear quinolinium ion at *m/z* 130.0652 (predicted *m/z* = 130.0651), in agreement with the spectrum of the IAasp standard. Similarly, IAglu [CID 25200808] was identified by its [M+H] at m/z 305.1130 (predicted for $C_{15}H_{17}N_2O_5$ - 305.1137 and the quinolinium ion at *m/z* 130.0652 (predicted *m/z* = 130.0651), in agreement with the spectrum of the IAglu standard. No other IAA conjugates within the targeted mass range were detected, indicating that these were the most abundant, and potentially the only, indolic auxin amino acid conjugates present.

Quantitative analysis of IAA and IAA conjugate levels

The ratio of free to conjugated IAA was determined in achenes by LC-MS/MS. Free IAA levels were determined by LC-MS/MS using [$^{13}C_6$]IAA as the internal standard in multiple lots of achenes harvested from *F. vesca* H4F7-3 fruit. Free IAA levels were remarkably stable across 3 biological replicates from 4 lots of achenes grown at different times, 155 ± 8 ng/g dry weight (Figure 2-2). Quantitative analysis of the IAasp and IAglu levels in H4F7-3 achenes was conducted using [$^{13}C_6$]IAasp and [$^{13}C_6$]IAglu internal standards. Spectral data were collected using LC-MS/MS as used for the identification, but measuring the peak intensity for both the labeled and native compounds. Using nine biological replicates we found 222±32 ng IAA/g for IAasp and 382±204 ng IAA/g for IAglu.

Related species and other lines of *F. vesca* had similar conjugate profiles. We looked at the 3-substituted indolic compounds in the mass range expected for IAA-amino acids in achenes in a comparative semi-quantitative study using the same high resolution LC-MS/MS methods used for identification (Figure 2-3). Here we also found only IAasp and IAglu, and although the ratio was typically about 0.5-10:1 IAsp:IAglu, and the ratio was notably different even between lots of *F. vesca* H4F7-3 which ranged from 0.6 (Figure 2-2) to 4.1 (Figure 2-3). *F. chiloensis* was notably different in having predominantly IAasp compared to IAglu, while IAglu was the predominant form in *D. indica.*

Release of free IAA from exogenous conjugates

To determine if these conjugates were simply remnants of IAA catabolism or were potentially stored conjugates for use during seedling growth, we grew germinated achenes on agar supplemented with either[$^{13}C_6$]IAasp or [$^{13}C_6$]IAglu, at the concentration used in LeClere et al. (2002) to test for inhibition of root growth. After 6 days growth, extracts of extensively rinsed seedlings contained the labeled conjugates (Figure 2-4), indicating that these compounds were taken up by the plants. In order to analyze IAA and its [$^{13}C_6$] isotopomer quantitatively by isotope dilution analysis (Barkawi et al., 2010), we used a second isotopomer, [$^{2}H_4$]IAA, as an internal standard that allowed all three isotopic forms

(unlabeled, [$^{13}C_6$], and [$^{2}H_4$]) to be detected simultaneously by GC-MS/MS (Figure 2-5). In this way the content of the seedling extracts were analyzed and quantitation of [$^{13}C_6$]IAA and unlabeled IAA was accomplished relative to the known quantity of the [$^{2}H_4$]IAA added to each sample (Figure 2-5). As shown in Figure 2-6, plants incubated with either conjugate, contained free [$^{13}C_6$]IAA released from the conjugate by apparent hydrolysis over a 6 day growth period. The level of [$^{13}C_6$]IAA in the tissues following growth on either [$^{13}C_6$]IAglu or [$^{13}C_6$]IAasp is about the same, about 4 ng/g fresh weight. A notable difference was found in the effect these supplied conjugates had on the level of endogenous free IAA in the seedlings. Where [$^{13}C_6$]IAglu appeared to have a strong suppressive effect on the accumulation of the unlabeled IAA, that effect was not as strong with [$^{13}C_6$]IAasp (Figure 2-6).

IAA-amino acid hydrolases of *F. vesca*

Six genes encoding IAA amino acid conjugate hydrolases were identified in the *F. vesca* genome by homology to those in Arabidopsis and the IAasp hydrolase identified in *Enterobacter agglomerans* (Chou et al., 1998). Each of the seven Arabidopsis hydrolase genes is specific for a small range of IAA amino acid conjugates (LeClere et al. 2002). None of the Arabidopsis hydrolases have a high degree of activity with IAasp and IAglu, in contrast to those from *Medicago truncatula* (Table 2-2). Transcriptome data for *F. vesca* (Darwish et al., 2013) and *F. ×ananassa* (Sánchez-Sevilla et al., 2017) indicate that all six strawberry hydrolase genes are expressed differentially in seedlings, leaves, and developing achenes, as well as in maturing and ripening receptacles (Supplement Figure 2-1). SignalP 4.1 (Petersen et al., 2011) identified a signal peptide in all the Arabidopsis and strawberry proteins except AtILL6. Comparison of the sequences of these proteins with 5 hydrolases from *Medicago* that are homologous to AtIAR3 (Campanella et al., 2008) places 3 of the *Medicago* (Mt) proteins in a clade with At and Fve IAR3 and ILL5 (Figure 2-7). *In silico* analysis indicated that the seven proteins in this clade localize to the ER, as do AtILL1, AtILL2, AtILR1, FveILR1 and FveILL6 (Table 2-2). All ER localized proteins except Fve ILR1 and FveILL6 have ER retention signals (KDEL, RDEL, HDEL or variants thereof) (Denecke et al., 1992). Sanchez Carranza et al. (2016) demonstrated *in vivo* that

AtILR1, AtILL2, and AtIAR3 localize to the ER, and that the variant KDEL sequence on AtILR1 (KSEL) is essential for ER localization, but the HEEL variant on ILL2 is not. The remaining Arabidopsis, strawberry, and *Medicago* hydrolases, including members of the ILL3 and ILL6 clades were predicted to localize to various cellular compartments, including the chloroplast, mitochondria, vacuole, cytoplasm, and extracellular space (Table 2-2). None of the *Arabidopsis*, *Fragaria*, or *Medicago* hydrolases group with the bacterial hydrolase (EaIAAH) or a hydrolase (MpILR1) recently identified in the genome of a liverwort, *Marchantia polymorpha* (Campanella et al. 2018) (Figure 2-7).

Discussion

The development of the strawberry fruit has long been known to be determined by auxin, which has a strong positive effect on the growth of the receptacle. Later in receptacle development, auxin levels decline, and it has been postulated that the cessation of auxin movement from achene to receptacle invokes the ripening process (Aharoni & O'Connell, 2002; Given et al., 1988). In contrast to what is known about the central importance of auxin to strawberry fruit growth which has led to strawberry becoming a model for auxin involvement in fruit development (Estrada-Johnson et al., 2017; Folta & Davis, 2006), relatively less is known about the biochemical relationships of the major auxin metabolites of IAA in strawberry. Here we applied a relatively new, high resolution LC-MS/MS method to probe the nature of the indolic auxins of the diploid strawberry achene. The Q Exactive mass spectrometer routinely delivered sub 2 ppm mass accuracy, providing the high selectivity required for the successful application of this approach.

IAA conjugated to the amino acids aspartate and glutamate are the only detectable IAA amino acid conjugates in the achene of *F. vesca* (Figure 2-1) and its close relatives (Figure 2-3). Although it is lower than the level of IAA amino acid conjugates, the level of free IAA in diploid strawberry achenes (Figure 2-2) is significantly higher than those previously reported for bioassay of *F. ×ananassa* in the classic paper by Nitsch (1955) (ranging from "0.5-5 ng/g DW") and the level reported in a recent mass spectrometric analysis by Symons et al. (2012) at 65 ng/g. The levels for IAasp and IAglu, when added

together, are well within the wide-ranging levels previously reported for IAA amide conjugates measured by hydrolysis, 100-28,000 ng/g (Dreher & Poovaiah, 1982; Archbold & Dennis, 1984, 1985). High levels in previous reports could possibly be related to the 1,100 ng/g protein bound IAA we previously reported in the achene (Park et al., 2006). However, previous quantitative studies need to be reconsidered because IAA amide conjugate levels determined using alkaline hydrolysis methods have been shown to be problematic in that hydrolysis can result in unexpected chemical conversions leading to significant overestimates of conjugate levels (Yu et al., 2015). As we demonstrate in this study, identification of the conjugates and the use of the chemically correct internal standards give results with a higher level of confidence. The conjugate data indicate significant variation between samples, perhaps reflective of the expected environmental or developmental impacts on the levels of these conjugates. The variation found is supportive of the role for conjugation in the plant's homeostatic mechanism resulting in a stable level of free IAA (Figure 2-2).

Identification of the stored conjugates of the strawberry achene as IAasp and IAglu creates an interesting quandary. It has long been postulated that stored conjugates of IAA are the precursors for auxin during early seedling growth, and in maize, the IAA-ester with *myo*-inositol was shown to have that function (Nowacki & Bandurski, 1980). A similar role was postulated for IAA-amino acid conjugates in dicots (J. D. Cohen & Bandurski, 1982). However, as noted by Sauer et al. (2013), based on work done on Arabidopsis, it is currently widely assumed that conjugation to form IAasp and IAglu is irreversible. IAasp and IAglu are thus considered to be intermediates for degradation (Kowalczyk & Sandberg, 2001; Ljung et al., 2001; Östin et al., 1998). The evidence for a single, catabolic role for these conjugates, however, lacked critical experimental testing, and, noted by Kowalczyk and Sandberg (2001), proper labeling studies to test this assumption are needed.

In their review, Korasick et al (2013) posited that the role of specific conjugates could differ among different plant species, and several previous experimental reports suggested to us that it was worth revisiting the possible role of IAasp and IAglu in strawberry. Consistent with this idea, the native conjugates in soybeans are IA-L-asp

(Cohen, 1982), IAglu (Epstein et al., 1986) and IAtrp (Yu et al., 2014). We had shown previously that IA-L-asp induced hypocotyl elongation in soybean while IA-D-asp was inactive, suggesting that the L-form was hydrolyzed (Cohen & Baldi, 1983). Thus, where IAasp is a predominant conjugate in the seed, it may have an active role as a stored IAA precursor. In another legume, *Medicago truncatula*, five genes encoding IAA-amino acid hydrolases with homology to *Arabidopsis thaliana* IAR3 were identified, four of which show their strongest hydrolase activity with IAasp as substrate (Campanella et al., 2008). Likewise, of all the amino acid conjugates tested, IAasp was hydrolyzed by PsIAR32, one of several AtIAR3 homologs found in *Picea sitchensis* (Campanella et al., 2014). A number of studies have shed light on specific aspects of the IAA amino acid hydrolase structure that defines substrate specificity. However, few of these past studies approached the issue of monocarboxylic verse dicarboxylic conjugate substrate specificity, the unresolved issue relative to understanding specific conjugate function. Nevertheless, analysis of the X-ray structure of AtILL2 highlighted Leu175 as important relative to discrimination against bulky amino acid side chains (Bitto et al. 2009). In the bacterial IAasp hydrolase, His405 was critical for activity and His404 reduced activity toward IAglu relative to IAasp (Chou et al., 2004). The truncation of *Medicago* MtIAR31/32/33/34/36 sequences increased activity toward IAasp in all cases except MtIAR33 were it significantly lowered the activity toward IAasp (Campanella et al., 2011). While it remains uncertain which specific residues direct activity toward IAasp and/or IAglu, in general, activity toward these substrates was found in the ILR3, ILR1 and ILL3 related sequences (Table 2-2).

To test the possible role of both IAasp and IAglu as potential seed auxin precursors, we grew seedlings of *F. vesca* on vertical plates containing media enriched with either [$^{13}C_6$]IAasp or [$^{13}C_6$]IAglu. As seen in Figure 2-6, both IAasp and IAglu are hydrolyzed by growing strawberry seedlings, and the supplied conjugate source provided a significant fraction of the free auxin in the seedling after 6 days of growth.

Previous studies indicated that exogenous IAA, and not other auxin-like compounds, has a negative influence on *de novo* IAA biosynthesis, strongly suggesting that IAA activates a feedback mechanism for the regulation of its own biosynthesis

(Ribnicky et al., 1996). If IAA from conjugate hydrolysis has a feedback activity on IAA biosynthesis, the IAA released from [$^{13}C_6$]IAglu showed a stronger influence on this mechanism than that seen with [$^{13}C_6$]IAasp (Figure 2-6). These results suggest that the hydrolysis of the two conjugates is perhaps occurring in different cellular compartments. Consistent with this possibility are the cellular targeting sequences and localizations predicted for the various IAA-amino acid hydrolase sequences found in *Arabidopsis*, *F. vesca*, and *Medicago* (Table 2-2). Localization predictions indicate that AtILL3 and *Medicago* (MtIAR33) homologs could be localized to the chloroplast. Recombinant MtIAR33 hydrolyzes IAasp *in vitro*, and it thus becomes important to investigate the substrate specificities of the other members of this clade as well. *Arabidopsis* and *Medicago* members of the ILL6 clade, as well as Fve IAR3 and ILL2, are also predicted to have non-ER localizations, pointing out the need for further investigation of whether, or how, localization of hydrolase activity influences growth and development.

Transcriptome data for *F. vesca* indicates that growing seedlings express *FveILL3* and *FveIAR3* (Supplement Figure 2-1) which encode proteins predicted to localize in different cellular compartments: the chloroplast and endoplasmic reticulum, respectively. IAA amino acid conjugate hydrolase genes are also expressed in the 6-7 day old *F. vesca* embryo, where it may be particularly important to maintain auxin homeostasis. More complex patterns of expression of these hydrolase genes are found in the receptacle, where during the early stages of development both the cortex and pith would require free IAA for rapid growth. This pattern was also found in transcriptome data from the octoploid strawberry receptacle (Sánchez-Sevilla et al., 2017). The pattern of hydrolase expression in the octoploid achene appears consistent with ripening of the achene, the true fruit, being complete by the time the receptacle begins to ripen. Although complex the expression data illustrates the dynamic nature of the processes involved in auxin metabolism in plants, in which various conjugates may play different roles in different families of plant.

Table 2-1: Plant materials used in this study

Plant	Abbreviation or identifier	Ploidy level	Source	Accession Number
F. vesca (Fve): Yellow Wonder	YW	Diploid	Johnny's Seed[a]	
Fve Yellow Wonder F7 inbred line[b]	YW5AF7	Diploid	NCGR Corvallis[c]	PI641092
Hawaii 4 inbred line	H4F7-3	Diploid	NCGR Corvallis	PI664444
Baron Solemacher inbred line	BSF7	Diploid	NCGR Corvallis	PI551507
Fve subspecies americana	Pawtuckaway	Diploid	NCGR Corvallis	PI657856
F. iinumae	J-17	Diploid	NCGR Corvallis	CFRA1855
F. virginiana	LH50-4	Octoploid	NCGR Corvallis	PI612495
F. chiloensis		Octoploid	NCGR Corvallis	PI612317
F. ×ananassa	(seedling from Family 825)	Octoploid	Adam Dale, University of Guelph	
Duchesnea indica		Unknown	Collected in Maryland USA	

[a]Johnny's Selected Seeds, Winslow, ME
[b]Slovin et al. (2009)
[c]USDA-ARS National Clonal Germplasm Repository, Corvallis, Oregon

Table 2-2: IAA conjugate hydrolase genes in *Arabidopsis thaliana* (At), *Fragaria vesca* (Fve), and *Medicago truncatula*

Gene ID	Signal Peptide (Signal P 4.1)	WoLF PSORT prediction[a]	KDEL, RDEL, etc	Expressed in Seedlings[b]	Expressed in immature seed[b]	At, Mt, or Fve locus	Fve gene#	Known IAA conjugated substrates[c,d]
AtIAR3	Yes	ER[e]	KDEL	Yes	Yes	At1g51760		Ala, Leu (Asn, Cys, **Glu**, Gly, Met, Ser)
FveIAR3	Yes	Chloro	RDEL	Yes	Yes	FvH4_1g06730	gene11364	
MtIAR31	Yes	ER	HDEL			11427153		**Asp** (Val)
MtIAR32	Yes	ER	HDEL			11441985		**Asp** (Ala, Gly, Phe)
MtIAR34	Yes	ER	HDEL			25500386		**Asp** (Leu, Ala, Gly, Val)
AtILR1	Yes	ERe	KSEL		Yes	At3g02875		Ala, **Asp**, Gln, **Glu**, Leu, Met, Phe, Tyr, (Gly, Thr)
FveILR1	Yes	Extra, ER	No		Yes	FvH4_6g19700	gene15613	
AtILL1	Yes	ER	HDEL	Yes	Yes	At5g56650		Ala, Asn, Tyr
AtILL2	Yes	ER[e], Extra, Vac	HEEL	Yes	Yes	At5g56660		Ala, Leu, Met, Phe, Ser, Thr, Tyr, Val, (Asn, Gly, His, **Asp**, Cys, Gln, **Glu**, Ile)
FveILL2	Yes	Chloro	No			FvH4_4g35100	gene00715	
AtILL3	Yes	Chloro, cyto	No	Yes	Yes	At5g54140		
FveILL3	Yes	Extra, chloro, mito	No	Yes		FvH4_7g33070	gene12442	
MtIAR33	Yes	Extra	No			11440453		**Asp** (Gly, Ala)
AtILL5	Yes	ER	KDEL	Yes	Yes	At1g51780		
FveILL5	Yes	ER	RDEL	Yes	Yes	FvH4_6g32830	gene23127	

AtILL6	No	Chloro	No	Yes	Yes	At1g44350		
FveILL6	Yes	Extra, ER	No	Yes		FvH4_2g27160	gene11194	
MtIAR36	Yes	Vac	No			11414033		Gly (Ile, Ala)

A compilation of information currently available for the 7 *Arabidopsis thaliana*, the 6 *Fragaria vesca*, and 5 *Medicago truncatula* IAA amino acid conjugate hydrolases. Genes are grouped according to clades predicted in Figure 2-7. *In silico* predictions of the presence of a signal peptide and the cellular localization of the protein were made using SignalP 4.1 (Petersen et al., 2011) and WoLF PSORT (Horton et al., 2007). The presence of a validated (Denecke et al., 1992; Sanchez Carranza et al., 2016) or variant endoplasmic reticulum retention signal at the carboxyl terminus of the protein is indicated by KDEL, RDEL etc. Where possible, the expression of a given gene in seedlings or young developing seeds as indicated on an efp Browser is indicated as "yes". Fve gene# refers to the number given each gene in the *F. vesca* genome v. 1 (Shulaev et al., 2011)

[a]Chloro=chloroplast/plastid; Cyto=cytoplasm; ER=endoplasmic reticulum; Extra=extracellular matrix; Mito=mitochondria; Vac=vacuole

[b]*Arabidopsis thaliana* expression based on data at: http://bar.utoronto.ca/efp2/Arabidopsis/Arabidopsis_eFPBrowser2.html, *Fragaria vesca* expression data is from http://bioinformatics.towson.edu/strawberry/

[c]LeClere et al. (2002), Campanella et al. (2011), Sanchez Carranza et al. (2016)

[d]Minor activities are indicated in parentheses

[e]Localized *in vivo* to the ER (Sanchez Carranza et al., 2016)

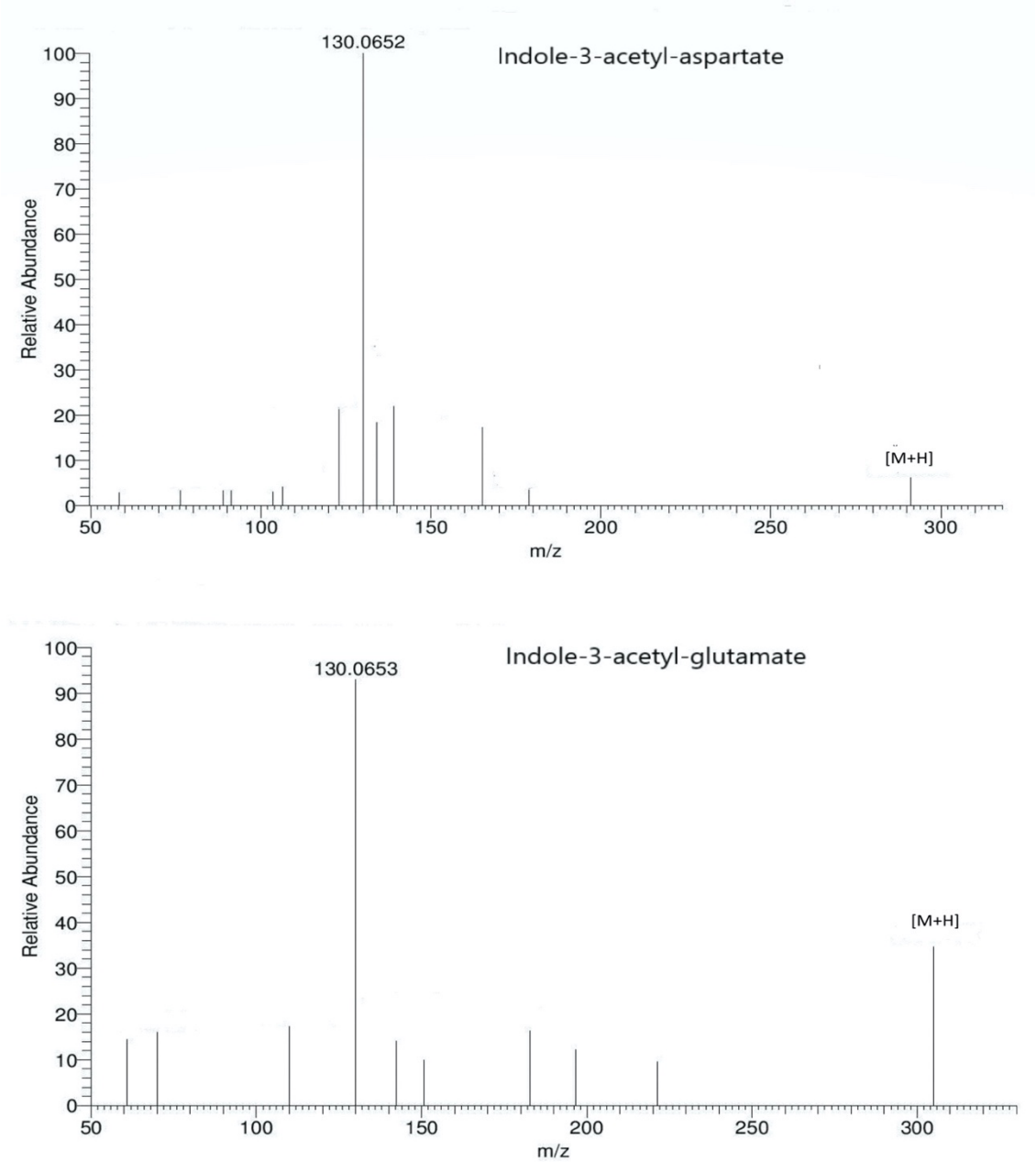

Figure 2-1: Mass spectra for IAasp (upper panel) and IAglu (lower panel) from *F. vesca* mature achenes using high sensitivity/high resolution LC-MS/MS which allows target analysis of all 3-substituted low molecular weight indole compounds without major prior assumptions about their chemical structures. IAasp was identified by the presence of a significant [M+H] at *m/z* 291.0878 and a clear quinolinium ion at *m/z* 130.0652, in agreement with the spectrum of the IAasp standard (not shown). Similarly, IAglu was identified by its [M+H] at *m/z* 305.0186 and the quinolinium ion at *m/z* 130.0652, also in agreement with the known standard (not shown)

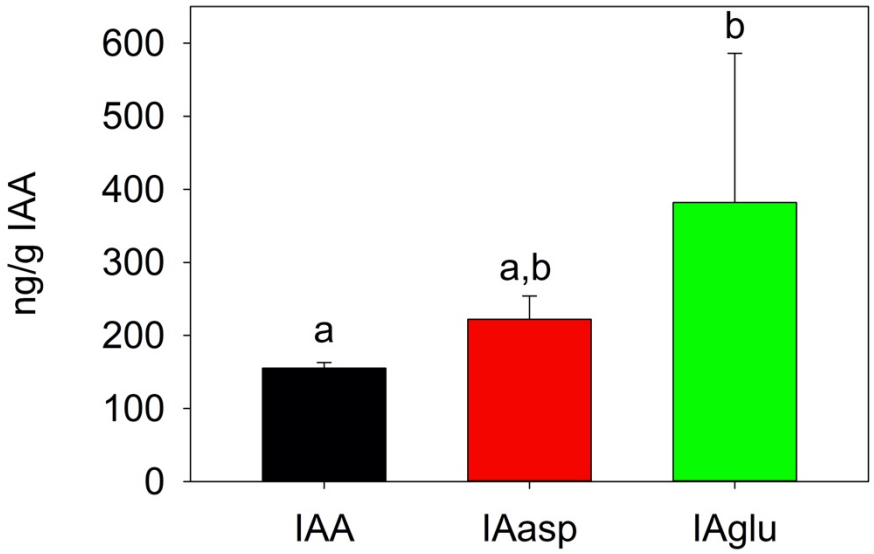

Figure 2-2: Levels of free IAA and of IAasp and IAglu measured by isotope dilution analysis LC-MS using [$^{13}C_6$]-labeled internal standards. Values for the conjugates were obtained from nine biological replicates from a single harvest of achenes while the free IAA levels represent 3 biological replicates from each of 4 individual harvests. As discussed in the text, the high variation in conjugate levels and the stability of the free IAA levels may suggest an active regulatory role for conjugate metabolism within the achene. Different letters above error bars indicate a significant difference (Tukey HSD, $P < 0.05$)

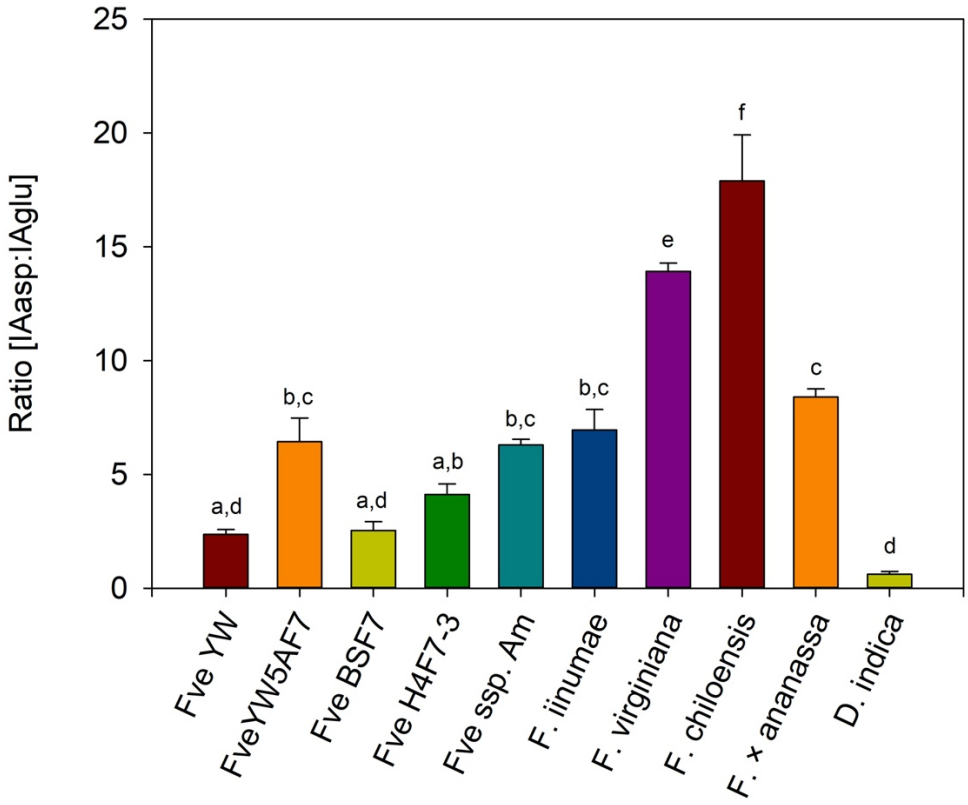

Figure 2-3: The ratio of peak abundance values for IAasp to IAglu for achenes from different lines of *F. vesca* and related species as determined by high resolution LC-MS/MS analysis. IAasp is the dominant chemical form in all species except for *D. indica*, where the apparent abundance is similar for both IAasp and IAglu. Different letters above error bars indicate a significant difference (Tukey HSD, $P < 0.05$)

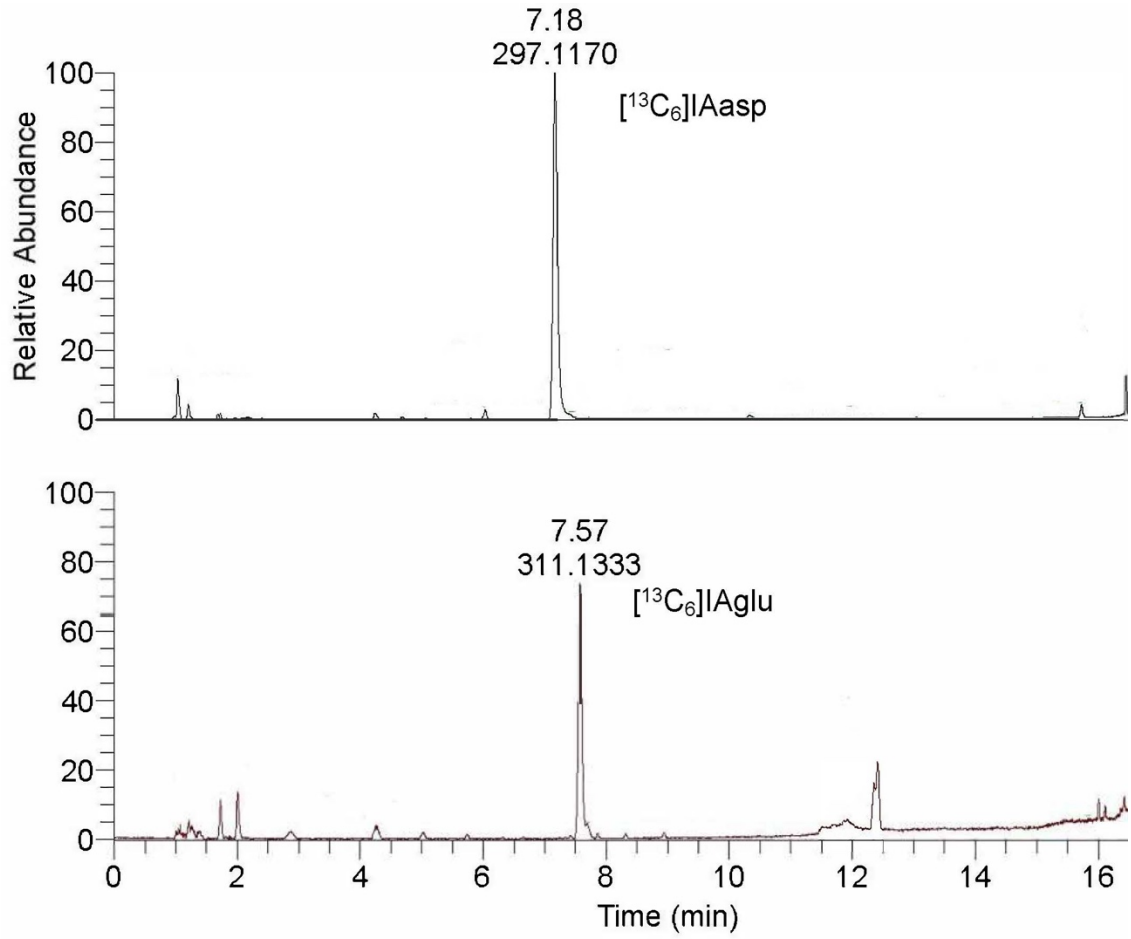

Figure 2-4: High resolution LC-MS/MS analysis confirms that *F. vesca* seedlings take up stable isotope labeled IAasp and IAglu from the medium during six days growth as seen with reconstructed ion chromatograms showing the molecular ions for [$^{13}C_6$]IAasp at *m/z* 297.1170 (upper chromatogram) and [$^{13}C_6$]IAglu at *m/z* 311.1333 (lower chromatogram)

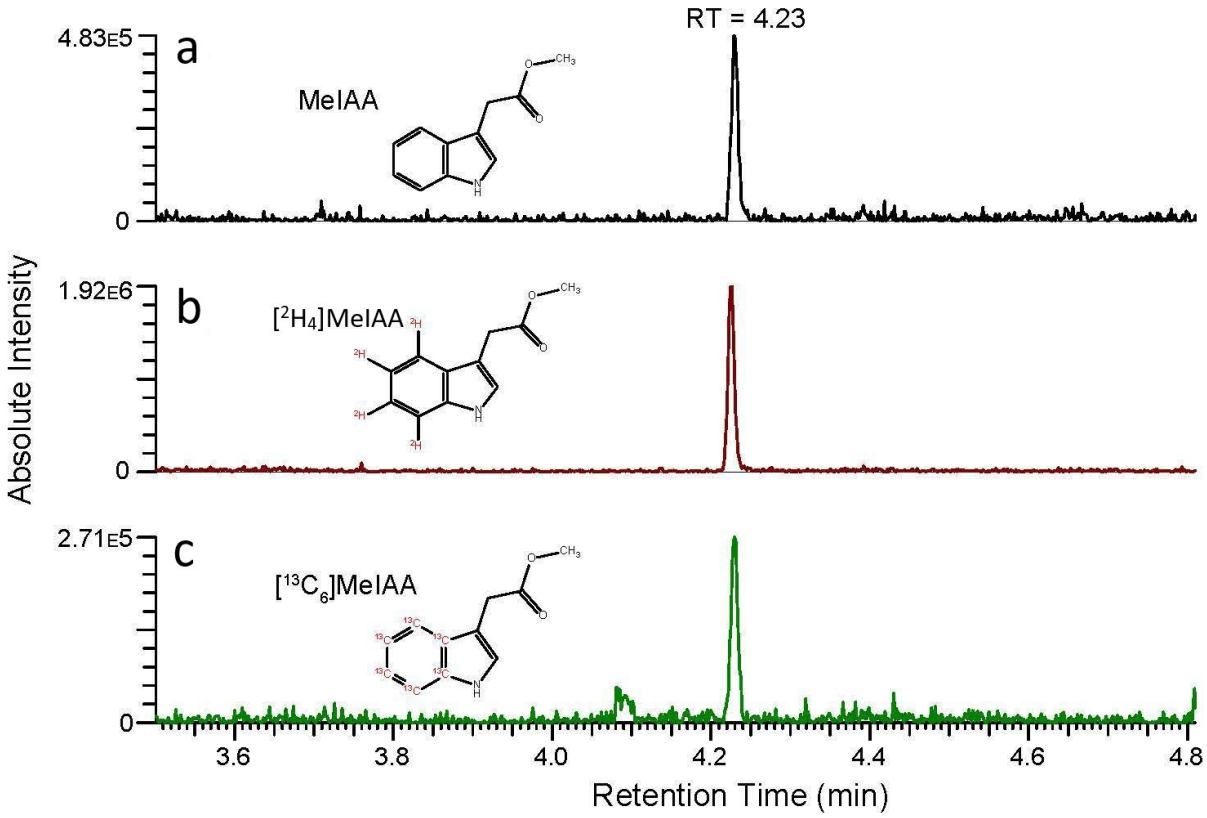

Figure 2-5: Selected Reaction Monitoring (SRM) ion chromatograms showing the quinolinium product ions of *m/z* 130, 134 and 136 of methyl esters of native IAA (a), [$^2H_4$]IAA (b) and [$^{13}C_6$]IAA (c). The quinolinium ions were detected after selection of their molecular ions at *m/z* 189, 193, and 195 followed by collision of the molecular ions with argon gas using a collision energy of 10 V and 1.5 mTorr collision gas pressure. This scheme allowed calculation of the quantity of both IAA and [$^{13}C_6$]IAA in the plant material by isotope dilution analysis using [$^2H_4$]IAA as the quantitative internal standard

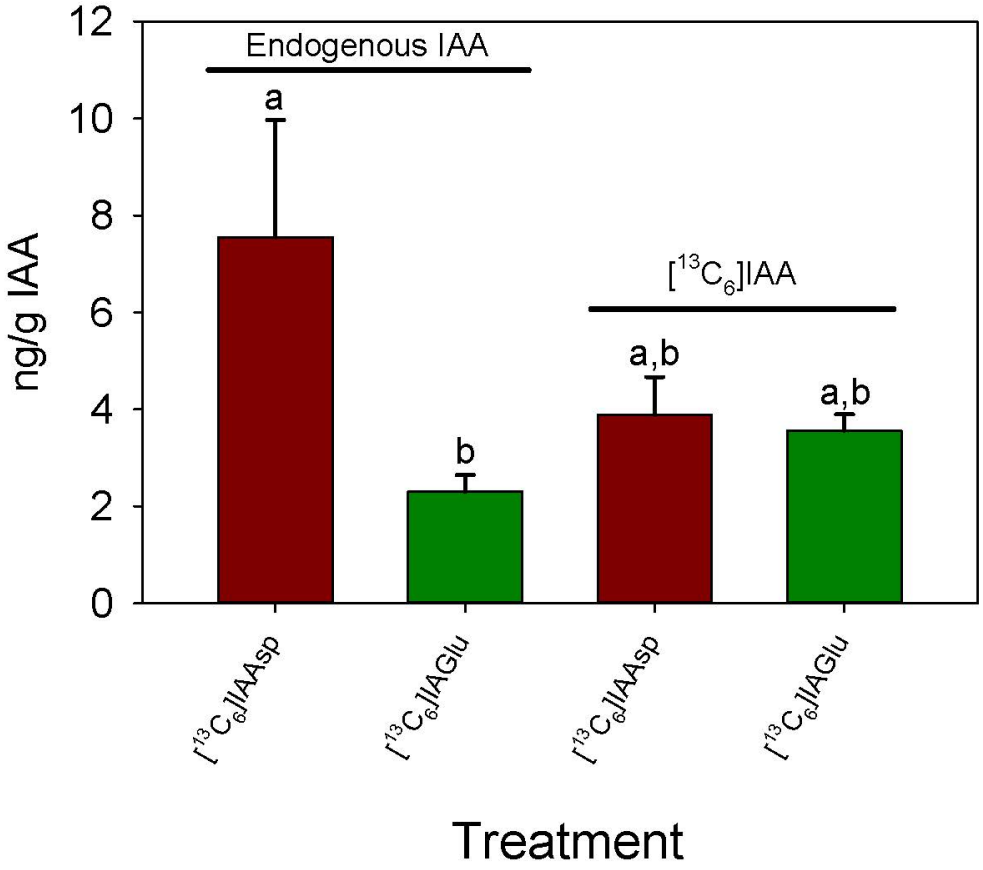

Figure 2-6: Isotope dilution quantitative analysis of native IAA and [$^{13}C_6$]IAA from *F. vesca* seedlings after 6 days growth on half strength Murashige and Skoog medium containing 40 µM of either [$^{13}C_6$]IAasp or [$^{13}C_6$]IAglu. Seedling samples were homogenized with buffered 2-propanol cantianing [$^{2}H_4$]IAA as the internal standard (1, 1.5 or 3 ng, depending of fresh weight of the sample from each plate, which ranged from 19-57 mg). This allowed calculation of the quantity of both IAA and [$^{13}C_6$]IAA, released by metabolic hydrolysis of the supplied conjugate, in the plant material. Different letters above error bars indicate a significant difference (Tukey HSD, $P < 0.05$)

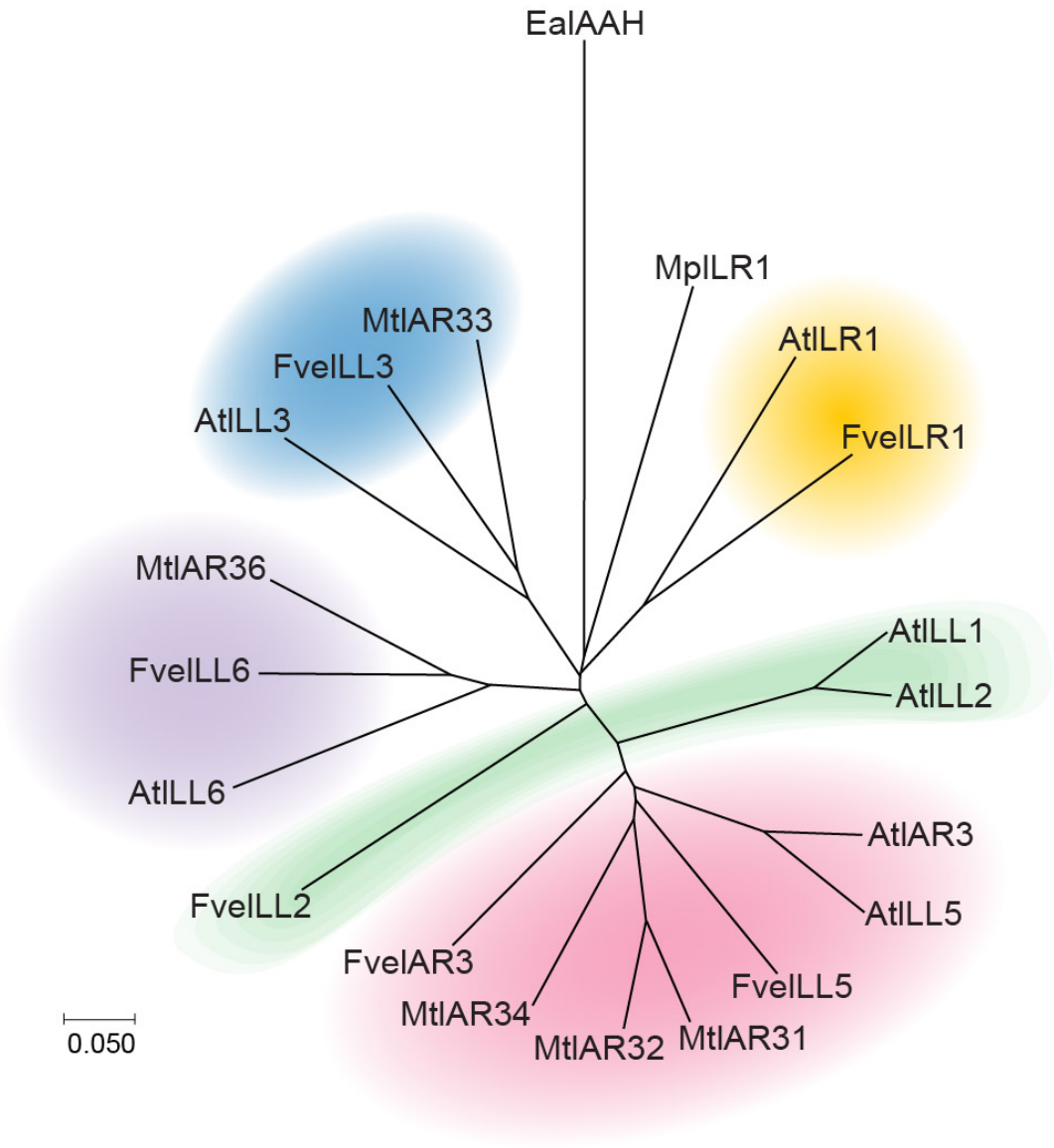

Figure 2-7: Evolutionary analysis of IAA amino acid conjugate hydrolases from *Arabidopsis thaliana* (At), *Fragaria vesca* (Fve), *Medicago truncatula* (Mt), *Marchantia polymorpha* (Mp), and *Enterobacter agglomerans* were conducted in MEGA X (Kumar et al., 2018). Sequences were aligned using Muscle in MEGA X and the evolutionary history, unrooted, inferred using the Neighbor-Joining method (Saitou & Nei, 1987). The tree is drawn to scale, with branch lengths in the same units as those of the evolutionary distances used to infer the phylogenetic tree. The evolutionary distances are in the units of the number of amino acid differences per site.

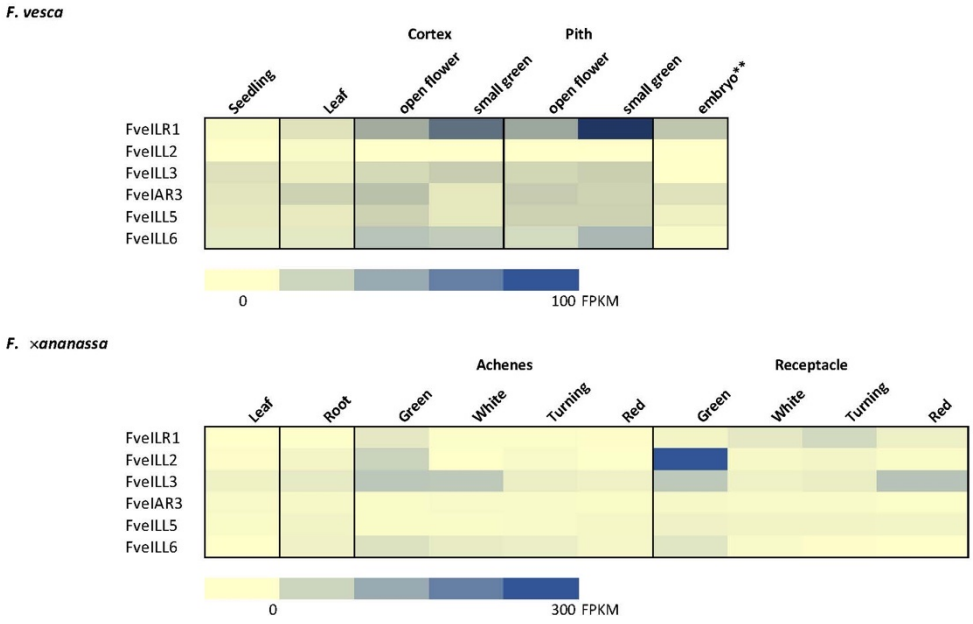

Supplement Figure 2-1: Expression of *Fragaria* homologs of Arabidopsis IAA-amino acid conjugate hydrolases estimated from *F. vesca* transcriptome data at SGR: Strawberry Genomic Resources, and *F. ×ananassa* transcriptome data in Sánchez-Sevilla et al. (2017)

Heat maps show that hydrolase genes identified in the *F. vesca* genome (Edger et al., 2018) are expressed in seedlings, leaves and roots, and that several of these genes are expressed in young receptacles of both species (cortex and pith for *F. vesca* and receptacles of *F. ×ananassa*). Hydrolases are also expressed in the achenes, the true fruits, which contain the embryo (data shown for 6-7 days after pollenation for *F. vesca*). These heatmaps are not meant to show quantitation of gene expression but to illustrate the dynamic nature of the processes involved in auxin metabolism. Color intensity represents the reported FPKM of each gene for the tissue.

Chapter 3. Analytical methods for visualizing the indolic precursor network leading to auxin biosynthesis

Introduction[2]

Plant life is characterized by strictly regulated developmental events that achieve optimum growth and reproduction. This is accomplished through an extremely complex hormonal signaling network in which the plant growth hormone auxin plays a central and defining role. To this end, auxin helps regulate almost all aspects of plant growth and development including embryogenesis, tissue architecture and tropic responses (Tivendale et al., 2014). Maintenance of auxin homeostasis involves multiple pathways for the biosynthesis of indole-3-acetic acid (IAA), the principal auxin in plants, and several regulatory pathways as well as subsequent catabolic events. These additional input/output processes include conjugation and hydrolysis of sugar and cyclitol conjugates, amino acid, peptide and protein conjugates, formation and β-oxidation of indole-3-butyric acid as well as deactivation by ring oxidation of IAA and its amino acid conjugates (Cooke et al., 2002). Nevertheless, how much IAA is made and accumulates remains the critical regulatory event in many aspects of plant development (Tivendale & Cohen, 2015).

Although several biosynthetic pathways for the bioactive auxin IAA have been proposed, many of them have not been well defined and flux information is largely lacking (Figure 3-1). The predominant biosynthetic route to IAA in *Arabidopsis thaliana* is widely believed to be through the YUCCA pathway, in which the amino acid tryptophan (Trp) is converted to indole-3-pyruvic acid (IPyA), which is then converted to IAA by YUCCA flavin monooxygenase enzymes (Mashiguchi et al., 2011). Species-specific evidence for the synthesis of IAA from Trp through indole-3-acetaldoxime (IAOx), which is converted to indole-3-acetamide (IAM) and sometimes an indole-3-acetonitrile (IAN) intermediate has been shown in *Arabidopsis* (Sugawara et al., 2009). Other potential intermediates of

[2]Tillmann, Tang & Cohen, 2021

IAA synthesis downstream of Trp have been proposed, such as indole-3-acetaldehyde (IAAld) (Rajagopal, 1971) and tryptamine (TAM) (Quittenden et al., 2009), though their places within the web of auxin biosynthesis have not been well detailed. A Trp-independent route has also been proposed based on tryptophan synthase mutants, metabolic flux analysis and *in vitro* analyses, in which indole or another upstream compound serves as the IAA precursor (Östin et al., 1999; Tivendale et al., 2014); however, unbound chemical intermediates, if they are involved in this pathway, have as yet not been identified (Nonhebel, 2015). The purpose of this protocol is to describe improved techniques for characterization of the auxin metabolic network utilizing recently discovered chemical inhibitors and technical advances in mass spectrometry (Figure 3-2). These tools will allow researchers to characterize auxin biosynthesis during specific developmental events or environmental responses.

Metabolic inhibitor approaches are complementary to genetic and biochemical studies and are particularly useful in studying IAA biosynthesis. While auxin biosynthesis mutants may have severe developmental defects that alter growth and confound comparisons to wild type plants (Cheng et al., 2007), biosynthetic reactions can be turned off at specific developmental time points with chemical inhibitors. Additionally, genetic redundancy can be overcome by inhibiting an entire enzyme family with a single chemical treatment (Fukui & Hayashi, 2018). Such is the case with inhibitors targeting both steps in the YUCCA pathway. The YUCCA enzymes are encoded by multiple genes in *Arabidopsis thaliana* and mutations in small sets of these genes encoding the flavin monooxygenase proteins results in significant morphological defects. A number of chemical inhibitors have been developed to inhibit the YUCCA pathway of auxin biosynthesis (Table 3-1), providing valuable tools to study the function of this pathway in different plant tissues and environmental conditions. Similarly, TAA1/TAR/ISS1/VAS1 (Tryptophan Aminotransferase of Arabidopsis 1/ Tryptophan Aminotransferase Related/ Indole Severe Sensitive 1 and reversal of sav3 phenotype 1) form a set of enzymes with overlapping biochemical functions that catalyze the penultimate step in the IPyA pathway (Pieck et al., 2015). Alternative aromatic amino acid substrates, such as L-kynurenine, can act as

competitive inhibitors of tryptophan aminotransferase and a series of potent inhibitors have been developed to pyridoxal phosphate-dependent enzymes with enhanced specificity to TAA1 and related enzymes ("pyruvamines"; see Table 3-1) (Narukawa-Nara et al., 2016).

The issues of redundancy with tryptophan synthase (TS) are a bit different. *Arabidopsis* and maize have two copies of the genes that encode each of the two proteins that form the αββα heterodimeric complex that catalyzes the formation of tryptophan from indole-glycerol-phosphate and serine in the plastids. In addition, maize has genes BX1 and IGL for TSα-like cytosolic enzymes that serve as sources of free indole. Arabidopsis also has a cytosolic TSα-like enzyme encoded by the indole synthase (INS) gene. TS is, however, a well-researched and highly conserved bi-enzyme complex (Watkins-Dulaney et al., 2020) such that inhibitors are available (Table 3-1) that target specifically TSα, TSβ as well as the 25-Å long tunnel to the β-subunit where indole diffuses in order to participate in the TSβ pyridoxal 5'-phosphate-mediated β-addition reaction with serine. Determining the possibility of a tryptophan-independent pathway is largely dependent on having Trp auxotroph mutants, which are difficult to obtain due to redundancy of Trp synthase genes and the fact that mutations in both copies of TSβ are seedling lethal. The protocols described here largely overcome these issues by employing chemical inhibitors, and can complement genetic studies.

Mass spectrometry (MS) has historically been and continues to be an important technique in deciphering routes of auxin biosynthesis, enabling accurate quantitation of IAA and its precursors, identification of intermediates, and tracking of isotopic labels through distinct pathways. Quantitative methods for IAA and precursor analysis by MS have been invaluable tools in elucidating auxin biosynthesis pathways and have continuously evolved over time with advances in analytical sensitivity and resolution (Liu et al., 2012; Ljung et al., 2005; Novák et al., 2012; Tivendale & Cohen, 2015). Stable isotope tracing experiments also lend insight into auxin biosynthesis when plant tissue is supplied with one or more labeled precursors, such as indole and/or anthranilate, and label incorporation into suspected downstream intermediates is monitored to determine whether synthesis from the labeled precursor has occurred. This approach can also provide

information regarding direction of flow and flux through different steps (Sugawara et al., 2009). Additionally, labeled precursors that are unique to one pathway in particular can be applied to measure contributions of a specific pathway to the IAA pool (Erdmann & Schiewer, 1971; Mashiguchi et al., 2011).

Results and Discussion

In this paper, we describe methods utilizing metabolic inhibitors coupled with a modified approach of isotope dilution/tracing and using liquid chromatography–high resolution-mass spectrometry (LC-HR-MS) for qualitative and quantitative analysis of a comprehensive set of IAA precursors and IAA itself to characterize auxin biosynthesis in *Arabidopsis* (see Supplement Figure 3-1). A distinct advantage of this method is its ability to resolve potential precursor compounds by chromatographic retention, absolute mass and by elemental composition, enabling complex mixtures of different stable isotopes (for example, multiple labeled compounds with ^{13}C and ^{15}N can be resolved) to be used in the experimental procedures (see Supplement Figure 3-2). Readers may also consult a complementary paper that was published while this manuscript was in preparation (Soeno et al., 2021). Growing seedlings on fully ^{15}N-labeled media as described here enables accurate quantitation of biosynthetic intermediates by reverse isotope dilution, using unlabeled internal standards which are typically more readily available than isotopically labeled standards (Bloch & Anker, 1948). The addition of one or more ^{15}N atoms at mass addition of 0.9970 can be resolved from the more abundant natural occurrence of ^{13}C, which is 1.0034 heavier than ^{12}C, which improves the utility of this approach when using high resolution analysis. Seedlings are first germinated on nylon mesh and are easily transferred onto media containing chemical treatments at the desired developmental time point. Next, stable isotope-labeled precursor compounds are fed to the plant. Labeled serine is used as a tracer for Trp-dependent biosynthesis specifically (Erdmann & Schiewer, 1971), while labeled indole and anthranilate can feed into both Trp-dependent and Trp-independent pathways (Pieck et al., 2015) (Figure 3-1). The techniques described here offer several advantages over previously described methods in their ease of preparation, high level of sensitivity, capacity for monitoring many compounds at once (see Supplement

Figure 3-2), and the ability of high resolution analysis to distinguish between different 'heavy' atoms, as might be required with [$^{13}C_1$]IAA and [$^{15}N_1$]IAA labeling products As shown in Supplement Figure 3-1, the use of multiple labels makes it easy to see that the addition of the tryptophan monooxygenase inhibitor YDF increases the incorporation of labeled indole into IAA but decreases labeling from labeled anthranilate and to a lesser degree from labeled tryptophan. Furthermore, this IAA labeling pattern for labeled indole and anthranilate is not reflected in any of the proposed intermediates following YDF treatment.

We also describe a technique for identifying novel intermediates based on the characteristic quinolinium ion produced from MS fragmentation of 3-substituted indolic compounds. This method involves using a series of injections of the same sample with increasingly narrow mass ranges, similar to the methods utilized by Yu et al. (2014) and Tang et al. (2019) where they targeted and identified novel indolic compounds. By monitoring exact masses of [$^{13}C_8$, $^{15}N_1$]- and [$^{15}N_1$]quinolinium ions after treatment with [$^{13}C_8$, $^{15}N_1$]- and [$^{15}N_1$]indole, this method can identify unknown compounds synthesized downstream from indole. A similar approach would likely be applicable in investigations of other classes of compounds that form characteristic signature ions. High resolution accurate mass analysis significantly reduces factors such as false negative molecular ions, low abundance ions, multiple isomers, and matrix effects, which otherwise would make it difficult to confirm possible compound identities.

Materials and Methods

Materials

Growing, labeling, and collecting plant material

Wild-type Columbia-0 ecotype *Arabidopsis thaliana* seeds or specific metabolic mutant lines need to be surface sterilized sodium hypochlorite then imbibed for 5-10 days at 4°C

to promote uniform germination. Typically seeds would be sown in a single row onto 20 μm nylon mesh covering the agar growth medium.

- 20 μm nylon mesh (Sefar, 03-20/14), cut into 9 cm × 9 cm squares and autoclave sterilized with 45 minute sterilization time at 121°C
- Sterile deionized water
- Forceps, flame sterilized
- 10 cm × 10 cm square Petri dishes (Fisherbrand, FB0875711A)
- Dilute bleach solution for seed sterilization: 20 mL concentrated regular liquid bleach (Clorox), 80 mL deionized water, 20 μL Tween 80 (Sigma-Aldrich, P1754)
- Plant growth medium: *Arabidopsis thaliana* salts (ATS)
- KimWipes delicate task wipes (Kimberly-Clark, KC34155EXL)
- 1.5 mL microcentrifuge tubes (Fisherbrand, 05-408-129)
- Liquid nitrogen
- Dry ice
- One or more isotopically labeled precursor solutions in aqueous ATS salts (see Notes 1 and 2; see Table 3-2 for description of example labeling strategies):
    - 3 mM [$^{13}C_3$]L-serine (Cambridge Isotope Laboratories, CLM-1574-H)
    - 500 μM [$^{13}C_6$]anthranilate (Sigma-Aldrich,709530)
    - 500 μM [$^{15}N_1$]indole (Cambridge Isotope Laboratories, NLM-792)
    - 500 μM [$^{13}C_8$, $^{15}N_1$]indole (Cambridge Isotope Laboratories, CNLM-4786-0)

Homogenization and extraction

Plant tissue samples, typically 20-50 mg, are homogenized for 4 min using a bead mill with three stainless steel balls and 40-100 μL of the extraction buffer/solvent.

- Tissue homogenizer (Retsch MM300)
- Microcentrifuge, temperature controlled at 4°C
- Repeater pipette (Eppendorf M4)
- Homogenization buffer: 65% isopropanol, 35% 0.2 M imidazole (pH 7.0), 100 mM methoxyamine hydrochloride (CH_3ONH_2·HCl) (Sigma-Aldrich, 226904) for targeted

analysis of IAA and biosynthesis intermediates (see Note 3); 50% isopropanol for analysis of unknown indolic compounds

  - For absolute quantitation, stable isotope internal standard is added into homogenization buffer. The amount of internal standard added to each sample should be similar to the amount of endogenous compound in the plant tissue (*see* Notes 4 and 5)

- Stainless steel beads for homogenization (1.6 mm diameter, Next Advance, SSB16)
- 2 mL screwcap tubes (Fisherbrand, 02-681-343)
- 10-200 µL Empty TopTips (Glygen, TT2EMT) and adaptors provided by Glygen for centrifugation
- Vacuum concentrator (SpeedVac, Savant)
- Additional materials required for specified extraction techniques are described in the sections below:

IAA extraction

Homogenized samples are incubated on ice for 50 minutes to allow isotopic standard equilibration with the endogenous IAA. They are then diluted 10-fold with water such that ion exchange will be effective, centrifuged to remove solid materials, and loaded onto two consecutive SPE micro spin column (TopTips) steps, first ion exchange on an amino phase and then on an epoxide support.

  - Bondesil-NH_2 resin (Agilent, 12213020) suspended in water, 1:4 w:v
  - IAA extraction solvents and solutions as described by Liu et al. (2012): hexane, acetonitrile, ethyl acetate, methanol, 0.2 M imidazole (pH 7.0), distilled water, 0.25% phosphoric acid (PA), 0.1 M succinic acid (SA, pH 6.0), 5:1 PA:SA solution
  - Macro-prep epoxide support resin (Bio-Rad, 156-0000), suspended in 0.1 M sodium bicarbonate (pH 7.0), 1:4 w:v

Extraction of proposed IAA biosynthesis intermediates: Anthranilate, Ser, IAAld, IPyA, IAOx, IAN, IAM, indole

Homogenized samples are incubated on ice for 50 minutes to allow isotopic standard equilibration with the endogenous compounds, diluted 10-fold with water to allow proper interaction with the solid phase, centrifuged to remove solids, and loaded onto a SPE micro spin column (TopTips) containing hydrophilic-lipophilic balanced (HLB) resin conditioned with acetonitrile followed by 20% acetonitrile in water. After loading, the spin columns are washed with 5% acetonitrile and compounds are eluted with 80% acetonitrile.

- RENSA HLB resin (MIP Technologies, 92001-0010) suspended in methanol, 1:5 w:v
- Acetonitrile: 100%, 80%, 20%, and 5% prepared in distilled water

Indole extraction

Indole is a very lipophilic and somewhat volatile compound that cannot be purified using the techniques used for the other compounds. Thus, its purification involves a simple solvent partitioning. It was important to select an apolar solvent with a boiling point below the melting point of indole. We found pentane to be well-suited as its boiling point is 36.0°C, well below the indole melting point of 52.5°C.

- Pentane

LC-MS analysis

UPLC utilizes a column with an end-capped octadecylsilane fully porous 1.8 µm silica resin with high carbon loading (20%) in order to obtain highest sensitivity for indolic compounds (see Supplement Figure 3-2).

- Amber autosampler vials (ChromTech, 404810) with 50 µL glass inserts (ChromTech, CTI-2405)
- Liquid chromatograph/mass spectrometer system: Dionex UltiMate 3000 UHPLC, Q Exactive mass spectrometer, Xcalibur software (Thermo Scientific)
- C_{18} HPLC column, 50 × 2.1 mm (Force, 9634252, Restek) with 0.2 µm precolumn filter (UltraShield, 25809, Restek)
- Mobile phase: A, 0.1% formic acid in water; B, 0.1% formic acid in acetonitrile. Different LC-MS methods are used to target compounds of interest:

- IAA analysis: Mobile phase gradient of 5% B (-1-0 min), 5-20% B (0-3 min), 20-80% B (3-6 min), 80% B (6-6.5 min) at a flow rate of 0.4 mL•min^{-1}. Mass spectra are collected in positive ion mode in a parallel reaction monitoring (PRM) scan and the inclusion list contains ions of 176, 177, 178, and 182 *m/z*. PRM resolution is 17500 full width at half maximum (FWHM), automatic gain control (AGC) target is 2×10^5, maximum ionization time is 50 milliseconds (ms), isolation window is 2.0 *m/z*, and normalized collision energy (NCE) is 20. Ion source conditions are: spray voltage: 4.00 kV, capillary temperature: 275°C, probe heater temperature: 300°C, sheath gas: 30 arbitrary units, aux gas: 20 arbitrary units, S-lens RF level: 50.
- For analysis of all the listed intermediates except indole, inject 5-10 µL plant extract into the LC system with the following mobile phase gradient: 5% B (-2-1 min), 5-15% B (1-3 min), 15-30% B (3-3.5 min), 30% B (3.5-5 min), 30-39% B (5-7.5 min), 39-80% B (7.5-8 min), 80% B (8-8.5 min) at a flow rate of 0.4 mL•min^{-1}. Mass spectra are collected in selected ion monitoring (SIM) mode. SIM resolution is 70,000 FWHM with maximum ionization time of 200 ms and AGC of 5×10^5. Ion source conditions are: spray voltage: 4.00 kV, capillary temperature: 275°C, probe heater temperature: 300°C, sheath gas: 30 arbitrary units, aux gas: 20 arbitrary units, S-lens RF level: 50. MS is set to acquire several segments of full scans each targeting 1-3 compounds. The segments are: 200-217 *m/z* (0-2.1 min), 157-173 *m/z* (2.1-3 min), 133-150 *m/z* (3-3.74 min), 170-188 *m/z* (3.74-5.4 min), 152-170 *m/z* (5.4-6 min), 227-245 *m/z* (6-6.7 min), 184-201 *m/z* (6.7-8.5 min).
- For indole analysis, 5-10 µL plant extract is injected with the following LC mobile phase gradient: 5% B (-1-1 min), 5-30% B (1-3 min), 30-39% B (3-5.5 min), 39-80% B (5.5-6.5 min), 80% B (6.5-7 min) at a flow rate of 0.4 mL•min^{-1}. Mass spectra are collected in SIM mode using a mass range of 110-132 *m/z*. SIM resolution is 70,000 FWHM with maximum ionization time of 200 ms and AGC of 5×10^5. Ion source conditions are: spray voltage: 4.00 kV, capillary

temperature: 275°C, probe heater temperature: 300°C, sheath gas: 30 arbitrary units, aux gas: 20 arbitrary units, S-lens RF level: 50.

- For analysis of compounds labeled by treatment with [$^{15}N_1$]- and [$^{13}C_8$, $^{15}N_1$]indole, multiple injections of the same sample are made using a series of methods (A-D, described below) with different MS parameters. The same mobile phase gradient is used with each method: 5% B (-2-2 min), 5-50% B (2-8 min), 50-85% B (8-10 min), 80% B (10-12 min) at a flow rate of 0.4 mL•min^{-1}.
  - Method A: Scan groups consist of one full MS-SIM scan followed by four PRM scans. For the SIM scan, Orbitrap resolution is 70,000 full width at half maximum (FWHM) with maximum ionization time of 200 ms, automatic gain control (AGC) target of 5×10^5, and scan range of 100-400 *m/z*. For the PRM scans, FWHM resolution is set to 17,500, maximum ionization time is 100 ms, AGC target is 2×10^5, normalized collision energy (NCE) is 35, and isolation window is 20 *m/z.* Four variations of this method (used in four separate injections) with different values in the inclusion list are used to cover a range of *m/z* values for potential compounds of interest:
    a) Method A.1: The inclusion list contains *m/z* values beginning at 130 and increasing by increments of 20 to 290 (130, 150, 170,… 250, 270, 290 *m/z*)
    b) A.2: *m/z* values begin at 140 and increase by increments of 20 to 300
    c) A.3: *m/z* values begin at 300 and increase by increments of 20 to 460
    d) A.4: *m/z* values begin at 310 and increase by increments of 20 to 470
  - Method B: LC-MS parameters are nearly identical to Method A, except that the isolation window is changed to 2 *m/z* and the inclusion list is designed to cover a 20 *m/z* range with values increasing by increments of 2 *m/z*. The inclusion list is customized to target features of interest observed using

Method A. For example, to investigate a candidate peak identified in the 210 *m/z* scan filter from Method A, the inclusion list for Method B would contain 200, 202, 204, … 216, 218, 220 *m/z.*

- Method C: Again, LC-MS parameters are nearly identical to Methods A and B, except that the isolation window is further narrowed to 1 *m/z* and the inclusion list is customized to isolate the isotopomers of interest observed with Method B. Values within 1-2 *m/z* of the scan range containing features of interest found from Method B are included. For example, to target a peak observed in the 206 *m/z* scan filter from Method B, 205, 206, and 207 *m/z* should be added to the inclusion list of Method C.
- Method D: Scan groups include one full MS- SIM scan followed by one PRM scan. MS parameters are the same as those described above except that the NCE is 15 and the isolation window is ≤1 *m/z*. The inclusion list is customized to contain only the [$^{13}C_8$, $^{15}N_1$]-, [$^{15}N_1$]-, and unlabeled molecular ions of interest with as much specificity as possible.

Methods

Growing seedlings with inhibitor and stable isotope precursor treatments

Seedlings are grown *in vitro* on mesh squares, allowing them to be easily transferred to chemical inhibitor treatments at the desired timepoints. A liquid solution containing stable isotope-labeled precursors is then supplied to seedlings, and synthesis of isotopically labeled IAA and intermediates can be identified and distinguished by LC-HR-MS.

1. In a laminar flow hood, moisten sterile nylon mesh squares with sterile water and use forceps to place squares flat on germination media (see Note 7 and Table 3-2) in square Petri dishes.
2. Clean *Arabidopsis* seeds by shaking in 20% bleach solution for 5 minutes and rinsing 4 times with sterile water.
3. Sow seeds approximately 0.5 cm apart in single row on mesh.

4. Store plates at 4°C in the dark for 3-7 days to stratify seeds. Remove plates from cold and place vertically in growth conditions.
5. Transfer seedlings onto inhibitor media (Table 3-1) to begin auxin biosynthesis inhibition treatment (see Note 8). In a laminar flow hood, use forceps to gently lift mesh with seedlings from germination plates and lay flat onto plates containing inhibitor media. Cover plates and place vertically under growth conditions.
6. Begin isotopic labeling treatments by flooding plates with 3 mL of labeling solution (Table 3-2). Gently rock plate back and forth 5-10 times to ensure labeling solution covers entire mesh square. Cover plates and place flat under growth conditions for 0-24 hours (see Note 8).
7. Collect samples by gathering 10-50 mg of plant tissue (see Notes 9 and 10), gently blotting away moisture on a KimWipe, and placing in a microcentrifuge tube. Immediately submerge tube in liquid nitrogen to flash freeze and place on dry ice. Store samples at -80° C until extraction.
8. Holding frozen samples on dry ice, add 20 µL of homogenization solution per 10 mg tissue and 2-3 beads to each sample.
9. Homogenize samples in tissue homogenizer for 4 minutes at 1500 RPM and incubate samples on ice for 1 hour (see Note 11)
10. Add 90 µL of water to each homogenized sample per 10 µL homogenization buffer and shake tube to mix.
11. Centrifuge samples at 25000 g for 10 min. at 4°C.
12. Prepare samples for LC-MS analysis using purification methods specified for compounds of interest:

Indole

Indole is a biosynthetic precursor of IAA and Trp, and is extracted by solvent partitioning.

13. Transfer 200 µL supernatant into a new tube. Add 100 µL pentane and vortex at room temperature for 5 minutes.

14. Spin samples a short time to clearly separate the organic and aqueous phases. Transfer the upper organic layer into a new tube. Save the aqueous phase for extraction of IAA (steps 16-21) or auxin biosynthesis intermediates (steps 22-26).
15. Evaporate pentane with vacuum concentrator and resuspend sample in 20 µL acetonitrile

IAA

IAA is typically present at low levels in plant tissues and can be extracted separately from other compounds using more selective methods for optimal detection. IAA samples are purified by solid phase extraction (SPE) using an amino (NH_2) resin followed by a second step with polymethylmethacrylate epoxide (PMME) resin.

16. Prepare TopTips with NH_2 resin for SPE according to Liu et al. (2012). Add 20 µL resin suspension per TopTip; wash with 50 µL each: hexane, acetonitrile, ethyl acetate; condition with 50 µL 0.2 M imidazole followed by 2 × 100 µL water.
17. Load supernatant from step 11 onto prepared TopTips. For larger samples, 250 µL of supernatant can be loaded at a time and spun through. Reload and spin until all supernatant has been loaded. Wash with 50 µL methanol.
18. Exchange tubes under TopTip adapters to fresh 2 mL tubes for elution. Elute with 3× 50 µL of PA, then add 25 µL of SA to each sample.
19. Prepare TopTips with PMME resin for solid phase extraction (SPE) according to Liu et al. (2012). Add 75 µL PMME resin suspension per TopTip; wash with 2 × 100 µL methanol; condition with 2 × 100 µL PA:SA.
20. Load samples onto prepared TopTips. Wash with 2 × 50 µL PA:SA.
21. Exchange tubes under TopTip adapters to clean 1.5 mL tubes for elution. Elute with 2 × 50 µL methanol. Reduce volume of each sample to approximately 20 µL with vacuum concentrator.

Proposed IAA biosynthesis pathway intermediates: Anthranilate, Ser, IPyA, IAAld, IAOx, IAN, IAM

Samples are prepared for analysis of biosynthesis intermediates by SPE using an HLB resin. SPE is an effective sample preparation technique for these compounds because it provides a high level of recovery and is relatively easy to use with large sample sets. IAA can also be extracted using the following method, but with some loss of sensitivity compared to methods described in the previous section.

22. Prepare TopTips with HLB resin for SPE. Add 25 µL resin suspension per TopTip; equilibrate with 2 × 50 µL 100% acetonitrile and 2 × 50 µL 20% acetonitrile.
23. Load supernatant onto prepared TopTips.
24. If highly sensitive detection and quantification of IAA is required, save 200-300 µL of supernatant for separate IAA analysis (steps 16-21). IAA may be extracted and analyzed simultaneously with precursor compounds if samples contain sufficiently high IAA levels (typically ≥ 2 ng).
25. Wash with 50 µL 5% acetonitrile.
26. Exchange tubes under TopTip adapters to clean 1.5 mL tubes for elution. Elute with 2 × 50 µL 80% acetonitrile. Reduce volume of each sample to approximately 20 µL using vacuum concentrator (about 10-12 minutes).

Unknown indolic compounds (double indole labeling samples)

An unbiased extraction method is used for discovery of unknown compounds synthesized from indole.

27. Transfer supernatant to a clean tube and centrifuge again at 25000 g for 10 min. at 4°C to remove all debris.

LC-MS analysis

Samples are analyzed using LC-HRAM-MS to chromatographically separate components of chemical matrix and obtain high resolution *m/z* data. Specific LC-MS methods are tailored for different sample types and analysis objectives (see method details in Materials section).

28. Carefully transfer each sample to a 50 µL glass insert so that no air pockets remain at the bottom of the insert. Assemble insert into autosampler vial with cap.
29. Inject 5-10 µL of sample for LC-MS analysis using methods described in the LC-MS analysis subsection of the Materials section.

Data analysis

IAA analysis

Extracted ion chromatograms (EICs) of labeled and unlabeled quinolinium ions generated by fragmentation of labeled internal standard and unlabeled endogenous IAA are viewed (see Supplement Figure 3-2). Narrow mass ranges are used to filter out background noise.

30. Under the "Ranges" tab in "Chromatogram Ranges" in Xcalibur, set the chromatogram viewing options to display two mass ranges: 130.0641-130.0661 (corresponding to unlabeled quinolinium ion), and 136.0843-136.0863 ([$^{13}C_6$] quinolinium produced from [$^{13}C_6$]IAA internal standard). Under "Display" tab, check "Peak Area." Use "peak selection" tool to select and calculate area of peaks corresponding to unlabeled IAA and the internal standard. Endogenous IAA levels can be calculated using isotope dilution.

Targeted IAA precursor analysis

Peak areas from EICs of multiple compounds are determined using a script. Mass ranges surrounding the exact masses of ions produced from the compounds of interest, as well as their labeled forms synthesized from the supplied labeled precursors, are kept within a narrow window to exclude background noise.

31. Raw data files are converted to mzXML format using the msconvert tool from the ProteoWizzard software prior to input into R. Quantitative data for each indolic compound is extracted using the Metabolite-Turnover script developed in the Hegeman lab (https://github.com/HegemanLab/Metabolite-Turnover). In this script, the ProteinTurnover (Fan et al., 2016) and the XCMS package (Smith et al.,

2006) are employed to extract EICs for each isotopmer of IAA and intermediates. This quantification approach using linear regression is preferred over that using peak area when the MS data has high background noise due to low analyte abundance.

32. Exact masses for isotopomers of interest are calculated using the University of Wisconsin—Madison Biological Magnetic Resonance Data Bank exact mass calculator (http://www.bmrb.wisc.edu/metabolomics/mol_mass.php). Isotopomers of proposed IAA biosynthetic intermediates derived from several isotopic labeling strategies are listed in Table 3-3. (See Note 12)
33. In the data output csv files, the slope of each linear regression line represents the ratio of the respective isotopic trace to its monoisotopmer. This ratio is used to calculate the relative abundance of labeled compounds, allowing us to track label incorporation from upstream precursors into IAA intermediates through multiple pathways.

Double indole labeling data analysis

Supplying plants two differentially labeled form of indole provides a way to identify indole-derived compounds, as downstream intermediates will incorporate both labels. These samples are analyzed in a series of LC-MS/MS injections, initially scanning broadly for formation of labeled quinolinium ions, and then narrowing in on precise ions in subsequent injections until a molecular ion can be identified and fragmented to provide further structural information.

34. Use LC-MS method A1 (described in Materials section "LC-MS analysis") to identify potential features producing [$^{15}N_1$]- and [$^{13}C_8$, $^{15}N_1$]quinolinium ions.
    a. Under the "Ranges" tab in "Chromatogram Ranges" in Xcalibur, set the chromatogram viewing options to display three mass ranges: 130.0641-130.0661 (corresponding to unlabeled quinolinium ion), 131.0612-131.0632 ([$^{15}N_1$]quinolinium ion), and 139.0880-139.0900 ([$^{13}C_8$, $^{15}N_1$]quinolinium ion).

b. Set “Scan Filter” to display chromatogram from the first ion of the inclusion list. Note any coeluting peaks present in both the [$^{15}N_1$]quinolinium and [$^{13}C_8$, $^{15}N_1$]quinolinium ion mass ranges. Ions producing these peaks may have incorporated label from the indole treatments.
c. View chromatograms through each Scan Filter, keeping the same mass ranges specified above, and continue to note any candidate peaks with matching retention times.

35. Repeat workflow described in step 33 with method A2 to identify additional candidate features.
36. Perform subsequent injection with method B, aiming to narrow *m/z* windows containing the parent ions. View data using the same settings in Xcalibur that were used in step 33, taking note of retention times and scan windows that show the presence of coeluting peaks for both quinolinium labeled mass ranges.
37. Perform subsequent injection with method C to progress toward pinpointing molecular ions. This method should be tailored to candidate peaks that were identified in steps 33-35.
    a. Using the same mass ranges settings to target quinolinium ion isotopomers, view EIC through each scan filter to identify the filter range containing the strongest quinolinium signal. The molecular ion is expected to be near (within 1 *m/z*) this value.
38. Customize method D to include approximate molecular ion values identified in step 35 in the inclusion list. Run sample using this method to obtain exact mass spectra.
39. Compare spectra produced from each of the three ions in the inclusion list of method D, taking note of exact mass differences between the major ions of different spectra. Exact mass differences of 0.9970, 9.0239, and 8.0268 *m/z* correspond to the differences between $^{15}N_1$ and unlabeled, $^{13}C_8{}^{15}N_1$ and unlabeled, and $^{13}C_8{}^{15}N_1$ and $^{15}N_1$, respectively.
40. If no molecular ions are observed, NCE settings in method D can be set to a lower intensity to preserve a greater abundance of molecular ion.

41. Unlabeled molecular ion and spectral data can be searched against mass spectral databases to identify potential compound identities: MassBank, METLIN, NIST Tandem Mass Spectral Library, m/zCloud, MS-DIAL.
42. Confirm compound identities by comparing retention time and mass spectral data against authentic standards.

Notes

1. 500 μM [$^{13}C_{11}$, $^{15}N_2$]Trp (or other labeled forms of Trp) may also be used as a labeled precursor treatment (Mashiguchi et al., 2011; Östin et al., 1999); however, results should be examined cautiously as high levels of exogenous Trp will feedback inhibit anthranilate synthase and anthranilate phosphoribosyltransferase , which may confound results.
2. To improve solubility, labeled indole can first be dissolved in a small volume of acetonitrile; anthranilate can first be dissolved in a small volume of isopropanol. Labeled indole and anthranilate concentrations were based on observation that significant labeling of IAA and biosynthetic precursors was achieved after incubation with 500 μM labeled precursor for 16 h, and labeled Ser concentrations were chosen to approximate endogenous Ser levels (Riens et al., 1991). However, concentrations may be adjusted as needed for use in other systems (see Table 3-4).
3. IPyA and IAAld degrade quickly and need to be derivatized with CH_3ONH_2 to generate their oximes (IPyA-MeOx and IAAld-MeOx). Standards should be derivatized and freshly prepared.
4. For IAA quantitation by isotope dilution, mix 10 ng of stable isotope labeled-IAA per 1 mL homogenization buffer. We recommend using [$^{13}C_6$]IAA (Cambridge Isotope Laboratories, CLM-1896) in experiments where other [$^{13}C_6$]-labeled precursors (such as [$^{13}C_6$]anthranilate) are not used.
5. For reverse isotope dilution quantitation, use unlabeled internal standards as endogenous compounds are [^{15}N]-labeled in plants germinated on [^{15}N]ATS media. Add 50 nM ANT, 500 nM indole, 5 μM Trp, 1 nM IAM, 2.5 μM IAN, 100 nM

IPyA, 10 nM IAAld, 10 nM IAA, 1 nM TAM, 10 nM IAOx and 100 mM freshly prepared methoxylamine hydrochloride ($CH_3ONH_2 \cdot HCl$) into homogenization buffer. In the data analysis output for reverse isotope dilution samples, the slope of each linear regression line represents the ratio of the respective isotopic trace (labeled compounds) to its monoisotopomer (unlabeled internal standard added) and is used to quantify the isotopic traces.

6. Although MS parameters are altered in subsequent injections, it is important to keep the LC gradient consistent with method A so that retention times are consistent across injections.
7. For absolute quantitation of compounds by reverse isotope dilution, use fully [^{15}N]-labeled salts in both germination and inhibitor media. If only relative label incorporation data is needed, unlabeled media can be used.
8. Timing for inhibitor treatments, isotopic labeling, and sample collection can be adapted to study auxin biosynthesis at different developmental stages. Significant IAA biosynthesis inhibition can be observed in 12-day seedlings (22°C, 10/14-hour photoperiod, cool white fluorescent lights at ~ 100 μmol m^{-2} s^{-1}) after 20 hours on 100 μM YDF and 30 μM PVM2153 media with 30 minutes labeling treatment. Under these conditions, we observed greater label incorporation into IAA from labeled indole compared to other precursors. Endogenous levels of IAA precursors such as Trp may increase in the presence of biosynthesis inhibitors (Narukawa-Nara et al., 2016).
9. For absolute quantitation, record fresh weight of harvested tissues. This data is later used for isotope dilution calculations.
10. Recommended amounts for tissue collection: 40-50 mg per sample for [$^{13}C_3$]serine labeling or double indole labeling; 10-30 mg for indole/anthranilate labeling experiments. More tissue may be needed depending on plant tissue type and inhibitor treatment
11. Plant tissue should be completely pulverized after homogenization. If significant plant material remains intact, repeat homogenization step.
12. We recommend using a mass range window of the calculated *m/z* value +/- 0.003.

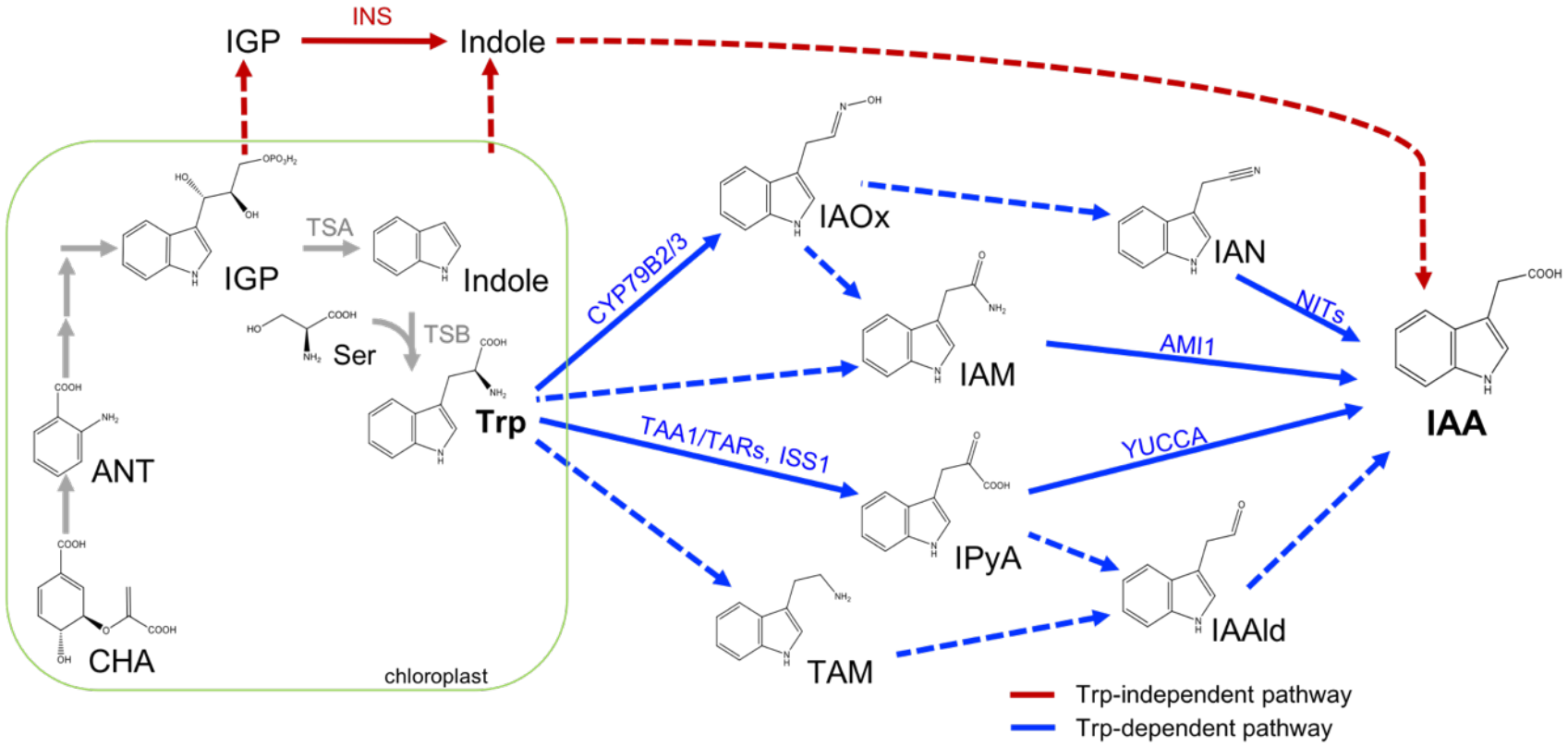

Figure 3-1: Major pathways for IAA biosynthesis. Solid arrows refer to pathways with enzymes identified in at least one species, and dashed arrows to undefined ones. AMI1, indole-3-acetamide hydrolase-1; ANT, anthranilate; CHA, chorismic acid; IAAld, indole-3-acetaldehyde; CYP79B2/3, cytochrome P450 (79B2/3); IAM, indole-3-acetamide; IAN, indole-3-acetonitrile; IAOx, indole-3-acetaldoxime; IGP, indole-3-glycerol phosphate; INS, indole synthase; IPyA, indole-3-pyruvic acid; ISS1, Indole Severe Sensitive 1; NIT, nitrilase; Ser, serine; TAA1, tryptophan aminotransferase of Arabidopsis 1; TAR, tryptophan aminotransferase-related; TAM, tryptamine; Trp, tryptophan; TSA, tryptophan synthase α; TSB, tryptophan synthase β; YUCCA, Arabidopsis flavin monooxygenase

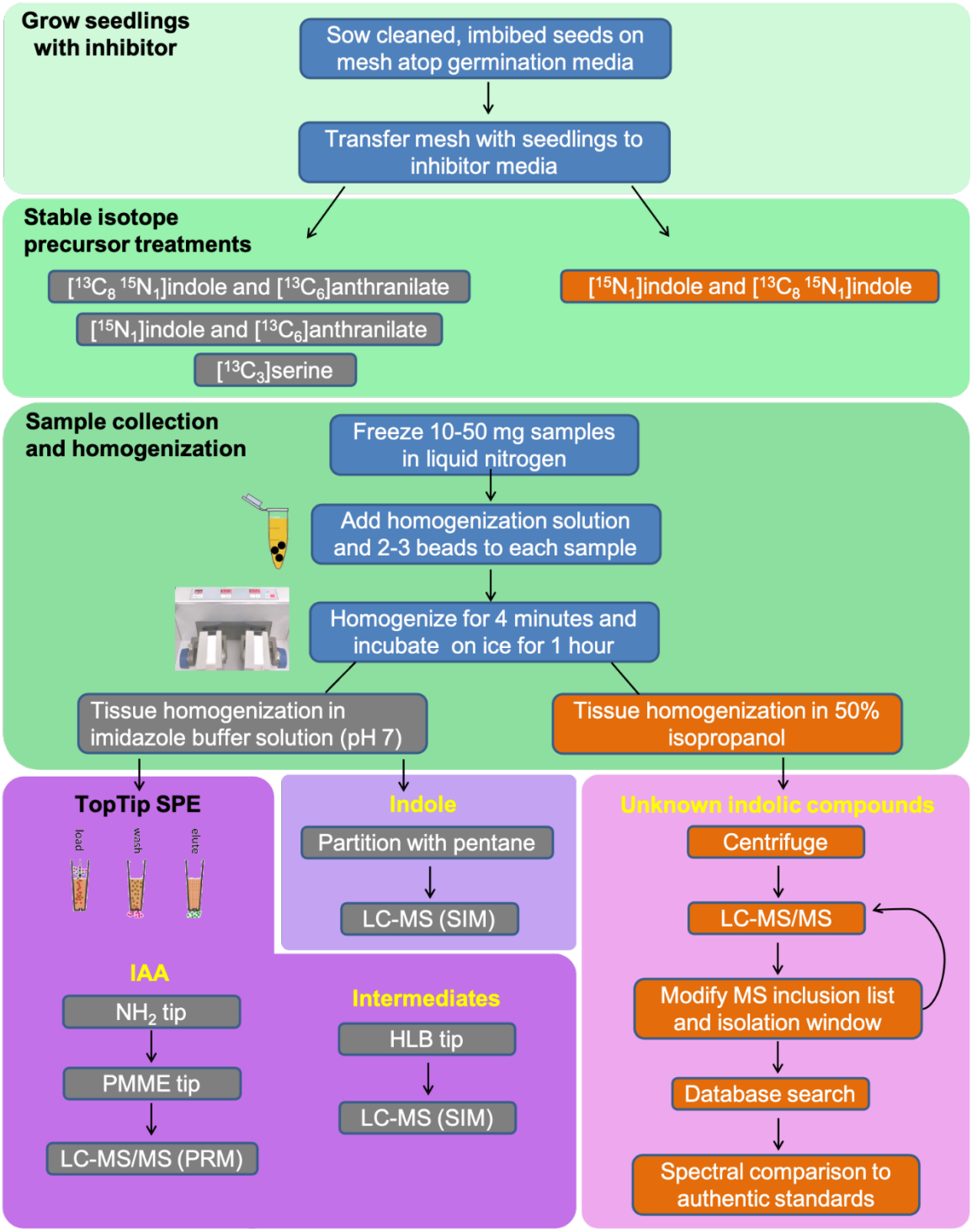

Figure 3-2: Workflow summary for labeling and analysis of the auxin metabolic network. Various labeling and analysis techniques are used to investigate different aspects of auxin biosynthesis. For absolute quantitation, internal standards are added to samples prior to homogenization

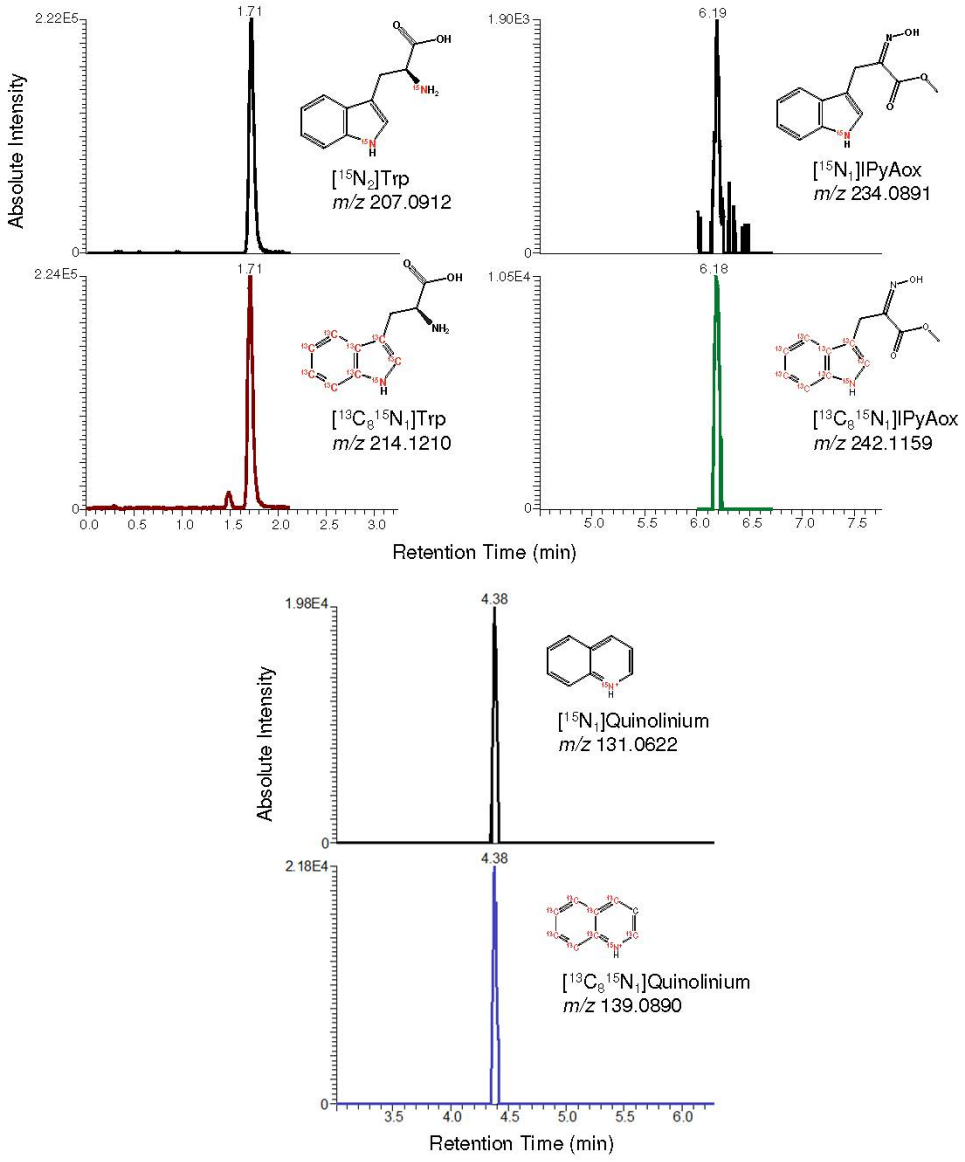

Figure 3-3: Representative results from analysis of Trp, IPyA, and IAA extracted from Arabidopsis seedlings. 13-day-old seedlings grown on ^{15}N media were subjected to mock inhibitor treatment (DMSO+ACN) for 22h, then labeled with 500 µM [$^{13}C_8$, $^{15}N_1$] indole for 1h. [$^{15}N_2$]Trp, [$^{13}C_8$, $^{15}N_1$]Trp, [$^{15}N_1$]IPyAox, and [$^{13}C_8$, $^{15}N_1$]IPyAox were monitored in SIM mode. [$^{15}N_1$] IAA →[$^{15}N_1$]quinolinium ion and [$^{13}C_8$, $^{15}N_1$]IAA → [$^{13}C_8$, $^{15}N_1$]quinolinium ion transitions were monitored in PRM mode

Table 3-1: Some chemical inhibitors of auxin biosynthesis

Inhibitor name	Representative Structure(s)	Target	Mode of action	Reference
BBo	3-chlorophenylboronic acid, 4-biphenylboronic acid	YUCCA	Competitive inhibitor	(Kakei et al., 2015)
PPBo	4-phenoxyphenyl-boronic acid	YUCCA	Competitive inhibitor	(Kakei et al., 2015)
Ponalrestat	2-(3-(4-bromo-2-fluorobenzyl)-4-oxo-3,4-dihydrophthalazin-1-yl)acetic acid	YUCCA	Substrate antagonist	(Zhu et al., 2019)
Yucasin	5-(4-chlorophenyl)-4H-1,2,4-triazole-3-thione	YUCCA	Competitive inhibitor	(Nishimura et al., 2014)
Yucasin DF (YDF)	5-[2,6-difluorophenyl]-2,4-dihydro-[1,2,4]-triazole-3-thione	YUCCA	Competitive inhibitor	(Tsugafune et al., 2017)
Pyruvamines (PVM) "Type I compounds"	PVM1169; L-alpha-(aminooxy)-3-(naphthalen-2-yl)propanoic acid	TAA1	Competitive inhibitor	(Narukawa-Nara et al., 2016)
Pyruvamines (PVM) "Type III compounds" (Derivatives of Type I compounds)	PVM2153; Benzene propanoic acid, 3,4-dichloro-α-[(1,3-dihydro-1,3-dioxo-2H-isoindol-2-yl)oxy]methyl ester	TAA1	Competitive inhibitor	(Narukawa-Nara et al., 2016)
L-Kynurenine (Kyn)	(2S)-2-amino-4-(2-aminophenyl)-4-oxobutanoic acid	TAA1	Alternative substrate/ Competitive inhibitor	(He et al., 2011)
AVG	Aminoethoxyvinyl-glycine	TAA1	Slow-binding inhibition	(Soeno et al., 2010)
AOPP	L-aminooxyphenyl-propionic acid	TAA1	Competitive inhibitor	(Soeno et al., 2010)

AOA	Amino-oxyacetic acid	TAA1		(Soeno et al., 2010)
AOIBA	2-amino-oxyisobutyric acid	TAA1		(Soeno et al., 2010)
Indoleacrylic acid	trans-indole-3-acrylic acid	Trp synthase β and α	Allosteric inhibitor	(Matchett, 1972); (Marabotti et al., 2000)
(1-Fluorovinyl)glycine	α-(1′-fluoro)vinyl glycine	Trp synthase β	PLP-enzyme mechanism-based inhibitor	(Xu & Abeles, 1993)
Arylsulfide phosphonates	[4-[(2-aminophenyl)sulfanyl]butyl] phosphonic acid	Trp synthase α	Transition state analog	(Finn et al., 1999); (Dias et al., 2006)
Indoline-5-sulfonamides	1-(2-fluorobenzoyl)-N-methyl-5-indoline sulfonamide N-methyl-1-[(5-methyl-2-thienyl)carbonyl]-5-indolinesulfonamide	Trp synthaseinter-subunit interface	Allosteric inhibitor	(Abrahams et al., 2017)
sulfolane and indole-5-sulfonamide	GSK1, (3R,4R)-4-[4-(2-chlorophenyl)piperazin-1-yl]-1,1-dioxothiolan-3-ol; GSK2, 1-[2-fluorobenzoyl]-N-methyl-2,3-dihydro-1H-indole-5-sulfonamide	Trp synthaseinter-subunit interface	Allosteric inhibitor	(Michalska et al., 2020)
Aryl sulfonamides	[F9]; N-(4’-trifluoromethoxy benzenesulfonyl)-2-aminoethyl phosphate	Trp synthase β	α-Site allosteric ligand	(Ngo et al., 2007)
Benzamide	N-(4-carbamoyl benzyl)-5-(3-chloro phenyl)-1,2-oxazole-3-carboxamide	Trp synthase α	α-Site ligand	(Naz et al., 2019)

Table 3-2: Labeling precursors used for different applications. Example labeling strategies employing different stable isotope-labeled precursors for studying IAA biosynthesis. These strategies can be used in combination with various inhibitors (Table 3-1) for targeted analysis of specific routes of IAA biosynthesis.

Labeled precursor treatment	Germination Media	Purpose/Description
3 mM [$^{13}C_3$]serine	[^{14}N] ATS	Traces synthesis of Trp and Trp-dependent pathway intermediates. [$^{13}C_3$]serine is condensed with indole to give [$^{13}C_3$]Trp ([$^{13}C_3$]-label is incorporated into Trp sidechain).
500 µM [$^{13}C_6$]anthranilate and 500 µM [$^{15}N_1$]indole	[^{14}N] ATS	Multiple auxin precursors upstream of Trp are applied to monitor label incorporation into various intermediates through multiple pathways.
500 µM [$^{13}C_8{}^{15}N_1$]indole and 500 µM [$^{15}N_1$]indole	[^{14}N] ATS	Multiple labeled forms of indole are applied to label indole-derived metabolites and potential IAA biosynthesis intermediates. LC-MS/MS analysis workflow for identifying candidate compounds is described in the Materials LC-MS analysis section.
500 µM [$^{13}C_6$]anthranilate and 500 µM [$^{13}C_8{}^{15}N_1$]indole	[^{15}N] ATS	Growing seedlings on [^{15}N] ATS media enables rapid [^{15}N]-labeling of newly synthesized IAA and biosynthesis intermediates during early seedling development (Figure 3-3). Unlabeled internal standards may be used for quantitation of IAA and biosynthetic intermediates in plant tissue grown on [^{15}N] ATS (reverse isotope dilution quantitation).

Table 3-3: The *m/z* values of isotopomers measured in the IAA and intermediates analyses.

	M(+H)	$^{15}N_1$	$^{13}C_1$	$^{15}N_2$	$^{13}C_1{}^{15}N_1$	$^{13}C_1{}^{15}N_2$
ANT	138.0550	139.0520	139.0583		140.0553	
IND	118.0651	119.0622	119.0685		120.0655	
Trp	205.0972	206.0942	206.1005	207.0912		
Ser	106.0499	107.0469	107.0532			
TAM	161.1073	162.1044	162.1107	163.1014	163.1077	164.1047
IAOx	175.0866	176.0836	176.0899	177.0807	177.0870	178.0840
IAM	175.0866	176.0836	176.0899	177.0807	177.0870	178.0840
IAN	157.0760	158.0731	158.0794	159.0701		160.0734
IPyAox	233.0921	234.0891	234.0954		235.0925	
IAAldox	189.1022	190.0993	190.1056		191.1026	
IAA	176.0706	177.0676	177.0740		178.0710	
Quinolinium	130.0651	131.0622	131.0685			
	$^{2}H_4$	$^{13}C_6$	$^{13}C_6{}^{15}N_1$	$^{13}C_7$	$^{13}C_7{}^{15}N_1$	$^{13}C_8{}^{15}N_1$
ANT		144.0751	145.0721	145.0784		147.0788
IND		124.0853	125.0823	125.0886		127.0890
Trp		211.1173	212.1143		213.1177	214.1210
Ser						
TAM			168.1245		169.1278	170.1312
IAOx			182.1038		183.1071	184.1105
IAM			182.1038		183.1071	184.1105
IAN			164.0932		165.0965	166.0999
IPyAox		239.1122	240.1092	240.1156		242.1159
IAAldox		195.1224	196.1194	196.1257		198.1261
IAA	180.0957	182.0907	183.0878	183.0941		185.0945
Quinolinium	134.0902	136.0853				139.0890

Table 3-4: Common problems and troubleshooting guide. Adapted from Liu et al. (2012)

Problem	Possible Reasons	Solutions
Liquid does not pass through TopTips before loading plant samples	The slit on TopTips is too narrow	Increase the centrifugal force to make liquid pass through, or switch to a new TopTip.
Liquid does not pass through TopTips after loading plant samples	Plant debris blocks the TopTip slit	Always try to avoid transferring plant debris into TopTips. Increase the centrifugal force to make liquid pass through. Use a dissecting probe to remove visible plant debris.
Drift of LC retention time	Injection volume is too large	Evaporate eluate or extract to a smaller volume with vacuum concentrator. Reduce the sample volume injected onto the LC.
	Change of LC mobile phase	Check that correct, freshly prepared mobile phase solvents are being used. Purge the LC lines after changing solvents.
	LC solvents are blocked or leaking	Replace the precolumn filter. Check column connections and reinstall if needed. Check LC lines for leaking solvent.
Low yield of labeled compounds, but normal yield of endogenous compounds and/or internal standards	Slow turnover	Increase the labeling time period.
	Insufficient intake of labeled precursors	Increase the concentration of labeled precursors in the labeling solution. Make sure plants are bathed in sufficient volume of labeling solution.

Broad/tailed LC peaks	Injection volume is too large	Evaporate eluate or extract to a lower volume with vacuum concentrator. Reduce the sample volume injected onto the LC.
	The precolumn filter is dirty	Replace the filter.
	The column is dirty	Disconnect the LC line from the MS source and wash the column with solvent according to manufacturer's instructions.
Analyte *m/z* values do not match calculated values	The MS needs to be calibrated	Perform mass calibration with calibration standard mixture according to instrument manual.
Reduced MS sensitivity	The MS needs to be calibrated	See above.
	The tune file needs to be modified	Adjust source parameters for optimal ion intensity using standard compounds.

Supplements

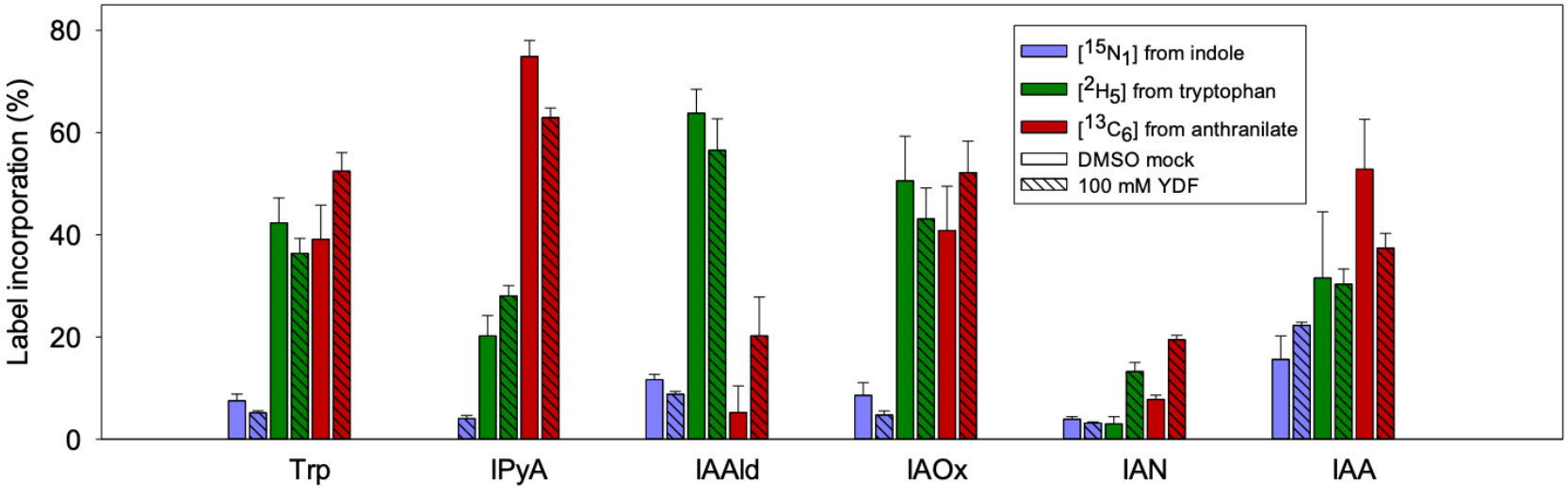

Supplement Figure 3-1: [$^{15}N_1$]indole, [$^{2}H_5$]tryptophan, and [$^{13}C_6$]anthranilate labeling of IAA precursors in Arabidopsis hypocotyls in the presence of YDF. Seedlings were grown in the dark for 7 d, then transferred onto media with or without 100 μM YDF. Seedlings were then exposed to a 16 h photoperiod of red light (660 nm, 135 μmol m^{-2} s^{-1}) for 1 day, and then treated by applying a solution containing 100 μM [$^{15}N_1$]indole, 500 μM [$^{2}H_5$]tryptophan, and 500 μM [$^{13}C_6$]anthranilate for 16 hours under red light. Samples containing approximately 20 hypocotyls were collected for LC-MS analysis of isotopic enrichment of IAA and IAA biosynthesis intermediates. Data are expressed as the percentage of total detected compound containing the specified isotopic label.

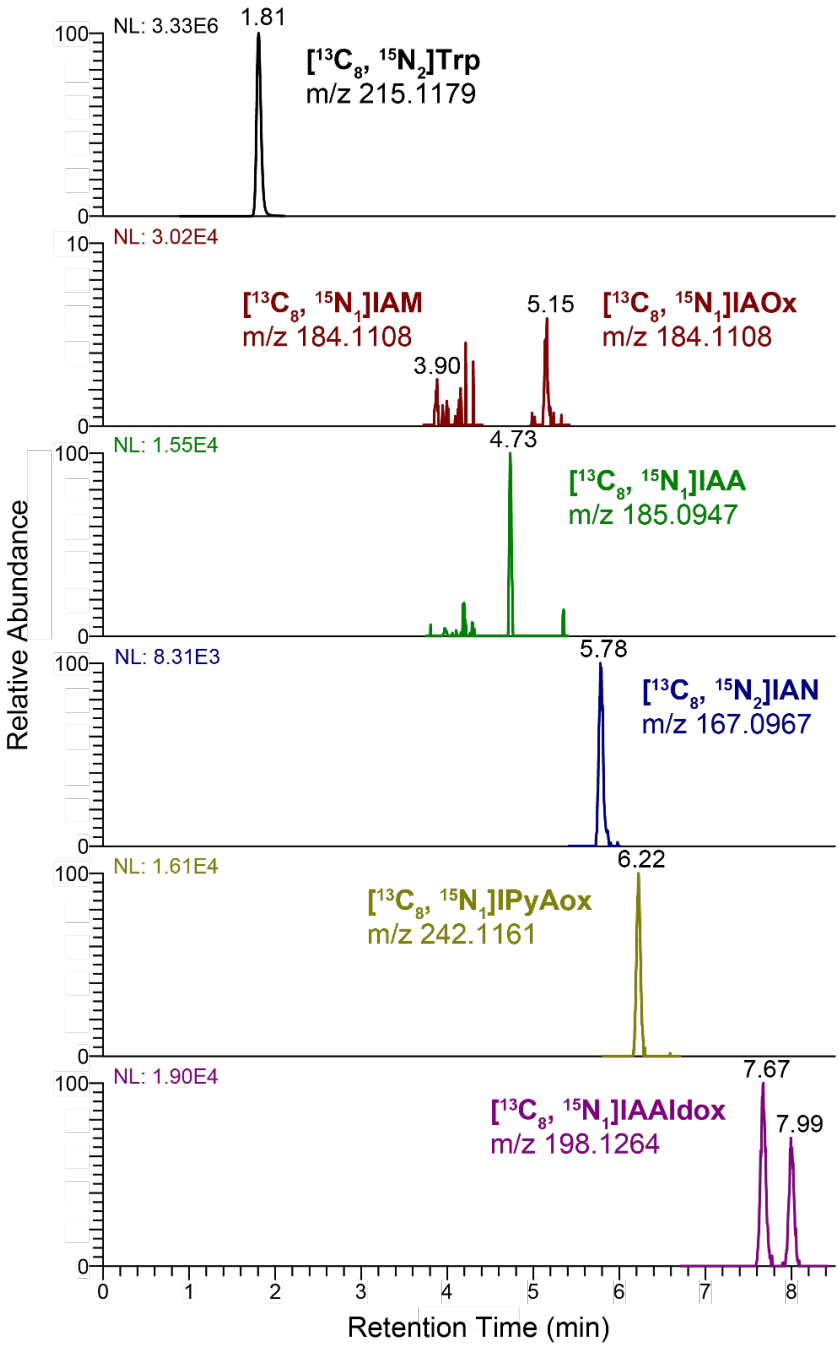

Supplement Figure 3-2: Extracted Ion Chromatogram (EIC) of targeted metabolites. Arabidopsis seedlings were grown for 12 days on [^{15}N]ATS salts at 22°C under ~ 100 µmol m^{-2} s^{-1} of cool white fluorescent lights for 10/14-hour photoperiod, then subjected to labeling with [$^{13}C_8$, $^{15}N_1$]indole. Resulting labeled compounds (tryptophan (Trp), indole-3-acetamide (IAM), indole-3-acetaldoxime (IAOx), indole-3-acetic acid (IAA), indole-3-acetonitrile (IAN), indole-3-pyruvic acid oxime (IPyAox), indole-3-acetaldehyde-oxime (IAAldox)) were extracted from plant tissue using solid phase extraction and analyzed by LC-MS.

Chapter 4. Protocols for stable isotope labeling to elucidate rapid auxin kinetics

Introduction

Plant growth control is regulated by changes in the levels of active hormones, their transport to and away from the site of action and the sensitivity of plant tissues to these concentration changes (Li et al., 2013). In particular, auxin levels in plants appear to be controlled by several different metabolic pathways. This combination of metabolic regulatory processes has been termed “auxin homeostasis” to delineate the expected high degree of control that plants exercise to maintain the appropriate rates of growth. Auxin homeostatic regulation involves an interactive network of redundant pathways, the complexity of which has been shown by the application of a combination of molecular, genetic, and analytical approaches (Jiang et al., 2017; Cohen & Gray, 2006; Ljung et al., 2002; Cooke et al., 2002).

A major limitation of many studies of phytohormone biosynthesis is the lack of dynamic information to allow interpretation of data in the context of metabolic fluxes. Metabolic analysis may demonstrate an increased abundance of a hormone or its metabolite under specific conditions. Often such studies cannot determine whether this is the result of increased flux from a biosynthetic enzyme, decreased flux by a catabolic enzyme, changes in formation or hydrolysis of conjugating moieties, or alteration in transport of the metabolite (Chokkathukalam et al., 2014). Furthermore, phytohormone metabolic pathways are largely interconnected, and a number of interacting metabolic processes maintain metabolite levels. These cannot be adequately resolved by measurement of steady-state metabolite concentrations alone.

These considerations are of concern because the vast bulk of studies analyzing phytohormone metabolism have approached physiological questions with measurements of hormone levels and/or levels of a metabolite to infer a metabolic origin, fate, or regulation with only a few notable exceptions. While many of these studies have been

informative, they are, nevertheless, often limited static 'windows' that are extrapolated to predict time-dependent metabolic activities. The full limitations of such approaches are difficult to predict with any certitude. Similarly, approaches that seek to measure reactions where a supplied metabolic precursor is applied and its conversions to a product of interest, typically using an isotopic label, provide different information but also are subject to some inherent limitations. These can be compounded by measurements that are limited in number of time points. Also, often measurements are made after protracted labeling periods. These times can range from somewhat less than an hour to several hours (Cooney & Nonhebel, 1991; Ljung et al., 2005; Nishimura et al., 2009, 2013; Jones et al., 2010; Pieck et al., 2015; Tivendale et al., 2010). In other cases, labeling times can continue for a day to even weeks (Epstein et al., 2002; Glawischnig et al., 2000; Wang et al., 2015). Clearly, temporal understanding can be a concern given that indole-3-acetic acid (IAA) turnover have been measured or modeled to be in the range of a few minutes to 1-10 hours (Kramer and Ackelsberg, 2015; Tam et al., 1995; Rapparini et al., 2002).

To overcome some of the possible limitations of prior efforts, we developed a method for the targeted metabolomic analysis of the indole auxin biosynthetic network (Tillmann et al., 2021). We have now further adapted this method by first analyzing when seedlings of Arabidopsis make the transition from heterotrophic to autotrophic auxin biosynthesis, and then by using seedlings of Arabidopsis to analyze the incorporation at stable isotopic labels into newly synthesized IAA as well as potential biochemical precursors at very short time intervals with time-dependent sampling. By these small molecule implementations of Stable Isotope Labeled Kinetics (SILK) methods, we demonstrate that measuring entire pathways over time and using different isotopic tracer precursor techniques offer improved and more detailed information about this complex interacting network of metabolic reactions.

Materials and Methods

Growing plant material

- Plant growth medium: *Arabidopsis thaliana* salts (ATS; Lincoln et al., 1990)

- Salts substituted to make [^{15}N]ATS: $K^{15}NO_3$ (Cambridge Isotope Laboratories, NLM-765-PK), $Ca(^{15}NO_3)_2$ (Cambridge Isotope Laboratories, NLM-499-PK)
- Media made with 1% agar (Phytotech, A111) and 10% sucrose (Millipore Sigma S5390)

- When required for labeling and inhibitor studies, 20 μm nylon mesh (Sefar, 03-20/14), cut into 9 cm × 9 cm squares and autoclaved to sterilize for 45 minutes at 121°C. In a laminar flow hood, moisten sterile nylon mesh squares with sterile water and use forceps to place squares flat on [^{15}N]ATS germination media in 10 cm × 10 cm square Petri dishes (Fisherbrand, FB0875711A).
- Grow Wild-type Columbia-0 Arabidopsis seeds on the Petri plates. Seeds were surface sterilized by soaking in dilute bleach solution (20% commercial bleach (Clorox, 6% sodium hypochlorite), 80 mL deionized water, 20 μL Tween 80 (Sigma-Aldrich, P1754)) for 5 minutes and then rinsing 4 times with sterile water.
- Store plates at 4°C in the dark for 3-7 days to stratify seeds. Remove plates from cold and place vertically in growth chamber (10/14-h photoperiod, ~100 μmol m^{-2} s^{-1} white light at 22°C).

Harvest, homogenization and extraction

- Harvest, homogenization and extraction are performed as detailed below in two separate protocols.
  - Option 1, for the absolute quantification of unlabeled IAA and [$^{15}N_1$]IAA.
  - Option 2, for labeling and inhibitor studies.
- In each case, samples are thoroughly homogenized (with added internal standard, if desired, for quantitative analysis) and equilibrated for a short time before centrifugation to remove large particles.

Option 1

For the absolute quantification of unlabeled and [$^{15}N_1$]IAA using [$^{13}C_6$]IAA as internal standard to find the change from the heterotrophic IAA utilization from stored reserves and precursors to autotrophic de novo IAA production.

- Similar growth conditions were used except seeds were geminated and grown on [^{15}N]ATS without using the nylon mesh.
- Collect samples by gathering 5-20 mg of seedlings every day at the same time from day 1 to day 14 after the transfer to the growth chamber. Seedlings are collected into a 1.6 mL microcentrifuge tube (Fisherbrand, 05-408-129).
- Weigh microcentrifuge tube before and after sample collection using an analytical balance to record sample fresh weight. Immediately after weighing, submerge tube in liquid nitrogen to flash freeze and place on dry ice. Store samples at -80°C until extraction.
- Mix 10 ng of [$^{13}C_6$]IAA (Cambridge Isotope Laboratories, CLM-1896) per 1 mL homogenization buffer(65% isopropanol, 35% 0.2 M imidazole (pH 7.0)).
- Holding frozen samples on dry ice, add 20 µL of homogenization buffer per 10 mg tissue and 2-3 stainless steel beads (1.6 mm diameter, Next Advance, SSB16) to each sample.
- Homogenize samples in Geno/Grinder (SPEX SamplePrep) for 3 minutes at 1750 RPM and incubate samples on ice for approximately 1 hour.
- Add 90 µL of water to each homogenized sample per 10 µL homogenization buffer and shake tube to mix.
- Centrifuge samples at 25,000 g for 10 min. at 4°C.

Extraction of IAA

IAA is typically present at low levels in plant tissues. IAA samples are purified by solid phase extraction (SPE) using an amino (NH_2) resin followed by a second step with polymethylmethacrylate epoxide (PMME) resin.

- Prepare TopTips (Glygen, TT2EMT) with Bondesil-NH_2 resin (Agilent, 12213020; suspended in water, 1:4 w:v) for SPE according to Liu et al. (2012). Add 20 µL resin suspension per TopTip; wash with 50 µL each: hexane, acetonitrile, ethyl acetate; condition with 50 µL 0.2 M imidazole (pH 7.0) followed by 2 × 100 µL water.

- Load supernatant onto prepared TopTips. For larger samples, 250 µL of supernatant can be loaded at a time and spun through. Reload and spin until all supernatant has been loaded. Wash with 50 µL methanol.
- Exchange tubes under TopTip adapters to fresh 2 mL tubes (Fisherbrand, 02-681-343) for elution. Elute with 3× 50 µL of 0.25% phosphoric acid (PA), then add 25 µL of 0.1 M succinic acid, pH 6.0 (SA) to each sample.
- Prepare TopTips with PMME resin (Macro-prep epoxide support resin (Bio-Rad, 156-0000), suspended in 0.1 M sodium bicarbonate (pH 7.0), 1:4 w:v) for SPE according to Liu et al. (2012). Add 75 µL PMME resin suspension per TopTip; wash with 2 × 100 µL methanol; condition with 2 × 100 µL 5:1 PA:SA.
- Load samples onto prepared TopTips. Wash with 2 × 50 µL 5:1 PA:SA.
- Exchange tubes under TopTip adapters to clean 1.5 mL tubes for elution. Elute with 2 × 50 µL methanol. Reduce volume of each sample to approximately 20 µL with vacuum concentrator (SpeedVac, Savant; about 8 minutes).

Option 2

For labeling and inhibitor studies

- Grow Arabidopsis seedlings onto 20 µm nylon mesh covering the agar growth medium.
- Transfer 12-day seedlings onto inhibitor media (Table 4-1) or to control (mock) media to begin auxin biosynthesis studies. In a laminar flow hood, use forceps to gently lift mesh with seedlings from germination plates and lay flat onto [^{15}N]ATS media containing 100 µM 5-[2,6-difluorophenyl]-2,4-dihydro-[1,2,4]-triazole-3-thione (YDF; CAS# 1094690-87-5, custom synthesis by LabSeeker, Wujiang City, China; dissolved in dimethyl sulfoxide (DMSO) and filter sterilized before adding to media), 30 µM 3,4-dichloro-α-[(1,3-dihydro-1,3-dioxo-2H-isoindol-2-yl)oxy]-benzene propanoic acid, methyl ester (PVM2153/KOK2153; CAS# 1394950-62-9, LabSeeker; dissolved in acetonitrile and filter sterilized), 50 µM [4-[(2-aminophenyl) sulfanyl]butyl] phosphonic acid (I26; CAS# 191411-61-7, Chemspace US, Monmouth Jct, NJ; dissolved in DMSO and filter sterilized), or solvent mock treatment. Cover plates and place vertically into the growth chamber for 20-30 hours.

- Begin isotopic labeling treatments by flooding plates with 3 mL of 500 µM [$^{13}C_6$]anthranilate (Sigma-Aldrich,709530) or 500 µM [$^{13}C_8$,$^{15}N_1$]indole (Cambridge Isotope Laboratories, CNLM-4786-0). Gently rock plate back and forth 5-10 times to ensure labeling solution covers entire mesh area. Cover plates and place flat under growth conditions.
- Collect samples by gathering 20-50 mg of plant tissue at time intervals range from 30 seconds to 4 hours, gently blotting away moisture on a KimWipe (Kimberly-Clark, KC34155EXL), and placing in a microcentrifuge tube then flash freezing in liquid nitrogen.
- Holding frozen samples on dry ice, add 20 µL of homogenization buffer per 10 mg tissue and 2-3 stainless steel beads, homogenize in Geno/Grinder for 3 minutes at 1750 RPM and incubate samples on ice for approximately 1 hour.
- Add 90 µL of water to each homogenized sample per 10 µL homogenization buffer and centrifuge at 25,000 g for 10 min. at 4°C.
- IAA extraction and quantification are similar to the steps for *de novo* IAA analysis described above except the internal standard mixed in homogenization buffer was [$^{2}H_4$]IAA (a gift from R.S. Bandurski; Magnus et al., 1980).

Extraction of proposed IAA biosynthesis intermediates: Anthranilate, IAAld, IPyA, IAOx, IAN, IAM, indole

- For reverse isotope dilution quantitation (Bloch & Anker, 1948), use unlabeled compounds as internal standards to quantify both endogenous compounds ([^{15}N]-labeled in plants germinated on [^{15}N]ATS media) and newly synthesized compounds (derived from a different isotopic form of labeled precursors (such as [$^{13}C_6$]anthranilate). Add 50 nM ANT (Sigma-Aldrich, A89855), 500 nM indole (Sigma-Aldrich, I0750), 5 µM Trp (Sigma-Aldrich, T8941), 1 nM IAM (Sigma-Aldrich, I1125), 2.5 µM IAN (Sigma-Aldrich, 129453), 100 nM IPyA (Sigma-Aldrich, I7017), 10 nM IAAld (Sigma-Aldrich, I1000), 10 nM IAA (Sigma-Aldrich, I3750), 1 nM TAM (Sigma-Aldrich, 193747), 10 nM IAOx (synthesized as described by Ahmad,

1960) and 100 mM freshly prepared methoxylamine hydrochloride ($CH_3ONH_2 \cdot HCl$; Sigma-Aldrich, 226904; see Tillmann et al., 2021) into homogenization buffer.

- Samples are purified for analysis of IAA intermediates by SPE using a hydrophilic-lipophilic balanced (HLB) resin. IAA can also be extracted using the following method, but with some loss of sensitivity compared to methods described in the previous section.
    - Prepare TopTips with RENSA HLB resin ((MIP Technologies, 92001-0010) suspended in methanol, 1:5 w:v) for SPE. Add 25 µL resin suspension per TopTip; equilibrate with 2 × 50 µL 100% acetonitrile and 2 × 50 µL 20% acetonitrile.
    - Load supernatant onto prepared TopTips.
    - If highly sensitive detection and quantification of IAA is required, save 200-300 µL of supernatant for separate IAA analysis (see previous section). IAA may be extracted and analyzed simultaneously with precursor compounds if samples contain sufficiently high IAA levels (typically ≥ 2 ng).
    - Wash with 50 µL 5% acetonitrile.
    - Exchange tubes under TopTip adapters to clean 1.5 mL tubes for elution. Elute with 2 × 50 µL 80% acetonitrile. Reduce volume of each sample to approximately 20 µL using SpeedVac (about 10-12 minutes).

LC-MS analysis

Samples are analyzed using LC-high resolution acurate mass (HRAM)-MS to chromatographically separate components of chemical matrix and obtain high resolution *m/z* data.

- Carefully transfer each sample to a 50 µL glass insert (ChromTech, CTI-2405). Assemble insert into autosampler vial (ChromTech, 404810) with cap. Gently tap the vial so that no air pockets remain at the bottom of the insert. Inject 5-10 µL of sample for LC-MS analysis using methods described in the LC-MS analysis subsection of the Materials section.

- UHPLC utilizes a column with an end-capped octadecylsilane fully porous 1.8 μm silica resin with high carbon loading (20%) in order to obtain highest sensitivity for indolic compounds.
    - C_{18} HPLC column, 50 × 2.1 mm (Force, 9634252, Restek) with 0.2 μm precolumn filter (UltraShield, 25809, Restek).
    - Liquid chromatograph/mass spectrometer system: Dionex UltiMate 3000 UHPLC, Q Exactive hybrid quadrupole/Orbitrap mass spectrometer, Xcalibur software (Thermo Scientific).
- Mobile phase: A, 0.1% formic acid in water (Optima™ LC/MS Grade, 7732-18-5 Fisher scientific); B, 0.1% formic acid in acetonitrile. Different LC-MS methods are used to target compounds of interest:
    - IAA analysis: Mobile phase gradient of 5% B (-1-0 min), 5-20% B (0-3 min), 20-80% B (3-6 min), 80% B (6-6.5 min) at a flow rate of 0.4 mL•min^{-1}. Mass spectra are collected in positive ion mode in a parallel reaction monitoring (PRM) mode. The inclusion list contains ions of 176.1000, 177.1000, 180.1000, and 182.1000 *m/z*. PRM resolution is 17500 full width at half maximum (FWHM), automatic gain control (AGC) target is 2×10^5, maximum ionization time is 50 milliseconds (ms), isolation window is 2.0 *m/z*, and normalized collision energy (NCE) is 20. Ion source settings are: spray voltage: 4.00 kV, capillary temperature: 275°C, probe heater temperature: 300°C, sheath gas: 30 arbitrary units, aux gas: 20 arbitrary units, S-lens RF level: 50.
    - For analysis of all the listed intermediates, inject 5-10 μL plant extract into the LC system with the following mobile phase gradient: 5% B (-2-1 min), 5-15% B (1-3 min), 15-30% B (3-3.5 min), 30% B (3.5-5 min), 30-39% B (5-7.5 min), 39-80% B (7.5-8 min), 80% B (8-8.5 min) at a flow rate of 0.4 mL•min^{-1}. Mass spectra are collected in selected ion monitoring (SIM) mode. SIM resolution is 70,000 FWHM with maximum ionization time of 200 ms and AGC of 5×10^5. Ion source settings are: spray voltage: 4.00 kV, capillary temperature: 275°C, probe heater temperature: 300°C, sheath gas: 30 arbitrary units, aux gas: 20 arbitrary units, S-lens RF level: 50. MS is set to acquire several segments of full scans each targeting

1-3 compounds. The segments are: 200-217 *m/z* (0-2.1 min), 157-173 *m/z* (2.1-3 min), 133-150 *m/z* (3-3.74 min), 170-188 *m/z* (3.74-5.4 min), 152-170 *m/z* (5.4-6 min), 227-245 *m/z* (6-6.7 min), 184-201 *m/z* (6.7-8.5 min).

Data analysis

IAA analysis

- Extracted ion chromatograms (EICs) of labeled and unlabeled quinolinium ions generated by fragmentation of labeled internal standard and endogenous IAA are viewed. Narrow mass ranges are used to filter out background noise.
- Under the "Ranges" tab in "Chromatogram Ranges" in Xcalibur, set the chromatogram viewing options to display:
  - three mass ranges for *de novo* IAA analysis: 130.0641-130.0661 (corresponding to unlabeled quinolinium ion), 131.0612-131.0632 (corresponding to [$^{15}N_1$]quinolinium ion from autotrophic IAA production) and 136.0843-136.0863 ([$^{13}C_6$]quinolinium ion produced from [$^{13}C_6$]IAA internal standard).
  - three mass ranges for IAA pathway analysis: 131.0612-131.0632 (corresponding to [$^{15}N_1$]quinolinium ion from endogenous IAA produced in [^{15}N]ATS media), 131.0612-131.0632 (corresponding to [$^{15}N_1$]quinolinium ion from autotrophic IAA production), 134.0892-134.0912(corresponding to [$^{2}H_4$] quinolinium ion from [$^{2}H_4$]IAA internal standard), and 136.0843-136.0863 ([$^{13}C_6$]quinolinium ion produced from [$^{13}C_6$]IAA after stable isotope labeling incorporation).
- Under "Display" tab, check "Peak Area." Use "peak selection" tool to select and calculate area of peaks corresponding to unlabeled IAA and the internal standard. Endogenous IAA levels can be calculated using isotope dilution (Barkawi et al., 2010).

Targeted IAA precursor analysis

- Peak areas from EICs of multiple compounds are determined using a script. Mass ranges surrounding the exact masses of ions produced from the compounds of interest, as well as their labeled forms synthesized from the supplied labeled precursors, are kept within a narrow window to exclude background noise.

- Raw data files are converted to *mzXML* format using the *msConvert* tool from the ProteoWizard software (Chambers et al., 2012) prior to input into R. Quantitative data for each indolic compound is extracted using the Metabolite-Turnover script developed in the Hegeman lab. (https://github.com/HegemanLab/Metabolite-Turnover, Evans et al., 2018). In this script, the *ProteinTurnover* (Fan et al., 2016) and the *XCMS* package (Smith et al., 2006) are employed to extract EICs for each isotopomer of IAA and intermediates. This quantification approach using linear regression (Huttlin et al., 2007) is preferred over that using peak area (Cohen et al., 1986) when the MS data has high background noise due to low analyte abundance.
- Exact masses for isotopomers of interest are calculated using the University of Wisconsin—Madison Biological Magnetic Resonance Data Bank exact mass calculator (http://www.bmrb.wisc.edu/metabolomics/mol_mass.php). Isotopomers of proposed IAA biosynthetic intermediates derived from several isotopic labeling strategies are listed in Tillmann et al. (2021).
- In the data output .CSV files, the slope of each linear regression line represents the ratio of the respective isotopic trace to its monoisotopmer. This ratio is used to calculate the relative abundance of labeled compounds, allowing us to track label incorporation from upstream precursors into IAA intermediates through multiple pathways.

Results and discussion

An important advantage of SILK is that it can be used to assess not only the status on on-going metabolic activity but also the effect of various metabolic modulators on a target metabolic network (Bateman et al., 2019). The quantification of compounds as well as the rate of labeling has several advantages over static measurements of concentration (Chokkathukalam et al., 2014). For example, both metabolic activity and pathway disruptions are not adequately visualized by simply quantifying the concentrations before and after treatments. SILK, however, quantifies the metabolism of target compounds and can, for example, reflect which side of the biosynthesis/catabolism process has been affected and may reveal metabolism changes even if overall metabolite concentrations are

essentially unchanged. In addition, SILK can be adapted, as employed in this method, to measure labeling patterns very rapidly in complex networks and determine changes in labeling as altered by metabolic disruptions over short time intervals (Jin & Moseley, 2021).

For the analysis of IAA biosynthesis in a seedling it is better defined after the plant has become fully autotrophic for its auxin needs; this limits inputs from large stores of storage forms (Bartel et al., 2001). There are only a few studies in Arabidopsis that have accessed this critical transition period, although a few reports exist employing deuterium oxide with plants with larger seeds such a maize (Jensen & Bandurski, 1996; Pengelly & Bandurski, 1983; Ribaut et al., 1993; Wright et al., 1991) and bean (Bialek et al., 1992). These prior studies utilized deuterium oxide primarily because of its rapid uptake into cellular compartments and because the low-resolution mass spectrometers available at the time were better suited to analyze multiple labels to avoid interference with naturally occurring heavy atoms, primarily endogenous ^{13}C, that gave IAA approximately a 11.1% *m+1/z* increase in the isotopic envelope. The growth of plants on deuterium oxide however was shown to be inhibited (Bialek et al., 1992; Yang et al., 2010) thus making evaluation of temporal changes difficult to reconcile. In addition, deuterium exchange processes (Bialek et al., 1992; Magnus et al., 1980; Pengelly & Bandurski, 1983) complicates isotopic analysis. Modern high resolution mass spectrometers, however, can easily distinguish between a mass increase of 1.00335 for ^{13}C, 1.00628 for ^{2}H and a mass increase of 0.99703 for ^{15}N, allowing the structural nitrogen atom to serve as a monitor of new synthesis. Methods for growth with ^{15}N have been developed (Tillmann et al., 2021). Structural atoms such as ^{15}N, ^{18}O and ^{13}C avoid many of the problems of exchangeable deuterium, as high concentrations are not toxic, nor do they alter growth rates, and they are not generally subject to rearrangements (Smith 2004) during mass spectrometry processes. One disadvantage to using inorganic ^{15}N to measure *de novo* synthesis of a nitrogen-containing molecule is the recycling of nitrogen that occurs (Müntz et al., 1998), however that change in the baseline of enrichment becomes important only where absolute rates of synthesis are being measured. As shown in Figure 4-1, low levels of ^{14}N become consistent at day 8, remains low, and "new IAA" with the [^{15}N]-label becomes the predominate form. Our

labeling experiments were thus done with 12-day-old seedlings so they are well beyond the “auxin autotropic” stage based on [^{15}N]-incorporation.

Previous studies using isotopic labeling measured label incorporation after hours (3 or 6 hrs, Tivendale et al. 2010; 6, 10, 21 hrs, Nonhebel et al. 1993) or days (3 or 6 days, Bialek et al. 1992; 19 days, Glawischnig et al. 2000) which has the potential to complicate data interpretation for a complex pathway where rates of reactions are potentially much faster than the analysis times (Tam et al., 1995). The goals of this current research were to develop a procedure where labeling times could be reduced, and the kinetics of labeling could be measured over relatively short time intervals.

By labeling plants with [$^{13}C_6$]anthranilate, the appearance of [$^{13}C_6$]IAA could be detected after 1 hour of incubation (Figure 4-2), with little or no change in the [$^{15}N_1$]IAA pool except for a decline immediately upon transfer to the label. Labeling from [$^{13}C_6$]anthranilate into IAA was reduced by treatment with the monooxygenase inhibitor YDF (Figure 4-2). Labeling with [$^{13}C_8$,$^{15}N_1$]indole was more rapid than labeling with [$^{13}C_6$]anthranilate, suggesting perhaps more rapid uptake as might be expected for a lipid soluble compound. Interestingly, YDF had little effect on the incorporation of label into [$^{13}C_8$,$^{15}N_1$]IAA (Figure 4-3). This is similar to what we previously reported after a longer-term incubation (Tillmann et al., 2022) but without time resolved data. The effect of IPyA pathway inhibition by both the tryptophan amino transferase inhibitor PVM2153 and the monooxygenase inhibitor YDF was more pronounced than YDF alone, with little incorporation of ^{13}C into IAA from [$^{13}C_6$]anthranilate labeling even after 4 hours with both inhibitors (Figure 4-4). With [$^{13}C_8$,$^{15}N_1$]indole and both inhibitors, labeling of IAA was reduced more than with YDF alone, but still not as pronounced as with [$^{13}C_6$]anthranilate (Figure 4-5).

Inhibition of the biosynthesis of tryptophan as well as reactions related to tryptophan is complex in plants in part because indolic compounds and derivatives are often accumulated as part of the biotic resistance system (Erb & Kliebenstein, 2020). In addition to two gene copies encoding most of the enzymes involved in the conversion of anthranilate to tryptophan, including tryptophan synthase (TS) α and β subunits,

Arabidopsis has the TSα-like indole synthase (INS), a type2 AtTSβ protein, and an undefined AtTSβtype1 (Zhang et al., 2008; Yin et al., 2010; Wang et al., 2015; Nonhebel, 2015; Liu et al., 2018). A number of different inhibitors are known for the canonical TSαββα heterotetramer (Tillmann et al., 2021), however, such metabolic modulators have not been explored as to how they alter the activities of INS, nor standalone type1 and type2 AtTSβ proteins. Nevertheless, compounds that inhibit the activity of these early steps related to IAA metabolism have promise for further analysis of the precursors involved in the pathways. In a proof-of-concept study we used a well-established inhibitor of TS, an arylsulfide phosphonate (I26; [4-[(2-aminophenyl) sulfanyl]butyl] phosphonic acid) that was originally designed as a transition state analog targeting TSα. TS inhibitors are, however, well known to exert pleiotropic effects across the TSαββα heterotetramer due to complex allosteric interactions and little is known about their effects on the TSα-like INS enzyme, AtTSβtype2 or AtTSβtype1 (Yin et al., 2010). As shown in Figure 4-6, I26 essentially blocks new Trp synthesis from [$^{13}C_6$]anthranilate over a 17 h period with a more measured inhibition on the levels of [$^{15}N_2$]Trp (Figure 4-6 insert) as would be predicted for a TSα inhibitor. I26 also, however, markedly inhibits Trp synthesis from [$^{13}C_8$,$^{15}N_1$]indole (Figure 4-7) as well as from endogenously derived indole/serine to form [$^{15}N_2$]Trp (Figure 4-7 insert). This result is not expected based on the first reports on I26 and its predicted mechanism. Nevertheless because, as discussed in Michalska et al. (2020), TSαβ is allosterically regulated by the physical switching of the α- and β-subunits between an open low activity confirmation and a closed high activity conformation, interaction between TSαβ can be complex. In their open conformations, active sites are freely accessible to supplied substrates while in their closed states, sites are inaccessible to external substrates. While this switching normally prevents the escape of the intermediate, indole, produced by the α subunit, “locking” the TSα in the closed confirmation could block supplied labeled indole from entry. Such an inhibitory mechanism was first postulated based on the protein structures in the presence of aryl sulfonamides, also proposed as TSα inhibitors (Hilario et al., 2016; Ngo et al., 2007). These structures showed the α and β subunits in closed conformations with blocked access into the α and β sites in the presence of inhibitors. Interestingly, the inhibition pattern seen with Trp labeling is recapitulated with IAA; the

low level of [$^{13}C_6$]anthranilate labeling of IAA is reduced to essentially zero by I26 (Figure 4-8) and [$^{13}C_8$,$^{15}N_1$]indole labeling is also reduced to near zero (Figure 4-9). This might seem in contrast with the data in Figure 4-3 and Figure 4-5 which show significant [$^{13}C_8$,$^{15}N_1$]indole labeling of IAA when the predominate Trp pathway to IAA (Tillmann et al., 2022), the IPyA pathway, is blocked. However, there are several possible explanations for the data. First, TS could be involved in both Trp-dependent and Trp-independent IAA biosynthesis, although data from Trp auxotrophic mutants would suggest otherwise (reviewed in Tivendale et al., 2014). Indole-3-glycerol-phosphate (IGP) could be the precursor to IAA. Its formation by a reverse activity of any TSα-like enzyme would be expected to be inhibited by I26 as described for the forward reaction. Finally, an enzyme activity that forms a product important for IAA biosynthesis from indole could be a secondary target for inhibition by this allosteric mimic.

Stable isotope labeling followed by high resolution LC-MS/MS analysis is a powerful technique that can be used effectively to investigate labeling kinetics between multiple experimental groups and in tissues exposed to effectors of metabolic pathway activities. Determining relative changes to specific steps over short time intervals in a less well characterized metabolic pathway can aid in the understanding of how specific steps respond to disruptions, especially in steps catalyzed by multiple enzymes with similar and overlapping functions. These technologies can be easily adapted to measure processes in particular cellular fractions to determine in real-time cellular compartment dynamics. Similarly, stable isotopes allow the methods to be extended to be used in dynamic pulse-chase experimental designs followed by LC-MS/MS in order to investigate individual compound turnover.

Tables and figures

Table 4-1: Chemical inhibitors used for auxin biosynthetic pathway analysis

Inhibitor name	Representative structure(s)	Chemical structures	Target	Mode of action	Reference
Yucasin DF (YDF)	5-[2,6-difluorophenyl]-2,4-dihydro-[1,2,4]-triazole-3-thione	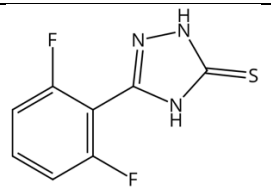	YUCCA	Competitive inhibitor	Tsugafune et al., 2017
Pyruvamines (PVM) "Type II compounds" (Derivatives of Type I compounds)	PVM2153; Benzene propanoic acid, 3,4-dichloro-α-[(1,3-dihydro-1,3-dioxo-2H-isoindol-2-yl)oxy]-methyl ester	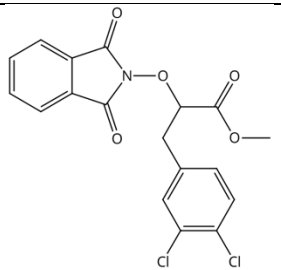	TAA1	Competitive inhibitor	Narukawa-Nara et al., 2016
Arylsulfide phosphonates	I26; RHA41161; [4-[(2-amino phenyl)sulfanyl] butyl]phosphonic acid	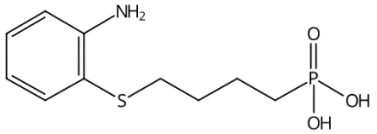	Trp synthase α	Transition state analog	Finn et al., 1999 ; Dias et al., 2006

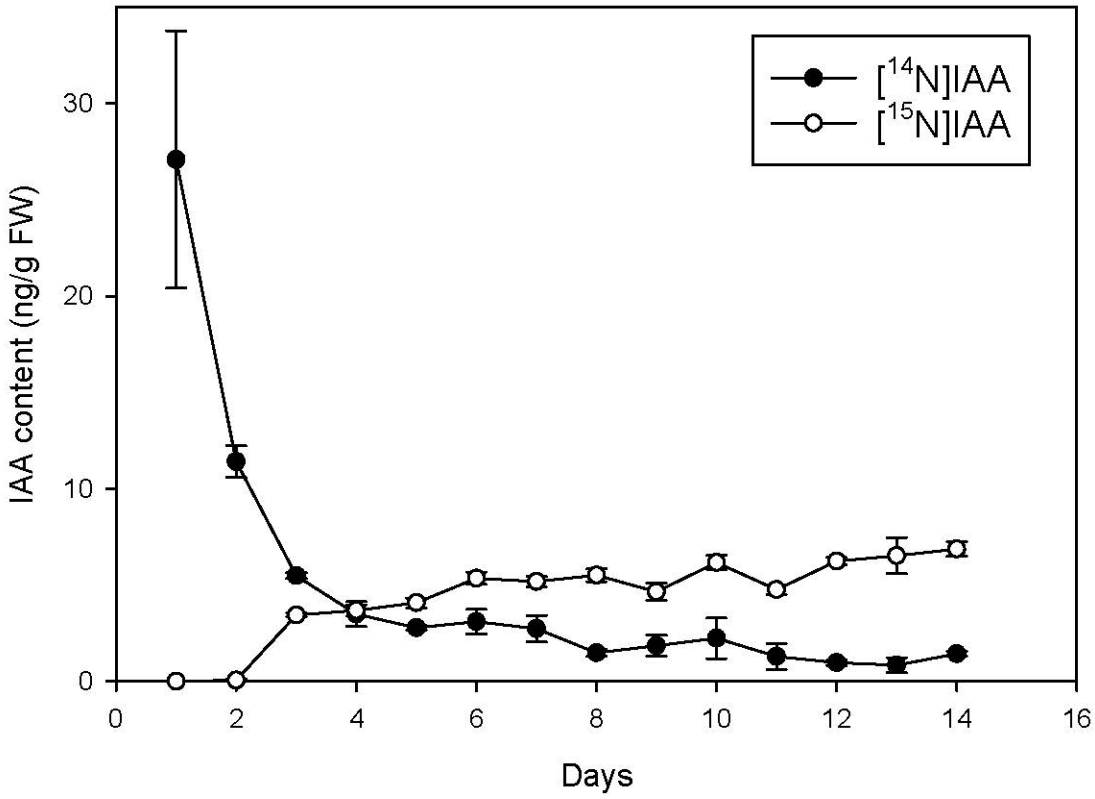

Figure 4-1: *De novo* IAA biosynthesis in Arabidopsis seed germination. Seeds were germinated on [^{15}N] ATS media under 10/14-h photoperiod, 89 μmol m^{-2} s^{-1} white light at 22°C. 5-20 mg of seedlings were collected every day for 14 days followed by LC-MS/MS. Unlabeled and [$^{15}N_1$]IAA were quantified by isotope dilution using [$^{13}C_6$]IAA internal standard. Each point represents the mean of 5 biological replicates; error bars represent SE.

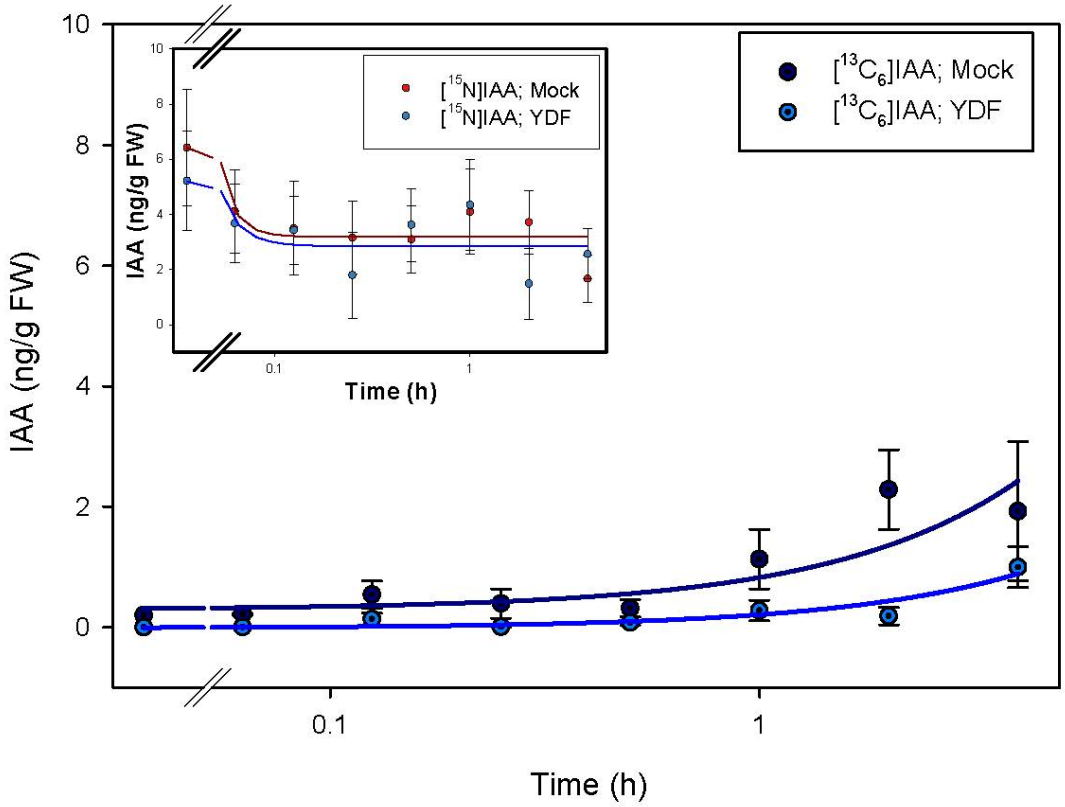

Figure 4-2: [$^{13}C_6$]anthranilate labeling patterns of IAA in Arabidopsis seedlings treated with YDF. Seedling were grown on [^{15}N] ATS media under 10/14-h photoperiod, 103 µmol m^{-2} s^{-1} white light at 22°C for 12 days, then transferred onto [^{15}N] ATS media containing 100 µM YDF or DMSO (mock). After 20 hours seedling were treated by applying to the inhibitor or mock plates ATS solution containing 500 µM [$^{13}C_6$]anthranilate. 20-30 mg of seedlings were collected at time points from 0-4 hours, then subject to LC-MS/MS analysis. [$^{15}N_1$]IAA and [$^{13}C_6$]IAA were quantified by isotope dilution using [$^{2}H_4$]IAA internal standard. Each point represents the mean of 3 biological replicates; error bars represent SE. Fitted lines were drawn using SigmaPlot 14.0 Dynamic Regression standard curve and four parameter procedures.

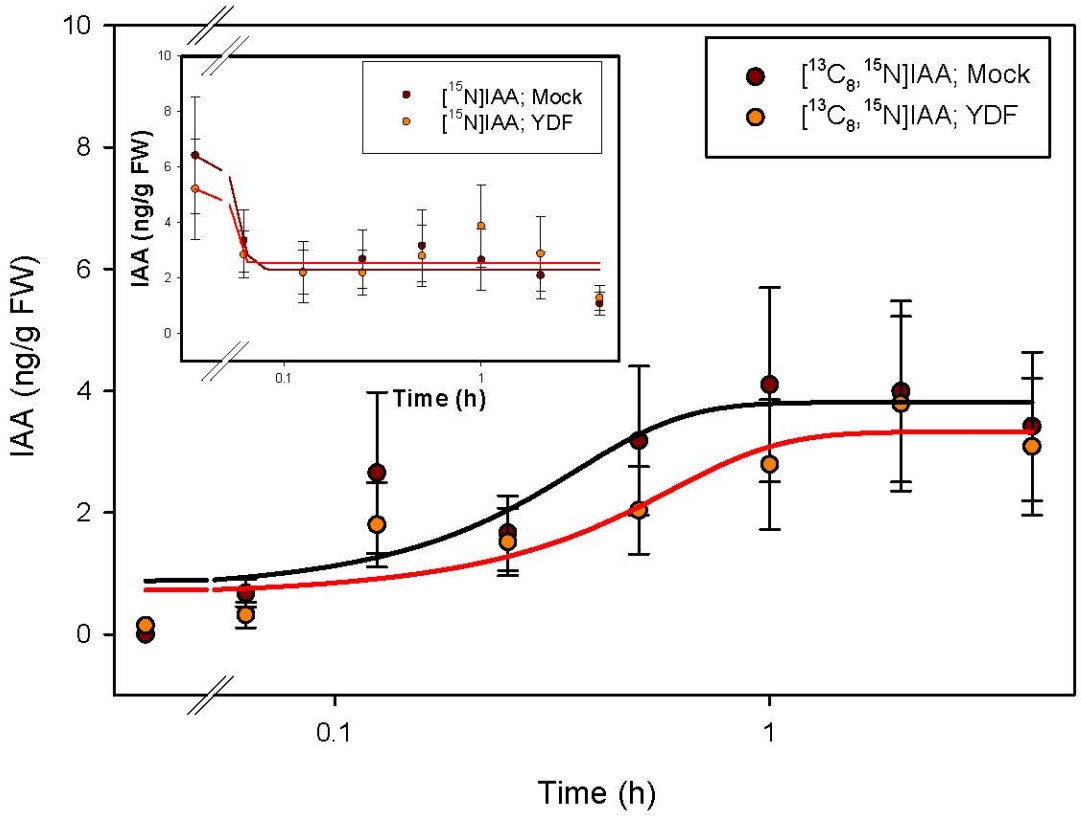

Figure 4-3: [$^{13}C_8$,$^{15}N_1$]indole labeling patterns of IAA in Arabidopsis **seedlings treated with YDF.** Seedling were grown on [^{15}N] ATS media under 10/14-h photoperiod, 103 µmol m^{-2} s^{-1} white light at 22°C for 12 days, then transferred onto [^{15}N] ATS media containing 100 µM YDF or DMSO (mock). After 20 hours seedling were treated by applying to the inhibitor or mock plates ATS solution containing 500 µM [$^{13}C_8$,$^{15}N_1$]indole. 20-30 mg of seedlings were collected at time points from 0-4 hours, then subject to LC-MS/MS analysis. [$^{15}N_1$]IAA and [$^{13}C_8$,$^{15}N_1$]IAA were quantified by isotope dilution using [$^{2}H_4$]IAA internal standard. Each point represents the mean of 3 biological replicates; error bars represent SE. Fitted lines were drawn using SigmaPlot 14.0 Dynamic Regression with sigmoid 3 and with four parameter procedures.

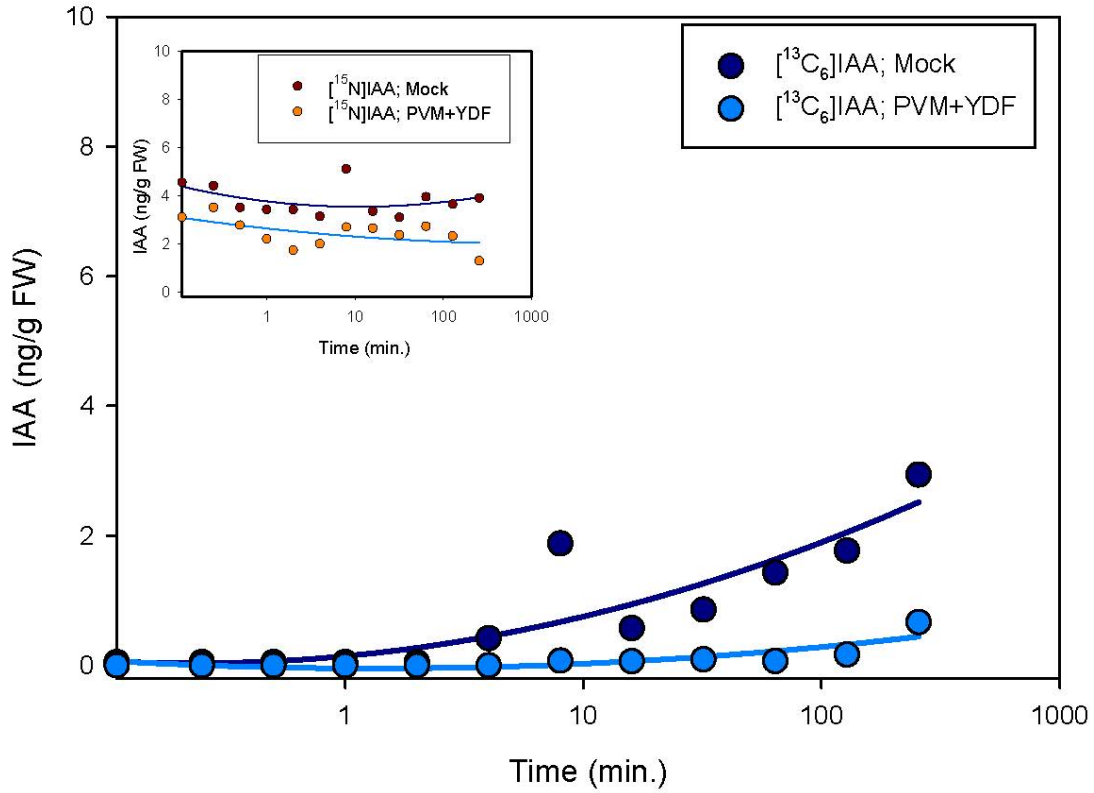

Figure 4-4: [$^{13}C_6$]anthranilate labeling patterns of IAA in Arabidopsis seedlings in the presence of IPyA pathway inhibitors. Seedling were grown on [^{15}N] ATS media under 10/14-h photoperiod, 103 µmol m^{-2} s^{-1} white light at 22°C for 12 days, then transferred onto [^{15}N] ATS media containing 100 µM YDF and 30 µM PVM2153, or DMSO and acetonitrile (mock). After 26 hours seedling were treated by applying to the inhibitor or mock plates ATS solution containing 500 µM [$^{13}C_6$]anthranilate. 20-30 mg of seedlings were collected at time points from 0-4 hours, then subject to LC-MS/MS analysis. [$^{15}N_1$]IAA and [$^{13}C_6$]IAA were quantified by isotope dilution using [$^{2}H_4$]IAA internal standard. Fitted lines were drawn using SigmaPlot 14.0 Dynamic Regression standard curve procedures.

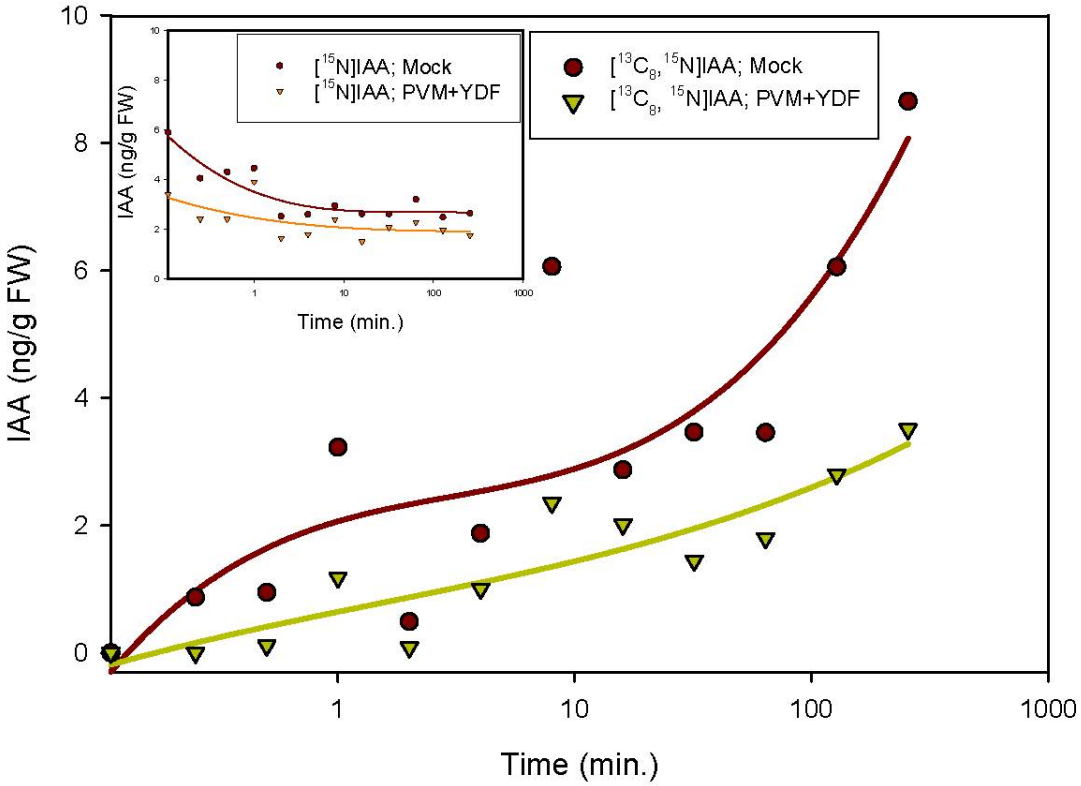

Figure 4-5: [$^{13}C_8$,$^{15}N_1$]indole labeling patterns of IAA in Arabidopsis seedlings in the presence of IPyA pathway inhibitors. Seedling were grown on [^{15}N] ATS media under 10/14-h photoperiod, 103 µmol m^{-2} s^{-1} white light at 22°C for 12 days, then transferred onto [^{15}N] ATS media containing 100 µM YDF and 30 µM PVM2153, or DMSO and acetonitrile (mock). After 20 hours seedling were treated by applying to the inhibitor or mock plates ATS solution containing 500 µM [$^{13}C_8$,$^{15}N_1$]indole. 20-30 mg of seedlings were collected at time points from 0-4 hours, then subject to LC-MS/MS analysis. [$^{15}N_1$]IAA and [$^{13}C_8$,$^{15}N_1$]IAA were quantified by isotope dilution using [$^{2}H_4$]IAA internal standard. Fitted lines were drawn using SigmaPlot 14.0 Dynamic Regression standard curve procedures.

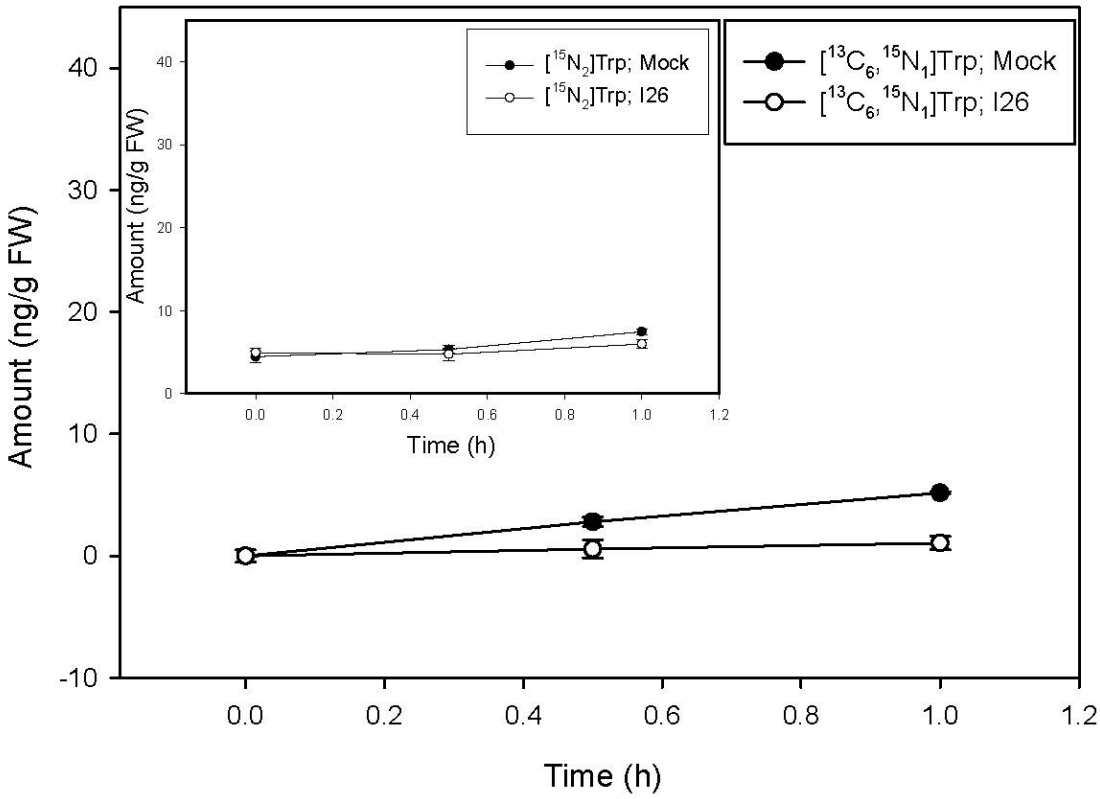

Figure 4-6: [$^{13}C_6$]anthranilate labeling patterns of Trp in Arabidopsis seedlings in the presence of TSα inhibitor compound 26 (arylsulfide phosphonate). Seedling were grown on [^{15}N] ATS media under 10/14-h photoperiod, 103 µmol m^{-2} s^{-1} white light at 22°C for 12 days, then transferred onto [^{15}N] ATS media containing 50 uM compound 26 or DMSO (mock). After 23 hours seedling were treated by applying to the inhibitor or mock plates ATS solution containing 500 µM [$^{13}C_6$]anthranilate. 20-30 mg of seedlings were collected at 0, 30 and 60 minutes, then subject to LC-MS analysis. [$^{15}N_2$]Trp and [$^{13}C_6$,$^{15}N_1$]Trp were quantified by using a linear regression approach employing the XCMS package in R. Each point represents the mean of 3 biological replicates; error bars represent SE.

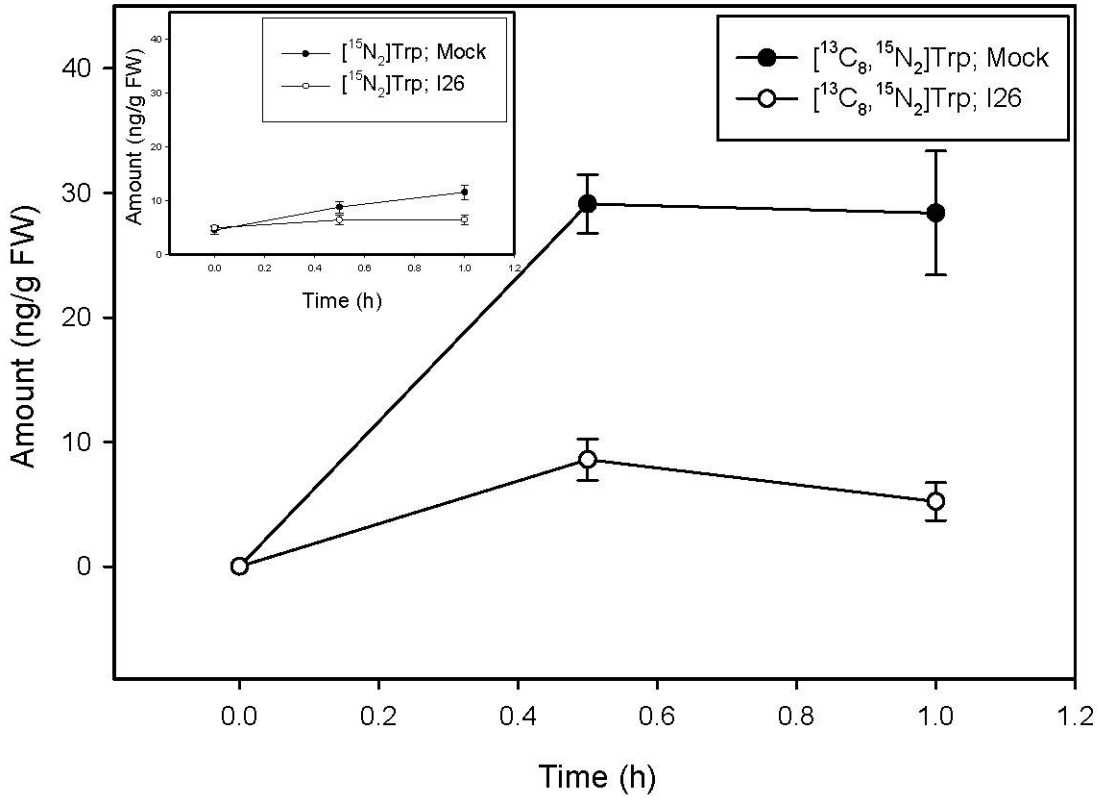

Figure 4-7: [$^{13}C_8$,$^{15}N_1$]indole labeling patterns of Trp in Arabidopsis seedlings in the presence of TSα inhibitor compound 26 (arylsulfide phosphonate). Seedling were grown on [^{15}N] ATS media under 10/14-h photoperiod, 103 μmol m^{-2} s^{-1} white light at 22°C for 12 days, then transferred onto [^{15}N] ATS media containing 50 uM compound 26 or DMSO (mock). After 23 hours seedling were treated by applying to the inhibitor or mock plates ATS solution containing 500 μM [$^{13}C_8$,$^{15}N_1$]indole. 20-30 mg of seedlings were collected at 0, 30 and 60 minutes, then subject to LC-MS analysis. [$^{15}N_2$]Trp and [$^{13}C_8$,$^{15}N_2$]Trp were quantified by using a linear regression approach employing the XCMS package in R. Each point represents the mean of 3 biological replicates; error bars represent SE.

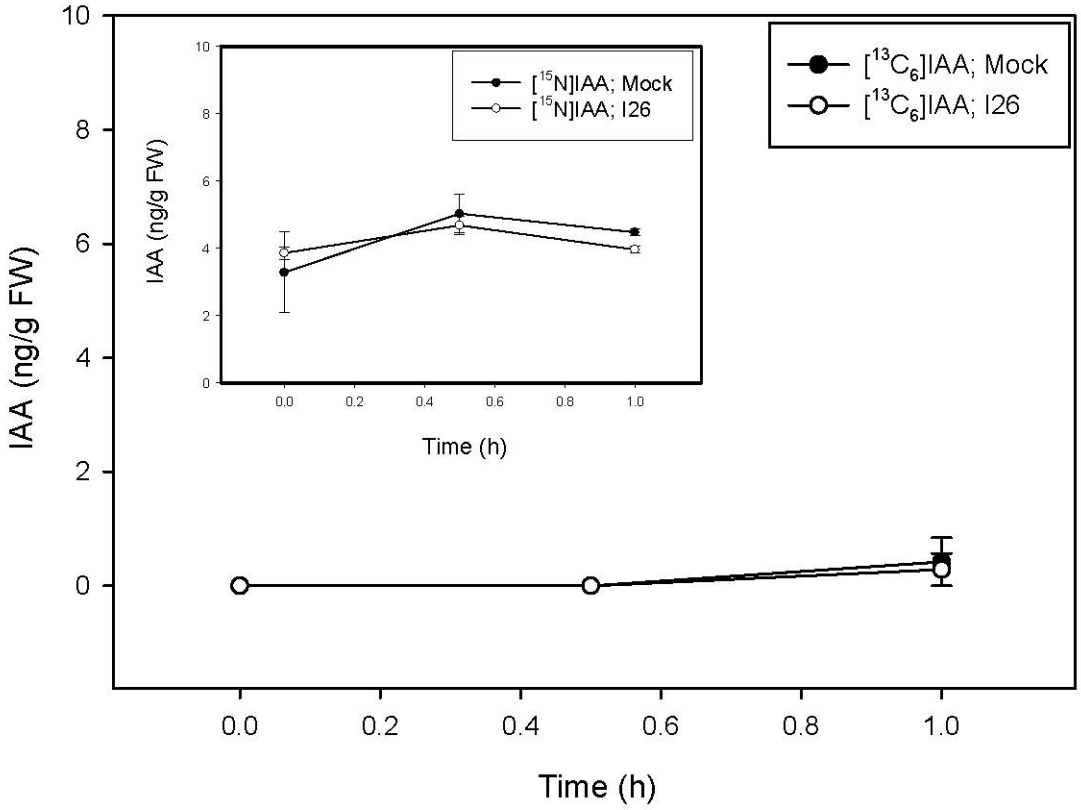

Figure 4-8: [$^{13}C_6$]anthranilate labeling patterns of IAA in Arabidopsis seedlings in the presence of TSα inhibitor compound 26 (arylsulfide phosphonate). Seedling were grown on [^{15}N] ATS media under 10/14-h photoperiod, 103 µmol m^{-2} s^{-1} white light at 22°C for 12 days, then transferred onto [^{15}N] ATS media containing 50 uM compound 26 or DMSO (mock). After 23 hours seedling were treated by applying to the inhibitor or mock plates ATS solution containing 500 µM [$^{13}C_6$]anthranilate. 20-30 mg of seedlings were collected at 0, 30 and 60 minutes, then subject to LC-MS analysis. [$^{15}N_1$]IAA and [$^{13}C_6$]IAA were quantified by isotope dilution using [$^{2}H_4$]IAA internal standard. Each point represents the mean of 3 biological replicates; error bars represent SE.

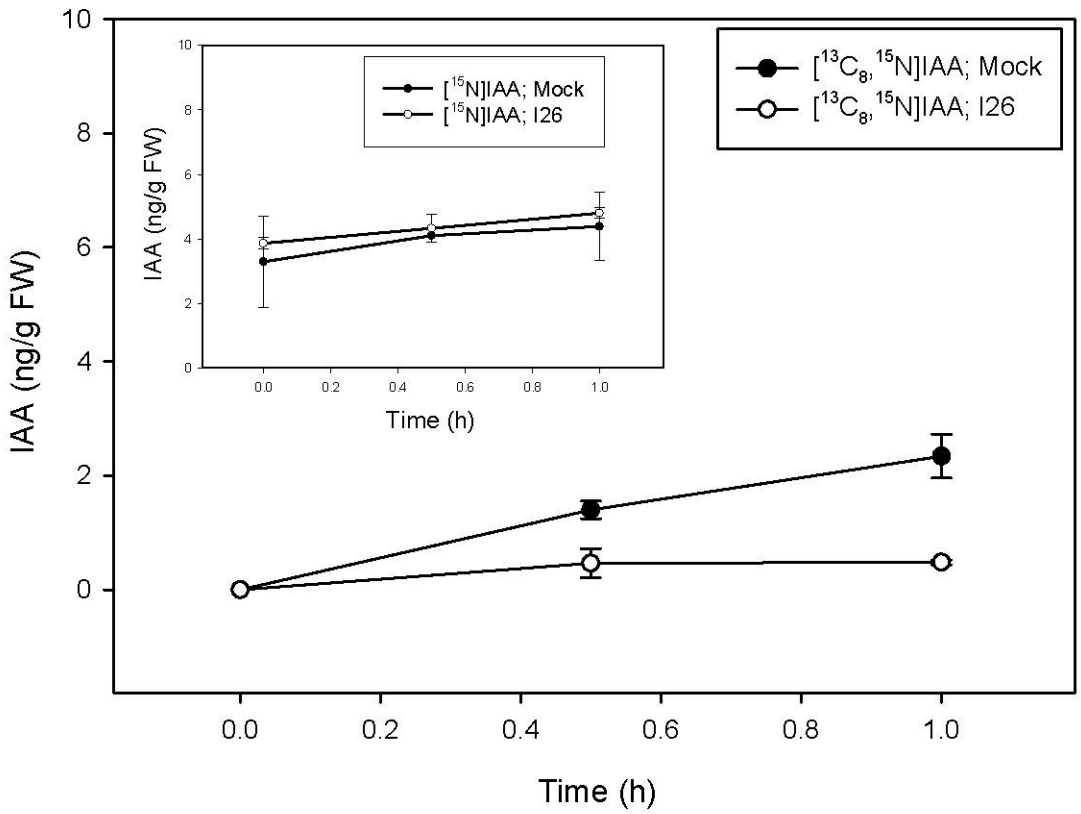

Figure 4-9: [$^{13}C_8$,$^{15}N_1$]indole labeling patterns of IAA in Arabidopsis seedlings in the presence of TSα inhibitor compound 26 (arylsulfide phosphonate). Seedling were grown on [^{15}N] ATS media under 10/14-h photoperiod, 103 µmol m^{-2} s^{-1} white light at 22°C for 12 days, then transferred onto [^{15}N] ATS media containing 50 uM compound 26 or DMSO (mock). After 23 hours seedling were treated by applying to the inhibitor or mock plates ATS solution containing 500 µM [$^{13}C_8$,$^{15}N_1$]indole. 20-30 mg of seedlings were collected at 0, 30 and 60 minutes, then subject to LC-MS analysis. [$^{15}N_1$]IAA and [$^{13}C_8$,$^{15}N_1$]IAA were quantified by isotope dilution using [$^2H_4$]IAA internal standard. Each point represents the mean of 3 biological replicates; error bars represent SE.

Chapter 5. Conclusion

The phytohormone auxin plays central roles throughout all developmental stages of a plant and facilitates its adaptation to different growth environments. Auxin homeostasis involves a complex metabolic interaction including biosynthesis, conjugation, catabolism and transport. Despite recent progress in elucidating biochemical pathways leading to the primary auxin, indole-3-acetic acid (IAA), the utilization of intermediates and the dynamic regulation of the proposed pathways in response to different environmental stimuli remain unknow. In Chapter 2, a highly sensitive and selective mass spectrometric method was used to identify low molecular weight indole-auxin amino acid conjugates in achenes of *F. vesca*. I found that indole-3-acetylaspartate (IAasp) and indole-3-acetylgutamate (IAglu) are the most abundant IAA amino acid conjugates in this diploid strawberry achenes. The data also suggest that IAasp and IAglu are auxin precursors that can be hydrolyzed by strawberry seedlings to provide a source of free IAA, in contrast to what had previously been proposed in Arabidopsis that the conjugation of IAA to the amino acids aspartate and glutamate has a sole catabolic role. Recent data suggests the assumption regarding the catabolic-only role in Arabidopsis is also not correct (Guo et al. 2022). To investigate further the utilization of different IAA biosynthetic pathways under various environmental conditions and developmental stages, I describe in Chapter 3 methods for monitoring incorporation of stable isotopes from labeled precursors into proposed intermediates. The application of chemical inhibitors aids to target specific steps or entire pathways of auxin biosynthesis. These methods were adapted, as described in Chapter 4, to survey dynamic changes in IAA metabolic pathways in Arabidopsis seedlings employing the Stable Isotope Labeled Kinetics (SILK) methods. The SILK approach was specifically developed to monitor the turnover rates of intermediates and IAA concurrently with a time scale of seconds to minutes. Altogether, the new protocols described in this thesis can be used to investigate this complex IAA metabolic network in greater detail in different plant tissues and under various environmental conditions.

In addition, this study of auxin metabolic pathways provides valuable insights into a number of biological questions. First of all, the fate of auxin amino acid conjugation

remains uncertain in different plant species, therefore it will be important to investigate when and where the hydrolysis of conjugates occurs and how this impacts plant growth. Secondly, auxin biosynthesis can be analyzed and/or redirected towards the step or pathway of interest by the application of different stable isotope labeled precursors and with chemical inhibitors. It is thus possible to identify and characterize novel intermediates and pathways implicated in auxin metabolic network. Finally, with the high sensitivity/high resolution LC-MS instrumentation, rapid measurements of the changing indolic profile over time will provide auxin metabolic flux information which allows for understanding how plants regulate the entire pathways at specific developmental stages with both spatial and temporal resolution.

Bibliography

Abrahams KA, Cox JA, Fütterer K, Rullas J, Ortega-Muro F, Loman NJ, Moynihan PJ, Pérez-Herrán E, Jiménez E, Esquivias J. (2017). Inhibiting mycobacterial tryptophan synthase by targeting the inter-subunit interface. *Scientific Reports*, *7*(1), 1–15. https://doi.org/10.1038/s41598-017-09642-y

Aharoni A, O'Connell AP. (2002). Gene expression analysis of strawberry achene and receptacle maturation using DNA microarrays. *Journal of Experimental Botany*, *53*(377), 2073–2087. https://doi.org/10.1093/jxb/erf026

Ahmad A, Eelnurme I, Spenser ID. (1960). Indolyl-3-acetaldoxime. *Canadian Journal of Chemistry*, *38*(12), 2523–2523. https://doi.org/10.1139/v60-342

Aleš Pěnčík, Simonovik B, Petersson SV, Henyková E, Simon S, Greenham K, Zhang Y, Kowalczyk M, Estelle M, Zazímalová E, Novák O, Sandberg G, Ljung K. (2013). Regulation of auxin homeostasis and gradients in Arabidopsis roots through the formation of the indole-3-acetic acid catabolite 2-oxindole-3-acetic acid. *The Plant Cell*, *25*(10), 3858–3870. https://doi.org/10.1105/tpc.113.114421

Altschul SF, Madden TL, Schäffer AA, Zhang J, Zhang Z, Miller W, Lipman DJ. (1997). Gapped BLAST and PSI-BLAST: a new generation of protein database search programs. *Nucleic Acids Research*, *25*(17), 3389–3402. https://doi.org/10.1093/nar/25.17.3389

Archbold D, Jr. FD. (1984). Quantification of free ABA and free and conjugated IAA in strawberry achene and receptacle tissue during fruit development. *Journal of the American Society for Horticultural Science*, *109*(3), 330–335.

Archbold D, Jr FD. (1985). Strawberry receptacle growth and endogenous IAA content as affected by growth regulator application and achene removal. *Journal of the American Society for Horticultural Science (USA)*.

Baldi BG, Maher BR, Slovin JP, Cohen JD. (1991). Stable isotope labeling, in vivo, of D- and L-tryptophan pools in *Lemna gibba* and the low incorporation of label into indole-3-acetic acid. *Plant Physiology*, *95*(4), 1203–1208. https://doi.org/10.1104/pp.95.4.1203

Barkawi LS, Cohen JD. (2010). A method for concurrent diazomethane synthesis and substrate methylation in a 96-sample format. *Nature Protocols*, *5*(10), 1619–1626. https://doi.org/10.1038/nprot.2010.119

Barkawi LS, Tam Y-Y, Tillman JA, Normanly J, Cohen JD. (2010). A high-throughput method for the quantitative analysis of auxins. *Nature Protocols*, *5*(10), 1609–1618. https://doi.org/10.1038/nprot.2010.118

Bartel B, Fink GR. (1995). ILR1, an amidohydrolase that releases active indole-3-acetic acid from conjugates. *Science*, *268*(5218), 1745–1748. https://doi.org/10.1126/science.7792599

Bartel B, LeClere S, Magidin M, Zolman BK. (2001). Inputs to the active indole-3-acetic acid pool: de novo synthesis, conjugate hydrolysis, and indole-3-butyric acid β-oxidation. *Journal of Plant Growth Regulation*, *20*(3), 198–216. https://doi.org/10.1007/s003440010025

Bateman RJ, West T, Yarasheski K, Patterson BW, Lucey B, Cirrito JR, Lehmann S, Hirtz C, Gabelle A, Miller T, Barthelemy N, Sato C, Bollinger JG, Kotzbauer P, Paumier K. (2019). Chapter 11 - Stable isotope labeling kinetics in CNS translational medicine: introduction to SILK technology. *Handbook of Behavioral Neuroscience*, *29*, 173–190. https://doi.org/10.1016/b978-0-12-803161-2.00011-4

Bialek K, Michalczuk L, Cohen JD. (1992). Auxin biosynthesis during seed germination in *Phaseolus vulgaris*. *Plant Physiology*, *100*(1), 509–517. https://doi.org/10.1104/pp.100.1.509

Bloch K, Anker H. (1948). An extension of the isotope dilution method. *Science*, *107*(2774), 228. https://doi.org/10.1126/science.107.2774.228

Calderon-Villalobos LI, Tan X, Zheng N, Estelle M. (2010). Auxin perception--structural insights. *Cold Spring Harbor Perspectives in Biology*, *2*(7), a005546–a005546. https://doi.org/10.1101/cshperspect.a005546

Campanella JJ, Larko D, Smalley J. (2003). A molecular phylogenomic analysis of the ILR1-like family of IAA amidohydrolase genes. *Comparative and Functional Genomics*, *4*(6), 584–600. https://doi.org/10.1002/cfg.340

Campanella JJ, Sigethy S, Ludwig-Müller J. (2011). Truncation of *Medicago truncatula* auxin conjugate hydrolases alters substrate specificity. *Plant Molecular Biology Reporter*, *29*(3), 745–752. https://doi.org/10.1007/s11105-010-0266-1

Campanella JJ, Smith SM, Leibu D, Wexler S, Ludwig-Müller J. (2008). The auxin conjugate hydrolase family of *Medicago truncatula* and their expression during the interaction with two symbionts. *Journal of Plant Growth Regulation*, *27*(1), 26–38. https://doi.org/10.1007/s00344-007-9027-2

Campanella JJ, Zaben N, Enriquez D, Smalley JV, Ludwig-Müller J. (2014). An enzymatic analysis of loblolly pine and sitka spruce auxin conjugate hydrolases and evolutionary implications. *Acta Horticulturae*, *1042*, 79–88. https://doi.org/10.17660/actahortic.2014.1042.9

Carranza APS, Singh A, Steinberger K, Panigrahi K, Palme K, Dovzhenko A, Bosco CD. (2016). Hydrolases of the ILR1-like family of *Arabidopsis thaliana* modulate auxin response by regulating auxin homeostasis in the endoplasmic reticulum. *Scientific Reports*, *6*(1), 24212. https://doi.org/10.1038/srep24212

Chambers MC, Maclean B, Burke R, Amodei D, Ruderman DL, Neumann S, Gatto L, Fischer B, Pratt B, Egertson J, Hoff K, Kessner D, Tasman N, Shulman N, … Mallick P. (2012). A cross-platform toolkit for mass spectrometry and proteomics. *Nature Biotechnology*, *30*(10), 918–920. https://doi.org/10.1038/nbt.2377

Chandler JW. (2009). Local auxin production: a small contribution to a big field. *BioEssays*, *31*(1), 60–70. https://doi.org/10.1002/bies.080146

Cheng Y, Dai X, Zhao Y. (2007). Auxin synthesized by the YUCCA flavin monooxygenases is essential for embryogenesis and leaf formation in Arabidopsis. *The Plant Cell*, *19*(8), 2430–2439. https://doi.org/10.1105/tpc.107.053009

Chisnell JR, Bandurski RS. (1988). Translocation of radiolabeled indole-3-acetic acid and indole-3-acetyl-myo-inositol from kernel to shoot of *Zea mays L*. *Plant Physiology*, *86*(1), 79–84. https://doi.org/10.1104/pp.86.1.79

Chokkathukalam A, Kim D-H, Barrett MP, Breitling R, Creek DJ. (2014). Stable isotope-labeling studies in metabolomics: new insights into structure and dynamics of metabolic networks. *Bioanalysis*, *6*(4), 511–524. https://doi.org/10.4155/bio.13.348

Chou J-C, Mulbry WW, Cohen JD. (1998). The gene for indole-3-acetyl-L-aspartic acid hydrolase from *Enterobacter agglomerans* : molecular cloning, nucleotide sequence, and expression in *Escherichia coli. Molecular and General Genetics MGG*, *259*(2), 172–178. https://doi.org/10.1007/s004380050802

Chou J-C, Welch WH, Cohen JD. (2004). His-404 and His-405 are essential for enzyme catalytic activities of a bacterial indole-3-acetyl-L-aspartic acid hydrolase. *Plant and Cell Physiology*, *45*(9), 1335–1341. https://doi.org/10.1093/pcp/pch153

Cohen J, Baldi B. (1983). Studies of endogenous indole-3-acetyl-L-aspartate during germination of soybeans. *Quarterly (Plant Growth Regulator Society of America)*, *10*, 117–122.

Cohen JD. (1981). Synthesis of ^{14}C-labeled indole-3-acetylaspartic acid. *Journal of Labelled Compounds and Radiopharmaceuticals*, *18*(9), 1393–1396. https://doi.org/10.1002/jlcr.2580180916

Cohen JD. (1982). Identification and quantitative analysis of indole-3-acetyl-L-aspartate from seeds of *Glycine max L. Plant Physiology*, *70*(3), 749–753. https://doi.org/10.1104/pp.70.3.749

Cohen JD. (1984). Convenient apparatus for the generation of small amounts of diazomethane. *Journal of Chromatography A*, *303*, 193–196. https://doi.org/10.1016/s0021-9673(01)96061-3

Cohen JD, Baldi BG, Slovin JP. (1986). $^{13}C_6$-[benzene ring]-indole-3-acetic acid: a new internal standard for quantitative mass spectral analysis of indole-3-acetic acid in plants. *Plant Physiology*, *80*(1), 14–19. https://doi.org/10.1104/pp.80.1.14

Cohen JD, Bandurski RS. (1978). The bound auxins: protection of indole-3-acetic acid from peroxidase-catalyzed oxidation. *Planta*, *139*(3), 203–208. https://doi.org/10.1007/bf00388631

Cohen JD, Bandurski RS. (1982). Chemistry and physiology of the bound auxins. *Annual Review of Plant Physiology*, *33*(1), 403–430. https://doi.org/10.1146/annurev.pp.33.060182.002155

Cohen JD, Gray WM. (2006). Auxin metabolism and signaling. *Plant Hormone Signaling*, *24*, 37–66. https://doi.org/10.1002/9780470988800.ch2

Cooke TJ, Poli D, Sztein AE, Cohen JD. (2002). Evolutionary patterns in auxin action. In C. Perrot-Rechenmann & G. Hagen (Eds.), *Auxin Molecular Biology* (pp. 319–338). Springer Dordrecht. https://doi.org/10.1007/978-94-010-0377-3_5

Cooney TP, Nonhebel HM. (1991). Biosynthesis of indole-3-acetic acid in tomato shoots: Measurement, mass-spectral identification and incorporation of ^{2}H from $^{2}H_2O$ into indole-3-acetic acid, D- and L-tryptophan, indole-3-pyruvate and tryptamine. *Planta*, *184*(3), 368–376. https://doi.org/10.1007/bf00195339

Darwish O, Slovin JP, Kang C, Hollender CA, Geretz A, Houston S, Liu Z, Alkharouf NW. (2013). SGR: an online genomic resource for the woodland strawberry. *BMC Plant Biology*, *13*(1), 223. https://doi.org/10.1186/1471-2229-13-223

Denecke J, Rycke RD, Botterman J. (1992). Plant and mammalian sorting signals for protein retention in the endoplasmic reticulum contain a conserved epitope. *The EMBO Journal*, *11*(6), 2345–2355. https://doi.org/10.1002/j.1460-2075.1992.tb05294.x

Dias MVB, Canduri F, Silveira NJF da, Czekster CM, Basso LA, Palma MS, Santos DS, Azevedo WF de. (2006). Molecular models of tryptophan synthase from *Mycobacterium tuberculosis* complexed with inhibitors. *Cell Biochemistry and Biophysics*, *44*(3), 375–384. https://doi.org/10.1385/cbb:44:3:375

Dreher T, Poovaiah BW. (1982). Changes in auxin content during development in strawberry fruits. *Journal of Plant Growth Regulation*, *1*, 267–276.

Edger PP, VanBuren R, Colle M, Poorten TJ, Wai CM, Niederhuth CE, Alger EI, Ou S, Acharya CB, Wang J, Callow P, McKain MR, Shi J, Collier C, … Knapp SJ. (2018). Single-molecule sequencing and optical mapping yields an improved genome of woodland strawberry (*Fragaria vesca*) with chromosome-scale contiguity. *GigaScience*, *7*(2), gix124. https://doi.org/10.1093/gigascience/gix124

Ehmann A. (1977). The van URK-Salkowski reagent — a sensitive and specific chromogenic reagent for silica gel thin-layer chromatographic detection and identification of indole derivatives. *Journal of Chromatography A*, *132*(2), 267–276. https://doi.org/10.1016/s0021-9673(00)89300-0

Epstein E, Baldi BG, Cohen JD. (1986). Identification of indole-3-acetylglutamate from seeds of *Glycine max L*. *Plant Physiology*, *80*(1), 256–258. https://doi.org/10.1104/pp.80.1.256

Epstein E, Cohen JD, Slovin JP. (2002). The biosynthetic pathway for indole-3-acetic acid changes during tomato fruit development. *Plant Growth Regulation*, *38*(1), 15–20. https://doi.org/10.1023/a:1020985715478

Erb M, Kliebenstein DJ. (2020). Plant secondary metabolites as defenses, regulators, and primary metabolites: the blurred functional trichotomy. *Plant Physiology*, *184*(1), 39–52. https://doi.org/10.1104/pp.20.00433

Erdmann N, Schiewer U. (1971). Tryptophan-dependent indoleacetic-acid biosynthesis from indole, demonstrated by double-labelling experiments. *Planta*, *97*(2), 135–141. https://doi.org/10.1007/bf00386761

Estrada-Johnson E, Csukasi F, Pizarro CM, Vallarino JG, Kiryakova Y, Vioque A, Brumos J, Medina-Escobar N, Botella MA, Alonso JM, Fernie AR, Sánchez-Sevilla JF, Osorio S, Valpuesta V. (2017). Transcriptomic analysis in strawberry fruits reveals active auxin biosynthesis and signaling in the ripe receptacle. *Frontiers in Plant Science*, *8*, 889. https://doi.org/10.3389/fpls.2017.00889

Evans EM, Freund DM, Sondervan VM, Cohen JD, Hegeman AD. (2018). Metabolic patterns in *Spirodela polyrhiza* revealed by ^{15}N stable isotope labeling of amino acids

in photoautotrophic, heterotrophic, and mixotrophic growth conditions. *Frontiers in Chemistry*, *6*, 191. https://doi.org/10.3389/fchem.2018.00191

Fan K-T, Rendahl AK, Chen W-P, Freund DM, Gray WM, Cohen JD, Hegeman AD. (2016). Proteome scale-protein turnover analysis using high resolution mass spectrometric data from stable-isotope labeled plants. *Journal of Proteome Research*, *15*(3), 851–867. https://doi.org/10.1021/acs.jproteome.5b00772

Finn J, Langevine C, Birk I, Birk J, Nickerson K, Rodaway S. (1999). Rational herbicide design by inhibition of tryptophan biosynthesis. *Bioorganic & Medicinal Chemistry Letters*, *9*(16), 2297–2302. https://doi.org/10.1016/s0960-894x(99)00340-6

Folta KM, Davis TM. (2006). Strawberry Genes and Genomics. *Critical Reviews in Plant Sciences*, *25*(5), 399–415. https://doi.org/10.1080/07352680600824831

Fukui K, Hayashi K. (2018). Manipulation and sensing of auxin metabolism, transport and signaling. *Plant and Cell Physiology*, *59*(8), 1500–1510. https://doi.org/10.1093/pcp/pcy076

Given NK, Venis MA, Gierson D. (1988). Hormonal regulation of ripening in the strawberry, a non-climacteric fruit. *Planta*, *174*(3), 402–406. https://doi.org/10.1007/bf00959527

Glawischnig E, Tomas A, Eisenreich W, Spiteller P, Bacher A, Gierl A. (2000). Auxin biosynthesis in maize kernels. *Plant Physiology*, *123*(3), 1109–1120. https://doi.org/10.1104/pp.123.3.1109

González-Lamothe R, Oirdi ME, Brisson N, Bouarab K. (2012). The conjugated auxin indole-3-acetic acid–aspartic acid promotes plant disease development. *The Plant Cell*, *24*(2), 762–777. https://doi.org/10.1105/tpc.111.095190

Guo R, Hu Y, Aoi Y, Hira H, Ge C, Dai X, Kasahara H, Zhao Y. (2022). Local conjugation of auxin by the GH3 amido synthetases is required for normal development of roots and flowers in Arabidopsis. *Biochemical and Biophysical Research Communications*, *589*, 16–22. https://doi.org/10.1016/j.bbrc.2021.11.109

Hayashi K, Arai K, Aoi Y, Tanaka Y, Hira H, Guo R, Hu Y, Ge C, Zhao Y, Kasahara H, Fukui K. (2021). The main oxidative inactivation pathway of the plant hormone auxin. *Nature Communications*, *12*(1), 6752. https://doi.org/10.1038/s41467-021-27020-1

He W, Brumos J, Li H, Ji Y, Ke M, Gong X, Zeng Q, Li W, Zhang X, An F. (2011). A small-molecule screen identifies L-kynurenine as a competitive inhibitor of TAA1/TAR activity in ethylene-directed auxin biosynthesis and root growth in Arabidopsis. *The Plant Cell*, *23*(11), 3944–3960. https://doi.org/10.1105/tpc.111.089029

Hilario E, Caulkins BG, Huang Y-MM, You W, Chang C-EA, Mueller LJ, Dunn MF, Fan L. (2016). Visualizing the tunnel in tryptophan synthase with crystallography: insights into a selective filter for accommodating indole and rejecting water. *Biochimica et Biophysica Acta (BBA) - Proteins and Proteomics*, *1864*(3), 268–279. https://doi.org/10.1016/j.bbapap.2015.12.006

Horton P, Park K-J, Obayashi T, Fujita N, Harada H, Adams-Collier CJ, Nakai K. (2007). WoLF PSORT: protein localization predictor. *Nucleic Acids Research*, *35*(Web Server issue), W585–W587. https://doi.org/10.1093/nar/gkm259

Huttlin EL, Hegeman AD, Harms AC, Sussman MR. (2007). Comparison of full versus partial metabolic labeling for quantitative proteomics analysis in *Arabidopsis thaliana*. *Molecular & Cellular Proteomics*, *6*(5), 860–881. https://doi.org/10.1074/mcp.m600347-mcp200

Ishimaru K, Hirotsu N, Madoka Y, Murakami N, Hara N, Onodera H, Kashiwagi T, Ujiie K, Shimizu B-I, Onishi A, Miyagawa H, Katoh E. (2013). Loss of function of the IAA-glucose hydrolase gene *TGW6* enhances rice grain weight and increases yield. *Nature Genetics*, *45*(6), 707–711. https://doi.org/10.1038/ng.2612

Iyer M, Slovin JP, Epstein E, Cohen JD. (2005). Transgenic tomato plants with a modified ability to synthesize indole-3-acetyl-β-1-O-D-glucose. *Journal of Plant Growth Regulation*, *24*(2), 142–152. https://doi.org/10.1007/s00344-004-0007-5

Jansky SH, Chung YS, Kittipadukal P. (2014). M6: a diploid potato inbred line for use in breeding and genetics research. *Journal of Plant Registrations*, *8*(2), 195–199. https://doi.org/10.3198/jpr2013.05.0024crg

Jensen PJ, Bandurski RS. (1996). Incorporation of deuterium into indole-3-acetic acid and tryptophan in *Zea mays* seedlings grown on 30% deuterium oxide. *Journal of Plant Physiology*, *147*(6), 697–702. https://doi.org/10.1016/s0176-1617(11)81480-x

Jiang Z, Li J, Qu L-J. (2017). Auxins. *Hormone Metabolism and Signaling in Plants*, 39–76. https://doi.org/10.1016/b978-0-12-811562-6.00002-5

Jin H, Moseley HNB. (2021). Hierarchical harmonization of atom-resolved metabolic reactions across metabolic databases. *Metabolites*, *11*(7), 431. https://doi.org/10.3390/metabo11070431

Jones B, Gunnerås SA, Petersson SV, Tarkowski P, Graham N, May S, Dolezal K, Sandberg G, Ljung K. (2010). Cytokinin regulation of auxin synthesis in Arabidopsis involves a homeostatic feedback loop regulated via auxin and cytokinin signal transduction. *The Plant Cell*, *22*(9), 2956–2969. https://doi.org/10.1105/tpc.110.074856

Jung S, Ficklin SP, Lee T, Cheng C-H, Blenda A, Zheng P, Yu J, Bombarely A, Cho I, Ru S, Evans K, Peace C, Abbott AG, Mueller LA, … Main D. (2014). The Genome Database for Rosaceae (GDR): year 10 update. *Nucleic Acids Research*, *42*(Database issue), D1237–D1244. https://doi.org/10.1093/nar/gkt1012

Kakei Y, Yamazaki C, Suzuki M, Nakamura A, Sato A, Ishida Y, Kikuchi R, Higashi S, Kokudo Y, Ishii T. (2015). Small-molecule auxin inhibitors that target YUCCA are powerful tools for studying auxin function. *The Plant Journal*, *84*(4), 827–837. https://doi.org/10.1111/tpj.13032

Kang C, Darwish O, Geretz A, Shahan R, Alkharouf N, Liu Z. (2013). Genome-scale transcriptomic insights into early-stage fruit development in woodland strawberry *Fragaria vesca*. *The Plant Cell*, *25*(6), 1960–1978. https://doi.org/10.1105/tpc.113.111732

Kohen R, Yamamoto Y, Cundy KC, Ames BN. (1988). Antioxidant activity of carnosine, homocarnosine, and anserine present in muscle and brain. *Proceedings of the National Academy of Sciences*, *85*(9), 3175–3179. https://doi.org/10.1073/pnas.85.9.3175

Korasick DA, Enders TA, Strader LC. (2013). Auxin biosynthesis and storage forms. *Journal of Experimental Botany*, *64*(9), 2541–2555. https://doi.org/10.1093/jxb/ert080

Kowalczyk M, Sandberg G. (2001). Quantitative analysis of indole-3-acetic acid metabolites in Arabidopsis. *Plant Physiology*, *127*(4), 1845–1853. https://doi.org/10.1104/pp.010525

Kramer EM, Ackelsberg EM. (2015). Auxin metabolism rates and implications for plant development. *Frontiers in Plant Science*, *6*, 150. https://doi.org/10.3389/fpls.2015.00150

Kriechbaumer V, Botchway SW, Hawes C. (2017). Localization and interactions between Arabidopsis auxin biosynthetic enzymes in the TAA/YUC-dependent pathway. *Journal of Experimental Botany*, *67*(14), 4195–4207. https://doi.org/10.1093/jxb/erw195

Kumar S, Stecher G, Li M, Knyaz C, Tamura K. (2018). MEGA X: Molecular Evolutionary Genetics Analysis across computing platforms. *Molecular Biology and Evolution*, *35*(6), 1547–1549. https://doi.org/10.1093/molbev/msy096

LeClere S, Tellez R, Rampey RA, Matsuda SPT, Bartel B. (2002). Characterization of a family of IAA-amino acid conjugate hydrolases from Arabidopsis. *Journal of Biological Chemistry*, *277*(23), 20446–20452. https://doi.org/10.1074/jbc.m111955200

Li W, Zhou Y, Liu X, Yu P, Cohen JD, Meyerowitz EM. (2013). LEAFY controls auxin response pathways in floral primordium formation. *Science Signaling*, *6*(270), ra23. https://doi.org/10.1126/scisignal.2003937

Lincoln C, Britton JH, Estelle M. (1990). Growth and development of the axr1 mutants of Arabidopsis. *The Plant Cell*, *2*(11), 1071–1080. https://doi.org/10.1105/tpc.2.11.1071

Lis E. (1974). Uptake and metabolism of sucrose-^{14}C and IAA-1-^{14}C in strawberry fruit explants cultivated in vitro. *Proceedings XIX International Horticultural Congress*, *1A*, 61 (Abstract).

Lis E, Borkowska B,, Antoszewski R. (1978). Growth regulators in the strawberry fruit. *Fruit Science Reports (Skierniewice, Poland)*, *V*, 17–29.

Liu C, Sun Q, Zhao L, Li Z, Peng Z, Zhang J. (2018). Heterologous expression of the transcription factor *EsNAC1* in Arabidopsis enhances abiotic stress resistance and retards growth by regulating the expression of different target genes. *Frontiers in Plant Science*, *9*, 1495. https://doi.org/10.3389/fpls.2018.01495

Liu X, Hegeman AD, Gardner G, Cohen JD. (2012). Protocol: high-throughput and quantitative assays of auxin and auxin precursors from minute tissue samples. *Plant Methods*, *8*(1), 1–17. https://doi.org/10.1186/1746-4811-8-31

Ljung K. (2013). Auxin metabolism and homeostasis during plant development. *Development (Cambridge, England)*, *140*(5), 943–950. https://doi.org/10.1242/dev.086363

Ljung K, Hul AK, Kowalczyk M, Marchant A, Celenza J, Cohen JD, Sandberg G. (2002). Biosynthesis, conjugation, catabolism and homeostasis of indole-3-acetic acid in *Arabidopsis thaliana*. *Plant Molecular Biology*, *50*(2), 309–332. https://doi.org/10.1023/a:1016024017872

Ljung K, Hull AK, Celenza J, Yamada M, Estelle M, Normanly J, Sandberg G. (2005). Sites and regulation of auxin biosynthesis in Arabidopsis roots. *The Plant Cell*, *17*(4), 1090–1104. https://doi.org/10.1105/tpc.104.029272

Ljung K, Östin A, Lioussanne L, Sandberg G. (2001). Developmental regulation of indole-3-acetic acid turnover in Scots pine seedlings. *Plant Physiology*, *125*(1), 464–475. https://doi.org/10.1104/pp.125.1.464

Magnus V, Bandurski RS, Schulze A. (1980). Synthesis of 4,5,6,7 and 2,4,5,6,7 deuterium-labeled indole-3-acetic acid for use in mass spectrometric assays. *Plant Physiology*, *66*(4), 775–781. https://doi.org/10.1104/pp.66.4.775

Marabotti A, Cozzini P, Mozzarelli A. (2000). Novel allosteric effectors of the tryptophan synthase α2β2 complex identified by computer-assisted molecular modeling. *Biochimica et Biophysica Acta (BBA)-Protein Structure and Molecular Enzymology*, *1476*(2), 287–299. https://doi.org/10.1016/s0167-4838(99)00242-3

Mashiguchi K, Tanaka K, Sakai T, Sugawara S, Kawaide H, Natsume M, Hanada A, Yaeno T, Shirasu K, Yao H. (2011). The main auxin biosynthesis pathway in Arabidopsis. *Proceedings of the National Academy of Sciences*, *108*(45), 18512–18517. https://doi.org/10.1073/pnas.1108434108

Matchett WH. (1972). Inhibition of tryptophan synthetase by indoleacrylic acid. *Journal of Bacteriology*, *110*(1), 146–154. https://doi.org/10.1128/jb.110.1.146-154.1972

Michalska K, Chang C, Maltseva NI, Jedrzejczak R, Robertson GT, Gusovsky F, McCarren P, Schreiber SL, Nag PP, Joachimiak A. (2020). Allosteric inhibitors of *Mycobacterium tuberculosis* tryptophan synthase. *Protein Science*, *29*(3), 779–788. https://doi.org/10.1002/pro.3825

Morrow E. (1954). A quick method of cleaning berry seed for breeders. *Proc. Amer. Soc. Hort. Sci.*, *63*, 265.

Müntz K, Becker C, Pancke J, Schlereth A, Fischer J, Horstmann C, Kirkin V, Neubohn B, Senyuk V, Shutov A. (1998). Protein degradation and nitrogen supply during germination and seedling growth of vetch (*Vicia sativa L.*). *Journal of Plant Physiology*, *152*(6), 683–691. https://doi.org/10.1016/s0176-1617(98)80030-8

Narukawa-Nara M, Nakamura A, Kikuzato K, Kakei Y, Sato A, Mitani Y, Yamasaki-Kokudo Y, Ishii T, Hayashi K, Asami T. (2016). Aminooxy-naphthylpropionic acid and its derivatives are inhibitors of auxin biosynthesis targeting L-tryptophan aminotransferase: structure–activity relationships. *The Plant Journal*, *87*(3), 245–257. https://doi.org/10.1111/tpj.13197

Naz S, Farooq U, Ali S, Sarwar R, Khan S, Abagyan R. (2019). Identification of new benzamide inhibitor against α-subunit of tryptophan synthase from *Mycobacterium tuberculosis* through structure-based virtual screening, anti-tuberculosis activity and molecular dynamics simulations. *Journal of Biomolecular Structure and Dynamics*, *37*(4), 1–24. https://doi.org/10.1080/07391102.2018.1448303

Ngo H, Harris R, Kimmich N, Casino P, Niks D, Blumenstein L, Barends TR, Kulik V, Weyand M, Schlichting I. (2007). Synthesis and characterization of allosteric probes of substrate channeling in the tryptophan synthase bienzyme complex. *Biochemistry*, *46*(26), 7713–7727. https://doi.org/10.1021/bi700385f

Ngo H, Kimmich N, Harris R, Niks D, Blumenstein L, Kulik V, Barends TR, Schlichting I, Dunn MF. (2007). Allosteric regulation of substrate channeling in tryptophan synthase: modulation of the L-serine reaction in stage I of the beta-reaction by alpha-site ligands. *Biochemistry*, *46*(26), 7740–7753. https://doi.org/10.1021/bi7003872

Nishimura T, Hayashi K, Suzuki H, Gyohda A, Takaoka C, Sakaguchi Y, Matsumoto S, Kasahara H, Sakai T, Kato J. (2014). Yucasin is a potent inhibitor of YUCCA, a key enzyme in auxin biosynthesis. *The Plant Journal*, *77*(3), 352–366. https://doi.org/10.1111/tpj.12399

Nishimura T, Nakano H, Hayashi K, Niwa C, Koshiba T. (2009). Differential downward stream of auxin synthesized at the tip has a key role in gravitropic curvature via TIR1/AFBs-mediated auxin signaling pathways. *Plant and Cell Physiology*, *50*(11), 1874–1885. https://doi.org/10.1093/pcp/pcp129

Nitsch JP. (1950). Growth and morphogenesis of strawberries as related to auxin. *American Journal of Botany*, *37*(3), 211–215. https://doi.org/10.1002/j.1537-2197.1950.tb12183.x

Nitsch JP. (1955). Free auxins and free tryptophane in the strawberry. *Plant Physiology*, *30*(1), 33–39. https://doi.org/10.1104/pp.30.1.33

Nonhebel H. (2015). Tryptophan-independent indole-3-acetic acid synthesis: Critical evaluation of the evidence. *Plant Physiology*, *169*(2), 1001–1005. https://doi.org/10.1104/pp.15.01091

Nonhebel H, Cooney T, Simpson R. (1993). The route, control and compartmentation of auxin synthesis. *Functional Plant Biology*, *20*(5), 527. https://doi.org/10.1071/pp9930527

Normanly J, Cohen JD, Fink GR. (1993). *Arabidopsis thaliana* auxotrophs reveal a tryptophan-independent biosynthetic pathway for indole-3-acetic acid. *Proceedings of the National Academy of Sciences*, *90*(21), 10355–10359. https://doi.org/10.1073/pnas.90.21.10355

Normanly J, Slovin JP, Cohen JD. (2010). Auxin biosynthesis and metabolism. In Davies, P.J. (Ed.) *Plant Hormones.* Springer, Dordrecht. https://doi.org/10.1007/978-1-4020-2686-7_3

Novák O, Hényková E, Sairanen I, Kowalczyk M, Pospíšil T, Ljung K. (2012). Tissue-specific profiling of the *Arabidopsis thaliana* auxin metabolome. *The Plant Journal*, *72*(3), 523–536. https://doi.org/10.1111/j.1365-313x.2012.05085.x

Nowacki J, Bandurski RS. (1980). Myo-inositol esters of indole-3-acetic acid as seed aux precursors of *Zea mays L.* *Plant Physiology*, *65*(3), 422–427. https://doi.org/10.1104/pp.65.3.422

Oetiker JH, Aeschbacher G. (1997). Temperature-sensitive plant cells with shunted indole-3-acetic acid conjugation. *Plant Physiology*, *114*(4), 1385–1395. https://doi.org/10.1104/pp.114.4.1385

Östin A, Ilić N, Cohen JD. (1999). An in vitro system from maize seedlings for tryptophan-independent indole-3-acetic acid biosynthesis. *Plant Physiology*, *119*(1), 173–178. https://doi.org/10.1104/pp.119.1.173

Östin A, Kowalyczk M, Bhalerao RP, Sandberg G. (1998). Metabolism of indole-3-acetic acid in Arabidopsis. *Plant Physiology*, *118*(1), 285–296. https://doi.org/10.1104/pp.118.1.285

Ouyang J, Shao X, Li J. (2000). Indole-3-glycerol phosphate, a branchpoint of indole-3-acetic acid biosynthesis from the tryptophan biosynthetic pathway in *Arabidopsis thaliana*. *The Plant Journal*, *24*(3), 327–334. https://doi.org/10.1046/j.1365-313x.2000.00883.x

Paponov IA, Paponov M, Teale W, Menges M, Chakrabortee S, Murray JAH, Palme K. (2008). Comprehensive transcriptome analysis of auxin responses in Arabidopsis. *Molecular Plant*, *1*(2), 321–337. https://doi.org/10.1093/mp/ssm021

Park S, Cohen JD, Slovin JP. (2006). Strawberry fruit protein with a novel indole-acyl modification. *Planta*, *224*(5), 1015–1022. https://doi.org/10.1007/s00425-006-0287-z

Pengelly WL, Bandurski RS. (1983). Analysis of indole-3-acetic acid metabolism in *Zea mays* using deuterium oxide as a tracer. *Plant Physiology*, *73*(2), 445–449. https://doi.org/10.1104/pp.73.2.445

Perkins-Veazie P. (1995). Growth and ripening of strawberry fruit. In J. J (Ed.), *Horticultural Reviews* (Vol. 17, pp. 267–297). John Wiley & Sons. https://doi.org/10.1002/9780470650585.ch8

Petersen TN, Brunak S, Heijne G von, Nielsen H. (2011). SignalP 4.0: discriminating signal peptides from transmembrane regions. *Nature Methods*, *8*(10), 785–786. https://doi.org/10.1038/nmeth.1701

Phillips KA, Skirpan AL, Liu X, Christensen A, Slewinski TL, Hudson C, Barazesh S, Cohen JD, Malcomber S, McSteen P. (2011). *vanishing tassel2* encodes a grass-specific tryptophan aminotransferase required for vegetative and reproductive development in maize. *The Plant Cell*, *23*(2), 550–566. https://doi.org/10.1105/tpc.110.075267

Pieck M, Yuan Y, Godfrey J, Fisher C, Zolj S, Vaughan D, Thomas N, Wu C, Ramos J, Lee N. (2015). Auxin and tryptophan homeostasis are facilitated by the ISS1/VAS1 aromatic aminotransferase in Arabidopsis. *Genetics*, *201*(1), 185–199. https://doi.org/10.1534/genetics.115.180356

Pratt JM, Petty J, Riba-Garcia I, Robertson DHL, Gaskell SJ, Oliver SG, Beynon RJ. (2002). Dynamics of protein turnover, a missing dimension in proteomics. *Molecular & Cellular Proteomics : MCP*, *1*(8), 579–591. https://doi.org/10.1074/mcp.m200046-mcp200

Quittenden LJ, Davies NW, Smith JA, Molesworth PP, Tivendale ND, Ross JJ. (2009). Auxin biosynthesis in pea: characterization of the tryptamine pathway. *Plant Physiology*, *151*(3), 1130–1138. https://doi.org/10.1104/pp.109.141507

Rajagopal R. (1971). Metabolism of indole-3-acetaldehyde. III. Some characteristics of the aldehyde oxidase of *Avena coleoptiles*. *Physiologia Plantarum*, *24*(2), 272–281. https://doi.org/10.1111/j.1399-3054.1971.tb03491.x

Rampey RA, LeClere S, Kowalczyk M, Ljung K, Sandberg G, Bartel B. (2004). A family of auxin-conjugate hydrolases that contributes to free indole-3-acetic acid levels during Arabidopsis germination. *Plant Physiology*, *135*(2), 978–988. https://doi.org/10.1104/pp.104.039677

Rapparini F, Tam YY, Cohen JD, Slovin JP. (2002). Indole-3-acetic acid metabolism in *Lemna gibba* undergoes dynamic changes in response to growth temperature. *Plant Physiology*, *128*(4), 1410–1416. https://doi.org/10.1104/pp.011005

Ribaut JM, Schaerer S, Pilet P-E. (1993). Deuterium-labelled indole-3-acetic acid neo-synthesis in plantlets and excised roots of maize. *Planta*, *189*(1), 80–82. https://doi.org/10.1007/bf00201347

Ribnicky DM, Ilic N, Cohen JD, Cooke TJ. (1996). The effects of exogenous auxins on endogenous indole-3-acetic acid metabolism (The implications for carrot somatic embryogenesis). *Plant Physiology*, *112*(2), 549–558. https://doi.org/10.1104/pp.112.2.549

Riens B, Lohaus G, Heineke D, Heldt HW. (1991). Amino acid and sucrose content determined in the cytosolic, chloroplastic, and vacuolar compartments and in the phloem sap of spinach leaves. *Plant Physiology*, *97*(1), 227–233. https://doi.org/10.1104/pp.97.1.227

Roscher A, Kruger NJ, Ratcliffe RG. (2000). Strategies for metabolic flux analysis in plants using isotope labelling. *Journal of Biotechnology*, *77*(1), 81–102. https://doi.org/10.1016/s0168-1656(99)00209-6

Ross JJ, Gélinas-Marion A. (2021). Two pathways become one. *Nature Plants*, *7*(12), 1546–1547. https://doi.org/10.1038/s41477-021-01036-3

Sairanen I, Novák O, Pěnčík A, Ikeda Y, Jones B, Sandberg G, Ljung K. (2012). Soluble carbohydrates regulate auxin biosynthesis via PIF proteins in Arabidopsis. *The Plant Cell*, *24*(12), 4907–4916. https://doi.org/10.1105/tpc.112.104794

Saitou N, Nei M. (1987). The neighbor-joining method: a new method for reconstructing phylogenetic trees. *Molecular Biology and Evolution*, *4*(4), 406–425. https://doi.org/10.1093/oxfordjournals.molbev.a040454

Sánchez-Sevilla JF, Vallarino JG, Osorio S, Bombarely A, Posé D, Merchante C, Botella MA, Amaya I, Valpuesta V. (2017). Gene expression atlas of fruit ripening and transcriptome assembly from RNA-seq data in octoploid strawberry (*Fragaria* × *ananassa*). *Scientific Reports*, *7*(1), 13737. https://doi.org/10.1038/s41598-017-14239-6

Sauer M, Robert S, Kleine-Vehn J. (2013). Auxin: simply complicated. *Journal of Experimental Botany*, *64*(9), 2565–2577. https://doi.org/10.1093/jxb/ert139

Shulaev V, Sargent DJ, Crowhurst RN, Mockler TC, Folkerts O, Delcher AL, Jaiswal P, Mockaitis K, Liston A, Mane SP, Burns P, Davis TM, Slovin JP, Bassil N, … Folta KM. (2011). The genome of woodland strawberry (*Fragaria vesca*). *Nature Genetics*, *43*(2), 109–116. https://doi.org/10.1038/ng.740

Simon S, Petrášek J. (2011). Why plants need more than one type of auxin. *Plant Science : An International Journal of Experimental Plant Biology*, *180*(3), 454–460. https://doi.org/10.1016/j.plantsci.2010.12.007

Slovin JP, Schmitt K, Folta KM. (2009). An inbred line of the diploid strawberry *Fragaria vesca f. semperflorens* for genomic and molecular genetic studies in the Rosaceae. *Plant Methods*, *5*(1), 15–15. https://doi.org/10.1186/1746-4811-5-15

Smith CA, Want EJ, O'Maille G, Abagyan R, Siuzdak G. (2006). XCMS: processing mass spectrometry data for metabolite profiling using nonlinear peak alignment, matching, and identification. *Analytical Chemistry*, *78*(3), 779–787. https://doi.org/10.1021/ac051437y

Smith RM. (2004). Important mass spectral rearrangements. In R. M. Smith (Ed.), *Understanding Mass Spectra: A Basic Approach, Second Edition* (pp. 207–237). https://doi.org/10.1002/0471479357.ch7

Smolko A, Ludwig-Müller J, Salopek-Sondi B. (2018). Auxin amidohydrolases – from structure to function: revisited. *Croatica Chemica Acta*, *91*(2), 233-239. https://doi.org/10.5562/cca3356

Soeno K, Goda H, Ishii T, Ogura T, Tachikawa T, Sasaki E, Yoshida S, Fujioka S, Asami T, Shimada Y. (2010). Auxin biosynthesis inhibitors, identified by a genomics-based approach, provide insights into auxin biosynthesis. *Plant and Cell Physiology*, *51*(4), 524–536. https://doi.org/10.1093/pcp/pcq032

Soeno K, Sato A, Shimada Y. (2021). Investigation of auxin biosynthesis and action using auxin biosynthesis inhibitors. *Methods in Molecular Biology*, *2213*, 131–144. https://doi.org/10.1007/978-1-0716-0954-5_12

Stepanova AN, Robertson-Hoyt J, Yun J, Benavente LM, Xie D-Y, Dolezal K, Schlereth A, Jürgens G, Alonso JM. (2008). TAA1-mediated auxin biosynthesis is essential for hormone crosstalk and plant development. *Cell*, *133*(1), 177–191. https://doi.org/10.1016/j.cell.2008.01.047

Stepanova AN, Yun J, Robles LM, Novak O, He W, Guo H, Ljung K, Alonso JM. (2011). The Arabidopsis YUCCA1 flavin monooxygenase functions in the indole-3-pyruvic acid branch of auxin biosynthesis. *The Plant Cell*, *23*(11), 3961–3973. https://doi.org/10.1105/tpc.111.088047

Sugawara S, Hishiyama S, Jikumaru Y, Hanada A, Nishimura T, Koshiba T, Zhao Y, Kamiya Y, Kasahara H. (2009). Biochemical analyses of indole-3-acetaldoxime-dependent auxin biosynthesis in Arabidopsis. *Proceedings of the National Academy of Sciences*, *106*(13), 5430–5435. https://doi.org/10.1073/pnas.0811226106

Symons GM, Chua Y-J, Ross JJ, Quittenden LJ, Davies NW, Reid JB. (2012). Hormonal changes during non-climacteric ripening in strawberry. *Journal of Experimental Botany*, *63*(13), 4741–4750. https://doi.org/10.1093/jxb/ers147

Tam YY, Slovin JP, Cohen JD. (1995). Selection and characterization of alpha-methyltryptophan resistant lines of *Lemna gibba* showing a rapid rate of indole-3-acetic acid turnover. *Plant Physiology*, *107*(1), 77–85. https://doi.org/10.1104/pp.107.1.77

Tang Q, Yu P, Tillmann M, Cohen JD, Slovin JP. (2019). Indole-3-acetylaspartate and indole-3-acetylglutamate, the IAA-amide conjugates in the diploid strawberry achene, are hydrolyzed in growing seedlings. *Planta*, *249*(4), 1073–1085. https://doi.org/10.1007/s00425-018-3061-0

Tao Y, Ferrer J-L, Ljung K, Pojer F, Hong F, Long JA, Li L, Moreno JE, Bowman ME, Ivans LJ, Cheng Y, Lim J, Zhao Y, Ballaré CL, … Chory J. (2008). Rapid synthesis of

auxin via a new tryptophan-dependent pathway is required for shade avoidance in plants. *Cell*, *133*(1), 164–176. https://doi.org/10.1016/j.cell.2008.01.049

Tillmann M, Tang Q, Cohen JD. (2021). Protocol: analytical methods for visualizing the indolic precursor network leading to auxin biosynthesis. *Plant Methods*, *17*(1), 63. https://doi.org/10.1186/s13007-021-00763-0

Tillmann M, Tang Q, Gardner G, Cohen JD. (2022). Complexity of the auxin biosynthetic network in Arabidopsis hypocotyls is revealed by multiple stable-labeled precursors. *Phytochemistry*, *200*, 113219. https://doi.org/10.1016/j.phytochem.2022.113219

Tivendale ND, Cohen JD. (2015). Analytical history of auxin. *Journal of Plant Growth Regulation*, *34*(4), 708–722. https://doi.org/10.1007/s00344-015-9519-4

Tivendale ND, Davies NW, Molesworth PP, Davidson SE, Smith JA, Lowe EK, Reid JB, Ross JJ. (2010). Reassessing the role of N-hydroxytryptamine in auxin biosynthesis. *Plant Physiology*, *154*(4), 1957–1965. https://doi.org/10.1104/pp.110.165803

Tivendale ND, Ross JJ, Cohen JD. (2014). The shifting paradigms of auxin biosynthesis. *Trends in Plant Science*, *19*(1), 44–51. https://doi.org/10.1016/j.tplants.2013.09.012

Tsugafune S, Mashiguchi K, Fukui K, Takebayashi Y, Nishimura T, Sakai T, Shimada Y, Kasahara H, Koshiba T, Hayashi K. (2017). Yucasin DF, a potent and persistent inhibitor of auxin biosynthesis in plants. *Scientific Reports*, *7*(1), 13992. https://doi.org/10.1038/s41598-017-14332-w

Tuominen H, Ostin A, Sandberg G, Sundberg B. (1994). A novel metabolic pathway for inole-3acetic acid in apical shoots of *Populus tremula (L.) x Populus tremuloides (Michx.)*. *Plant Physiology*, *106*(4), 1511–1520. https://doi.org/10.1104/pp.106.4.1511

Tzin V, Galili G. (2010). The biosynthetic pathways for shikimate and aromatic amino acids in *Arabidopsis thaliana*. *The Arabidopsis Book*, *8*(8), e0132. https://doi.org/10.1199/tab.0132

Wang B, Chu J, Yu T, Xu Q, Sun X, Yuan J, Xiong G, Wang G, Wang Y, Li J. (2015). Tryptophan-independent auxin biosynthesis contributes to early embryogenesis in Arabidopsis. *Proceedings of the National Academy of Sciences*, *112*(15), 4821–4826. https://doi.org/10.1073/pnas.1503998112

Watkins-Dulaney E, Straathof S, Arnold F. (2020). Tryptophan synthase: biocatalyst extraordinaire. *ChemBioChem*, *22*(1), 5–16. https://doi.org/10.1002/cbic.202000379

Won C, Shen X, Mashiguchi K, Zheng Z, Dai X, Cheng Y, Kasahara H, Kamiya Y, Chory J, Zhao Y. (2011). Conversion of tryptophan to indole-3-acetic acid by TRYPTOPHAN

AMINOTRANSFERASES OF ARABIDOPSIS and YUCCAs in Arabidopsis. *Proceedings of the National Academy of Sciences of the United States of America*, *108*(45), 18518–18523. https://doi.org/10.1073/pnas.1108436108

Woodward AW, Bartel B. (2005). Auxin: regulation, action, and interaction. *Annals of Botany*, *95*(5), 707–735. https://doi.org/10.1093/aob/mci083

Wright AD, Sampson MB, Neuffer MG, Michalczuk L, Slovin JP, Cohen JD. (1991). Indole-3-acetic acid biosynthesis in the mutant maize orange pericarp, a tryptophan auxotroph. *Science*, *254*(5034), 998–1000. https://doi.org/10.1126/science.254.5034.998

Xu Y, Abeles RH. (1993). Inhibition of tryptophan synthase by (1-fluorovinyl)glycine. *Biochemistry*, *32*(3), 806–811. https://doi.org/10.1021/bi00054a010

Yang S, Gao M, Xu C, Gao J, Deshpande S, Lin S, Roe BA, Zhu H. (2008). Alfalfa benefits from *Medicago truncatula*: The *RCT1* gene from *M. truncatula* confers broad-spectrum resistance to anthracnose in alfalfa. *Proceedings of the National Academy of Sciences*, *105*(34), 12164–12169. https://doi.org/10.1073/pnas.0802518105

Yang X-Y, Chen W-P, Rendahl AK, Hegeman AD, Gray WM, Cohen JD. (2010). Measuring the turnover rates of Arabidopsis proteins using deuterium oxide: an auxin signaling case study. *The Plant Journal : For Cell and Molecular Biology*, *63*(4), 680–695. https://doi.org/10.1111/j.1365-313x.2010.04266.x

Yin R, Frey M, Gierl A, Glawischnig E. (2010). Plants contain two distinct classes of functional tryptophan synthase beta proteins. *Phytochemistry*, *71*(14–15), 1667–1672. https://doi.org/10.1016/j.phytochem.2010.07.006

Yu P, Hegeman AD, Cohen JD. (2014). A facile means for the identification of indolic compounds from plant tissues. *The Plant Journal*, *79*(6), 1065–1075. https://doi.org/10.1111/tpj.12607

Yu P, Lor P, Ludwig-Müller J, Hegeman AD, Cohen JD. (2015). Quantitative evaluation of IAA conjugate pools in *Arabidopsis thaliana*. *Planta*, *241*(2), 539–548. https://doi.org/10.1007/s00425-014-2206-z

Yuan J, Bennett BD, Rabinowitz JD. (2008). Kinetic flux profiling for quantitation of cellular metabolic fluxes. *Nature Protocols*, *3*(8), 1328–1340. https://doi.org/10.1038/nprot.2008.131

Zazímalová E, Murphy AS, Yang H, Hoyerová K, Hosek P. (2010). Auxin transporters--why so many? *Cold Spring Harbor Perspectives in Biology*, *2*(3), a001552. https://doi.org/10.1101/cshperspect.a001552

Zhang J, Peer WA. (2017). Auxin homeostasis: the DAO of catabolism. *Journal of Experimental Botany*, *68*(12), 3145–3154. https://doi.org/10.1093/jxb/erx221

Zhang R, Wang B, Ouyang J, Li J, Wang Y. (2008). Arabidopsis indole synthase, a homolog of tryptophan synthase alpha, is an enzyme involved in the Trp-independent indole-containing metabolite biosynthesis. *Journal of Integrative Plant Biology*, *50*(9), 1070–1077. https://doi.org/10.1111/j.1744-7909.2008.00729.x

Zhao Y. (2008). The role of local biosynthesis of auxin and cytokinin in plant development. *Current Opinion in Plant Biology*, *11*(1), 16–22. https://doi.org/10.1016/j.pbi.2007.10.008

Zhao Y. (2012). Auxin biosynthesis: a simple two-step pathway converts tryptophan to indole-3-acetic acid in plants. *Molecular Plant*, *5*(2), 334–338. https://doi.org/10.1093/mp/ssr104

Zhao Z, Zhang Y, Liu X, Zhang X, Liu S, Yu X, Ren Y, Zheng X, Zhou K, Jiang L, Guo X, Gai Y, Wu C, Zhai H, … Wan J. (2013). A role for a dioxygenase in auxin metabolism and reproductive development in rice. *Developmental Cell*, *27*(1), 113–122. https://doi.org/10.1016/j.devcel.2013.09.005

Zhou Z-Y, Zhang C-G, Wu L, Zhang C-G, Chai J, Wang M, Jha A, Jia P-F, Cui S-J, Yang M, Chen R, Guo G-Q. (2011). Functional characterization of the *CKRC1/TAA1* gene and dissection of hormonal actions in the Arabidopsis root. *The Plant Journal : For Cell and Molecular Biology*, *66*(3), 516–527. https://doi.org/10.1111/j.1365-313x.2011.04509.x

Zhu Y, Li H, Su Q, Wen J, Wang Y, Song W, Xie Y, He W, Yang Z, Jiang K. (2019). A phenotype-directed chemical screen identifies ponalrestat as an inhibitor of the plant flavin monooxygenase YUCCA in auxin biosynthesis. *Journal of Biological Chemistry*, *294*(52), 19923–19933. https://doi.org/10.1074/jbc.ra119.010480

Appendix

Complexity of the auxin biosynthetic network in Arabidopsis hypocotyls is revealed by multiple stable-labeled precursors

Molly Tillmann*, Qian Tang, Gary Gardner, and Jerry D. Cohen

Published in Phytochemistry, August 2022, Volume 200, Article 113219

Abstract

Auxin is a key regulator of plant development and in *Arabidopsis thaliana* can be synthesized through multiple pathways; however, the contributions of various biosynthetic pathways to specific developmental processes are largely unknown. To trace the involvement of various biosynthetic routes to indole-3-acetic acid (IAA) under conditions that induce adventitious root formation in Arabidopsis hypocotyls, we treated seedlings with three different stable isotope-labeled precursors ([$^{13}C_6$]anthranilate, [$^{15}N_1$]indole, and [$^{13}C_3$]serine) and monitored label incorporation into a number of proposed biosynthesis intermediates as well as IAA. We also employed inhibitors targeting tryptophan aminotransferases and flavin monooxygenases of the IPyA pathway, and treatment with these inhibitors differentially altered the labeling patterns from all three precursors into intermediate compounds and IAA. [$^{13}C_3$]Serine was used to trace utilization of tryptophan (Trp) and downstream intermediates by monitoring ^{13}C incorporation into Trp, indole-3-pyruvic acid (IPyA), and IAA; most ^{13}C incorporation into IAA was eliminated with inhibitor treatments, suggesting Trp-dependent IAA biosynthesis through the IPyA pathway is a dominant contributor to the auxin pool in de-etiolating hypocotyls that can be effectively blocked using chemical inhibitors. Labeling treatment with both [$^{13}C_6$]anthranilate and [$^{15}N_1$]indole simultaneously resulted in higher label incorporation into IAA through [$^{15}N_1$]indole than through [$^{13}C_6$]anthranilate; however, this trend was reversed in the proposed precursors that were monitored, with the majority of isotope label originating from [$^{13}C_6$]anthranilate. An even greater proportion of IAA became [$^{15}N_1$]-labeled compared to [$^{13}C_6$]-labeled in seedlings treated with IPyA pathway inhibitors, suggesting that, when the IPyA pathway is blocked, IAA biosynthesis from labeled indole may also come from an origin independent of the measured pool of Trp in these tissues.

Extraction and analysis of IAA and biosynthesis intermediates

For analysis of proposed IAA biosynthesis intermediates (Trp, TAM, IPyA, IAAld, IAOx, IAN, and IAM), samples of 20-50 mg plant tissue were prepared and analyzed as previously described (Tillmann et al., 2021), where IPyA and IAAld were derivatized with CH_3ONH_2 to generate their methyl oximes (IPyA-MeOx and IAAld-MeOx). Retention times and exact mass data from unlabeled compounds were matched to authentic standards that were analyzed using identical LC-MS parameters. Exact mass values of standards, endogenous unlabeled compounds, and labeled isotopomers were within 0.0015 *m/z* of calculated values listed in Supplement Table A - 1.

Samples for IAA quantitation by LC-MS/MS were prepared and analyzed essentially as described by (Tang et al., 2019), using imidazole buffered aqueous 2-propanol for extraction. These procedures have five advantages: speed, small sample size, polar enzyme inactivating solvents, and a solvent-soluble buffer/antioxidant (Liu et al. 2012). Imidazole has been shown to have antioxadant activitiy (Kohen et al., 1988) and, as noted by Tivendale et al. (2015), IPyA is, at neutral pH in methanol, relatively stable. Data points were removed if recovery of internal standard was too low for accurate quantitation, or if the measurement deviated from the mean by more than 10 standard deviations (presumably due to contamination or interferring compounds).

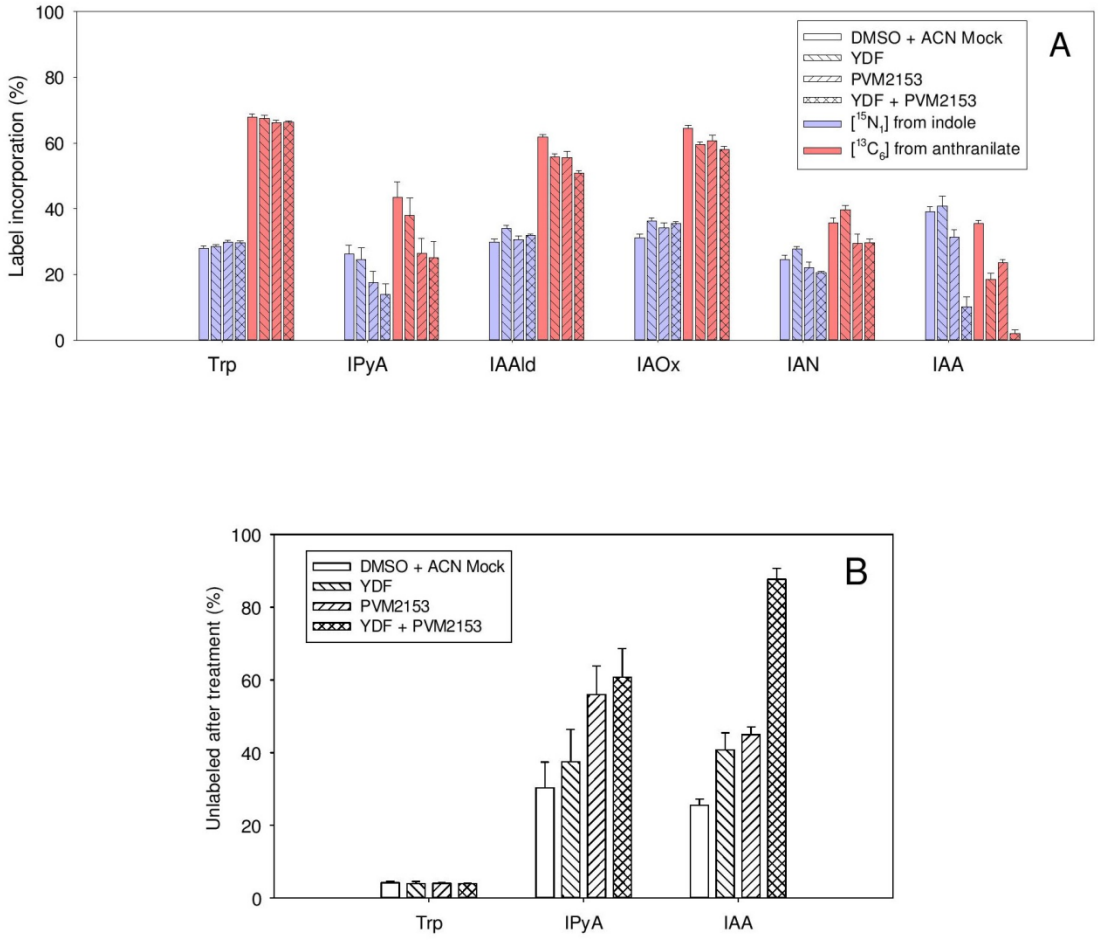

Figure A - 1: **[$^{15}N_1$]indole and [$^{13}C_6$]anthranilate labeling of IAA precursors in Arabidopsis hypocotyls in the presence of IPyA pathway inhibitors.** Seedlings were grown in the dark for 7 d, then transferred onto media containing 100 µM YDF and/or 30 µM PVM2153, or DMSO and acetonitrile (mock). Seedlings were then exposed to a 16 h photoperiod of red light (660 nm, 135 µmol m^{-2} s^{-1}) for 3 days, and then treated by applying to the inhibitor or mock plates a solution containing 500 µM [$^{15}N_1$]indole and 500 µM [$^{13}C_6$]anthranilate for 16 hours under red light. Samples containing approximately 20 hypocotyls were collected for LC-MS analysis of isotopic enrichment of IAA and IAA biosynthesis intermediates. Data are expressed as the percentage of total detected compound containing the specified isotopic label (A), or for Trp, IPyA, and IAA the percentage of compound remaining unlabeled after treatment (B) and have been corrected for the natural abundance of ^{15}N. In panel B we show only those compounds discussed in the text, Trp, IPyA, and IAA. Each bar represents the mean of 5-7 biological replicates; error bars represent SE.

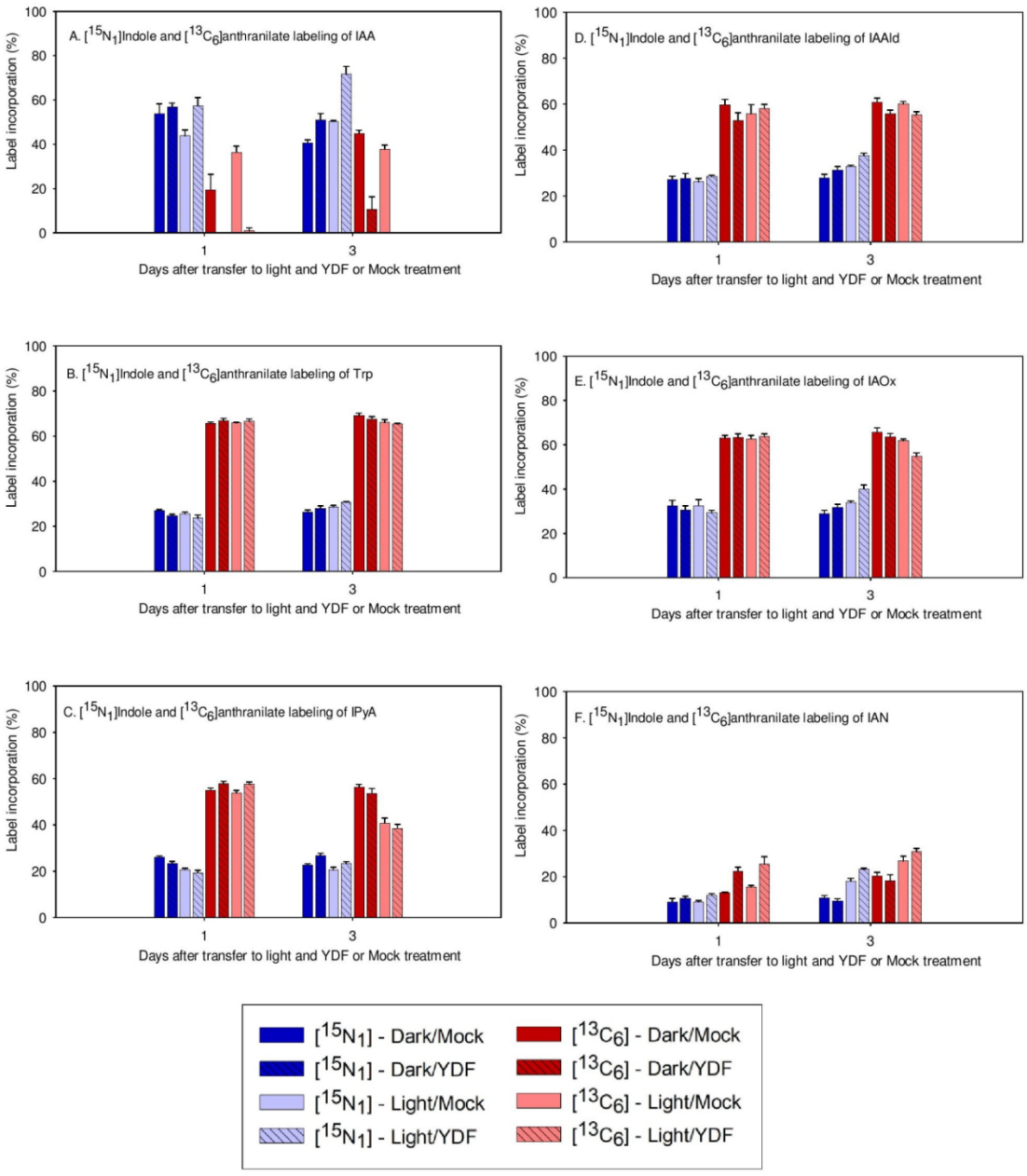

Figure A - 2: [$^{15}N_1$]indole and [$^{13}C_6$]anthranilate labeling of IAA precursors in Arabidopsis hypocotyls treated with YDF under light and dark. Seedlings were grown in the dark for 7 d, then transferred onto media containing 100 µM YDF or DMSO (mock) and exposed to a 16 h photoperiod of red light or continued darkness for 1 or 3 days. Seedlings were then treated by applying to the inhibitor or mock plates a solution containing 500 µM [$^{15}N_1$]indole and 500 µM [$^{13}C_6$]anthranilate for 16 hours. Samples containing approximately 20 hypocotyls were collected for LC-MS analysis of isotopic

enrichment of IAA (A) and potential IAA biosynthesis intermediates: Trp (B), IPyA (C), IAAld (D), IAOx (E), IAN (F). Data are expressed as the percentage of total detected compound containing the specified isotopic label and have been corrected for the natural abundance of ^{15}N. Each bar represents the mean of 4 biological replicates; error bars represent SE.

Supplement Table A - 1: Retention times, chemical formulas, and calculated *m/z* values of isotopomers of IAA and proposed biosynthesis intermediates. Retention times were determined with authentic standards. Tryptophan (Trp), Tryptamine (TAM), indole-3-acetaldoxime (IAOx), indole-3-acetamide (IAM), indole-3-acetonitrile (IAN), indole-3-pyruvate methyl oxime (IPyA-MeOx), indole-3-acetaldehyde methyl oxime (IAAld-MeOx), indole-3-acetic acid (IAA).

	Retention time (min)	**Formula**	***m/z* [M]+H**	***m/z* $^{15}N_1$**	***m/z* $^{13}C_1$**	***m/z* $^{13}C_2$**	***m/z* $^{13}C_3$**	***m/z* $^{13}C_6$**
Trp	1.87	$C_{11}H_{12}N_2O_2$	205.0972	206.0942	-	-	208.1072	211.1173
TAM	2.60	$C_{10}H_{12}N_2$	161.1073	162.1044	-	-	-	167.1275
IAOx	5.01/5.17*	$C_{10}H_{10}N_2O$	175.0866	176.0836	-	-	-	181.1067
IAM	3.96	$C_{10}H_{10}N_2O$	175.0866	176.0836	-	-	-	181.1067
IAN	5.87	$C_{10}H_8N_2$	157.0760	158.0731	-	-	-	163.0962
IPyA-MeOx	6.27	$C_{12}H_{12}N_2O_3$	233.0921	234.0891	-	-	236.1021	239.1122
IAAld-MeOx	7.74/8.07*	$C_{11}H_{12}N_2O$	189.1022	190.0993	-	-	-	195.1224
IAA	4.44	$C_{10}H_9NO_2$	176.0706	177.0676	-	178.0773	-	182.0907
Quinolinium ion (IAA)	-	C_9H_7N	130.0651	131.0622	131.0685	-	-	136.0853

*IAOx and IAAld-MeOx each produced two peaks